Formulation and evaluation of the biocompatibility of chitosan-dextran nanoparticles using a blood-brain barrier model

UNIVERSITY *of the*
WESTERN CAPE

Ziphozihle Ntwatwa

A mini-thesis submitted in partial fulfilment of the requirements for the degree of Magister Scientiae in Nanoscience in the Department of Medical Bioscience, University of the Western Cape.

Supervisor: Prof. Admire Dube

Co-supervisor: Prof. David Fisher

May 2018

ABSTRACT

Central nervous system (CNS) infections are a therapeutic challenge. This is partly due to insufficient drug penetration across the blood-brain barrier (BBB). The BBB is a specialized, highly selective, metabolically active physiological barrier that regulates the movement of molecules into-and-out of the brain. As a result, large hydrophilic antibiotics such as colistin poorly penetrate to the CNS. Colistin is an old ‘last line of defence'; a gram-negative antibiotic that has seen its clinical re-emergence due to the surge of multidrug resistance (MDR) infections. However, owing to systemic toxicity, increasing the intravenous dosage, in order to obtain higher CNS penetration, is inimical. Chitosan (CS) based nanoparticles (NPs) have been proposed as drug delivery systems across the BBB. CS is a cationic, natural polysaccharide that has the ability to be complexed with multivalent polymers like dextran (DS) thus forming CS-DS NPs. Naturally, CS has remarkable inherent features such as biocompatibility, biodegradability, ability to encapsulate poorly soluble drugs and it is favourable for endothelial cell uptake. However, polymeric NPs (even those derived from natural polysaccharides) have limited use due to toxicity. Considering the vital role of the BBB, toxicity would denote dire effects on CNS functioning. Therefore, treatment of CNS infections fringes on a deeper understanding of the interactions between drug delivery systems and the BBB.

The aim of this study was to (1) synthesize colistin encapsulated CS-DS NPs as a nano-drug delivery system, (2) characterize its biocompatibility to the BBB by assessing toxicity. This was achieved through the synthesis, optimization and characterization of CS-DS NPs with precise physicochemical characteristics; monodispersity, negative charge, hydrodynamic diameter less than 200 nm and encapsulation abilities. BBB biocompatibility was measured with reference to endothelial toxicity, influence on the transendothelial electrical resistance (TEER). Additionally, Scanning Electron Microscopy (SEM) was used to assess the topographical localization and interaction of the CS-DS NPs with the endothelial cell monolayer.

The polyelectrolyte complexation method was used to synthesize colloidal CS-DS NPs using the electrostatic interactions between CS and DS functional groups (positive amine and negative sulphate groups, respectively). The ratio between functional groups, charge index, was manipulated in order to assess its relationship to the physicochemical characteristics. An inverse relationship was observed; an increase in the charge index from 0.03 to 43.5 correlated to a significant decrease in hydrodynamic diameter, i.e., 551 ± 84.05 nm to 144.4 ± 10.89 nm, respectively ($P < 0.0001$). Charge index increase also significantly divided NP into positively

charged populations with large hydrodynamic diameters (61.27 ± 7.27 mV, 551 ± 84.05 nm) and negatively charged populations with small hydrodynamic diameters (-54.77 ± 23.29 mV, 144.4 ± 10.89 nm) ($P<0.0001$) with no significant effects on dispersity. The CS-DS NP had 24% encapsulation efficacy of colistin (colistin sulphate salt, CSS).

Cell viability studies showed that the CS-DS NPs had a protective effect on the BBB. CSS encapsulation into the NP significantly mitigated toxicity whereas free CSS was toxic to the BBB (after a 24-hour treatment with 9.6 µg/ml free CSS and CSS-CS-DS NPs) ($P<0.01$). The NPs also showed to maintain the physiological tautness of BBB as no changes in TEER were observed. SEM revealed that topographical interaction of CS-DS NPs with endothelial monolayer was on a structurally intact and healthy Bend5 monolayer versus unhealthy cells in CSS treated monolayer.

Evaluation of CS-DS NPs showed remarkable neuroprotective role, *in vitro*. The NPs extenuated the effects of neurotoxic drug (colistin) on the BBB and therefore strongly supports their use as potential drug delivery system.

Keywords: CNS infections, BBB, drug delivery system, CS-DS NPs, colistin, neuroprotection.

DECLARATION

I, Ziphozihle Ntwatwa, declare that 'Formulation and evaluation of the biocompatibility of chitosan-dextran nanoparticles using a blood-brain barrier model'is my own work, that it has not been submitted before for any degree or assessment in any other university, and that all the sources I have used or quoted have been indicated and acknowledged by means of complete references.

Full name: Ziphozihle Ntwatwa

Date: May 2018

Signed

ACKNOWLEDGMENTS

So many people have made a significant contribution to firstly who I am as a person and secondly constantly encouraging me to always keep going. Jeremiah 29 verse 11: “For I know the plans I have for you, plans to prosper you and not to harm you, plans to give you a future and a hope.

To all of those who have been a part of this journey

I would especially like to thank the following people,

Prof. D. Fisher, Prof I have such a profound appreciation for the depth in which you teach; academically, spiritually and emotionally. Thank you for the manner in which you directed this body of work and for reminding me about the importance of consistency. Most importantly, thank you for the platform that you have provided for me to grow in the direction that is a reflection of my true self and potential. Potential is key. May the Lord bless and keep you.

Prof. A Dube, thank you for introducing me to natural polymers. In light of who I am, I am incredibly blessed to focus my academics into the world of natural materials. Thank you for your transparency and having an open-door policy, it is grounding to always feel welcome

To my Mama I love you

To my brother, Qhama, you are my true love and I hope one day you will read this

To my partner Bart, you are an alpha

To God be the Glory

LIST OF ABBREVIATIONS

AE	Adsorptive endocytosis
AJ	Adherence junction
AP	Alkaline phosphatase
ATP	Adenosine triphosphate
BBB	Blood brain barrier
BM	Basement membrane
BMECs	Brain micro vascular endothelial cells
CA	Cornu Ammonis
CMS	Colistin methanesulfonate
CMT	Carrier-mediated transport
CNs	Carbon nanotubes
CNS	Central nervous system
CS	Chitosan
CS-DS NPs	Chitosan-dextran nanoparticles
CSS	Colistin sulphate salt
Da	Daltons
Dab	Diaminobutyric
DI	Deionized water
DLVO	Derjaguin, Landau, Verwey and Overbeek thoery
DOX	Doxorubicin
DS	Dextran
ECM	Extracellular matrix
EE	Encapsulation efficiency
FDA	Food and Drug Administration
GAGs	Glycosaminoglycans

GLUT	Glucose transporter
GUK	Guanylate kinase
HPMA	N-2-hydroxypropyl methacrylamide
JAMs	Junctional adhesion molecules
LDL	Low density lipoprotein
L-DOPA	L-3,4-dihydroxyphenylalanine
Log *P*	Lipophilicity
LPS	Lipopolysaccharide
Mac-1	Macrophage-1 antigen-complement receptor
MAO	Monoamine oxidase
MDR	Multidrug resistant
MRPs	Multidrug resistance-associated proteins
Mwt	Molecular weight
NAGs	N-acetyl glucosamines
NF-κB	Nuclear factor kappa-light-chain-enhancer of activated
NGF	Nerve growth factor
NINDS	National Institute of Neurological Disorders and Stroke
NPs	Nanoparticles
NVU	Neurovascular unit
OAT	Organic anion transporter
OATP	Organic anion transporting polypeptide
OCT	Organic cation transporter
PBCA	Poly (butylcanocrylates)
PBS	Phosphate buffer solution
PDI	Polydispersity index
PE	Polyelectrolyte

PECAM-1	Platelet Endothelial Cell Adhesion Molecule
PECs	Polyelectrolyte complexes
PEG	Poly (ethylene) glycol
P-gp	P-glycoprotein
PKC-α	Protein kinase C alpha
PLA	Poly (lactic acid)
PLGA	Poly (Lactide-co-glycocides)
PPE	Paracellular permeability enhancer
QSAR	Computational Quantitative Structure Activity Relationship
RMT	Receptor-mediated transcytosis
RNA	Ribonucleic acid
RT	Room temperature
SCENIHR	Scientific Committee on Emerging and Newly Identified Health Risks
SEM	Scanning Electron Microscopy
SLC	Solute carrier
TJs	Tight junctions
TPP	Tripolyphosphate
UV-Vis	Ultraviolet-visible spectroscopy
VEGF	Vascular endothelial growth factor
ZO	Zona occludin
γ-GTP	γ-glutamyl transpeptidase
ζ-potential	Zeta potential

LIST OF FIGURES

TABLE OF CONTENTS

CHAPTER ONE: INTRODUCTION

To date, there are more than 600 CNS disorders. These vary from the most common neurodegenerative diseases (mostly found in the elderly population; Alzheimer's, Parkinson's and Huntington's) to cerebrovascular strokes and neuro-infections (herpes encephalitis, acquired immunodeficiency syndrome) (Mc Carthy *et al.*, 2015). Such diseases have a poor prognosis and a likelihood of degeneration of the affected CNS area. Subsequently, this causes a loss in cognition with significant implications to patient morbidity and mortality (Cordell *et al*., 2013; Kowal *et al*., 2013; Olsesen *et al*., 2012). The number of patients suffering from neurodegenerative diseases significantly outweighs those associated with systemic cancers and cardiovascular diseases (Chen and Liu, 2012), hence the economic significance of CNS disorders and infections is enormous. In 2010, the global economic impact of neurodegenerative diseases alone was more than 600 billion USD with an estimated 35.6 million suffering from Alzheimer's associated dementia. Additionally, over a billion people have suffered from a CNS infection at any given point (WHO, 2012). Alarmingly, there has been an upturn in CNS infections due to (1) the emergence of MDR strains and (2) the stagnation in the development of novel antibiotics (Wallace, 2007). Hence, the last line of defence; large hydrophilic drugs colistin has had frequent use for CNS infections (Dai *et al*., 2013). Given the considerable economic impact of CNS diseases and infections, significant research efforts currently focus on the development of novel and improved therapeutics. However, the application of novel- even traditional- therapeutics is however, highly limited by the delicate ecosystem of the BBB (Tian *et al*., 2012).

The high impedance system established by the BBB selectively excludes most conventional therapeutics. Therefore, only lipophilic drugs with a molecular weight (Mwt) between 300 and 500 Daltons (Da) can cross in therapeutically significant doses. Essentially, 98% of small molecules, as well as large molecule drugs such as recombinant proteins, monoclonal antibodies and peptides are impenetrable to the BBB (Masserini, 2013; Busquets *et al.*, 2015). The BBB is a selectively permeable component of the neurovascular unit (NVU) made up of a monolayer of specialized endothelial cells lining the cerebral micro-vessel walls (Cardoso *et al*., 2010). Inherently, it has organized cell types whose structural components synergistically function to establish the tautness across the monolayer (Hawkins *et al*., 2005). This maintains the homeostatic environment required for optimal neuronal synapsing. There are three main cell types; endothelial cells, pericytes and astrocytes (Zlokovic, 2008). Adjacent endothelia are

connected by transmembranous proteins, tight junctions (TJs), which span the inter-endothelial space. TJs have a gate-function which impedes paracellular flux thus forcing substances to opt for a transcellular route (Wolburg *et al*., 1994). The endothelia have a plethora of specialized receptors transport mechanisms to support the transcellular movement. These mechanisms include carrier-mediated transport (CMT), receptor-mediated transcytosis (RMT), as well as other pathways like adsorptive endocytosis (AE) (Fu, 2012).

In this right the BBB, although physiologically necessary, is a therapeutic challenge. Enhanced drug delivery methods such as mechanical perturbation using hypertonic and non-electrolyte solutions for (transient vasoactive opening of TJ), and focused ultrasound (FUS), (intravenous injection of gas bubbles enhanced with focus ultrasound) are used to overcome the BBB (Martinho, 2011; Shetab and Lamprecht, 2015). Given the intricate functioning of BBB as an anatomic, metabolic and physiological barrier, such techniques are invasive and bare significant surgical and post-surgical complications (nosocomial infections and patient morbidity) (Malhotra and Prakash, 2011).

NPs have gained significant consideration as a proposed mechanism of (enhanced) drug delivery. NPs have improved drug kinetics and delivery of chemically diverse therapeutics (Martinho, 2011; Kulkarn *et al*., 2013). NPs are colloidal systems between 1 to 1000 nm with unique physical and chemical properties due to their high surface area and nanoscale size (Shetab and Lamprecht, 2015). They have the ability to carry therapeutic agents (drug, gene, protein, vaccine) through surface adsorption, encapsulation or electrostatic attachment (Gao and Jiang, 2006). Polymeric NPs have shown to be chemically stable, able to encapsulate diverse therapeutic agents, have controlled drug release kinetics as well as having surface modification abilities for cell-specific targeting (Masserini, 2013). However, the theoretical abilities of polymeric NPs may not necessarily translate to a biological environment. For example, Polysorbate-8- functionalized poly (butyl cyanoacrylate) (PBCA) NPs have successfully delivered endorphins across the BBB through LDL-mediated-receptor entry. However, the use of PBCA has been limited due to its toxicity (Honary and Zahir, 2013a). A noteworthy polymer is chitosan (CS), a linear polysaccharide obtained from the deacetylation of chitin. CS is composed of alternating units of glucosamine to N-acetyl glucosamine groups linked together by glycosidic bonds (Morris *et al*., 2009). The biocompatible nature of CS is denoted by its structural resemblance to the mammalian glycosaminoglycans (GAGs) - a group of heteropolysaccharides residing on cell surface membranes (Griffon *et al*., 2006). Other

unique physicochemical properties include a variety of functional groups, especially the free amino groups that can be protonated at low pH to ionically cross-link with multivalent anions like dextran (DS) (Abbas, 2010). DS is an anhydroglucose polysaccharide consisting of a high concentration of glucose molecules formed in chains of varying lengths. Respectively, each polymer has biomedical applications such as tissue engineering, non-viral gene delivery and enzyme immobilization due to their biocompatible and biodegradable nature (Goycoolea *et al.*, 2007).

It is possible that biocompatibility differs according to the intrinsic properties of CS and DS (i.e. Mwt) as well as cell types and experimental conditions. Some studies have shown that, in solution, CS tends to increase paracellular permeability by opening TJs across epithelial membranes (Vllasaliu *et al*., 2010). This could potentially cause sub-lethal toxicity, especially when applied to a highly regulated and specialized interface such as BBB. Toxicity and immune-modulation are two significant consequences following NP uptake by cells. NPs have the proclivity to dissolve due to the acidity of cellular lysosomes, therefore contributing to toxicity (Saptarshi *et al*., 2013). Moreover, the physicochemical properties of NPs influence their reactivity *in vivo*, specifically the way in which they bind proteins (Ehrenberg *et al*., 2009; Fischer and Chan, 2007; Lynch and Dawson, 2008). This, in turn, influences NP cellular interactions. Studies have shown that negatively charged poly (acrylic acid)-conjugated gold NPs bound fibrinogen from blood plasma resulting in unfolding. Subsequently, this activated the receptor Mac-1 (macrophage-1 antigen-complement receptor) on THP-1 cells (human monocytic cell line), resulting in inflammatory cytokines release through the NF-κB pathway (nuclear factor kappa-light-chain-enhancer of activated B cells) (Deng et al., 2001). Unlike other organs, the brain has limited regenerative capacity (Hawkins *et al*., 2005). NP formulations targeting the brain should, therefore, be assessed for toxicity, especially considering the cationic nature of CS-based formulations (Elnaggar *et al*., 2015).

It is clear that there is a need to design and characterize non-invasive drug delivery systems that are capable of encapsulating chemically active therapeutics for the treatment of CNS infections. Owing to the significant and complex role of the BBB on CNS functioning, the befitting NP would have to be biodegradable, biocompatible, non-toxic, non-immunogenic and stable in a biological environment. Although they are a new design in polymeric NPs, CS-DS NPs have shown abilities in encapsulating hydrophilic biologically active molecules whilst maintaining structural integrity (Goycoolea *et al.*, 2007; Mahmoud *et al*., 2010). Therefore, the

aim of this study was to characterize CS-DS NPs as a drug delivery system according to their physicochemical properties; hydrodynamic diameter, dispersity index, zeta potential (ζ-potential) and encapsulation efficiency (EE%). As well as biocompatibility with the BBB measured as physiological parameters; cytotoxicity, permeability and topographical localization.

CHAPTER TWO: LITERATURE REVIEW

2.1 An overview of the blood-brain barrier

Blood supply to the mammalian brain is achieved through vasculature that structurally and functionally differs from the peripheral. One such structure is the BBB which is a selectively permeable constituent of the NVU (Figure 2.1) (Muoio *et al*., 2014). Primarily, it comprises of a monolayer of specialized brain microvascular endothelial cells (BMECs) which form the circumference of cerebral micro-vessel walls (Nag, 2003; Cardoso *et al*., 2010; Masserini *et al*, 2013). Anatomically, opposing BMECs are linked by interconnected transmembranous junctional complexes; TJs and adherence junctions (AJs) that limit paracellular flux (Ballabh *et al*., 2004). BMECs and pericytes are enclosed by a basement membrane (BM), a 30-40 nm membrane that contains a complex of extracellular matrix proteins. The BM, in turn, is continuous with astrocyte end-feet processes which are associated with cerebral vessel membrane (Hawkins *et al*., 2005). A noteworthy characteristic of the BBB is its' large total surface area-which is attributed to endothelial cells covering approximately 100 billion branched vascular capillaries (Muoio *et al*., 2014). Endothelial coverage ensures that there is a short diffusion distance (20 µm) between capillaries and the underlying neuronal structures (Fu, 2012; Nagpal *et al*., 2013) thus each neuron is perfused by its own capillary allowing efficient nutrient supply to the brain (Rodriguez-Baeza *et al*., 2003).

The BBBs dynamic interface effectively demarcates the peripheral circulatory system from the CNS (Wolburg *et al*., 1994; Cardoso *et al*., 2010). In doing so, a border which allows for the discriminatory exchange of compounds between the blood and the brain is established. Simply, the BBB allows for the transcellular permeation of nutrients such as glucose and amino acids to the brain, as well as, the elimination of metabolic wastes from the CNS (Nagpal *et al*., 2013). The duality of this system effectively and efficiently protects the neuronal microenvironment from endogenous and exogenous neurotoxins, chemicals and infections thus maintaining homeostasis (Mikitsh and Chacko, 2014 ; Mc Carthy *et al*., 2015). This is important as 'normal' neuronal functioning is highly determined by the neuronal microenvironment; where the concentration of ions such as sodium, potassium and calcium must be retained within very narrow ranges (Chen and Liu, 2012; Masserini *et al*., 2013; Muoio *et al*., 2014).

Fluctuations in ionic concentration within the extracellular space alter neuronal reversal potentials and firing patterns. Hence, there is an association between ionic concentration and

pathological conditions such as hypoxia, anoxia, ischaemia, epilepsy and spreading depression (Jensen and Yaari, 1997). Studies showed that perfusion of rat hippocampal slices with high potassium saline encouraged transient bursts in neuronal action potential firing. The bursts were initiated at the Cornu Ammonis 1 (CA) (a subsection of the hippocampus proper) at 0.5–1 Hz and propagated deeper into CA1 regions. In 42% of the slices, the transient burst effects excelled to sustained ictal episodes with tonic and clonic features every (0.5–2 seconds) (Jensen and Yaari, 1997). Boosts in hippocampal ictal activity have also been shown in other studies using saline deficient in calcium (Haas and Jefferys, 1984; Heinemann *et al*. 1986), magnesium (Anderson *et al*., 1986) and potassium (Traynelis and Dingledine, 1988). Considering the imperative role of the CNS on human physiology, it is essential that the interface between the CNS and the peripheral system is met by a stringent structure as BBB disruption can compromise CNS functioning (Ballabh *et al*., 2004).

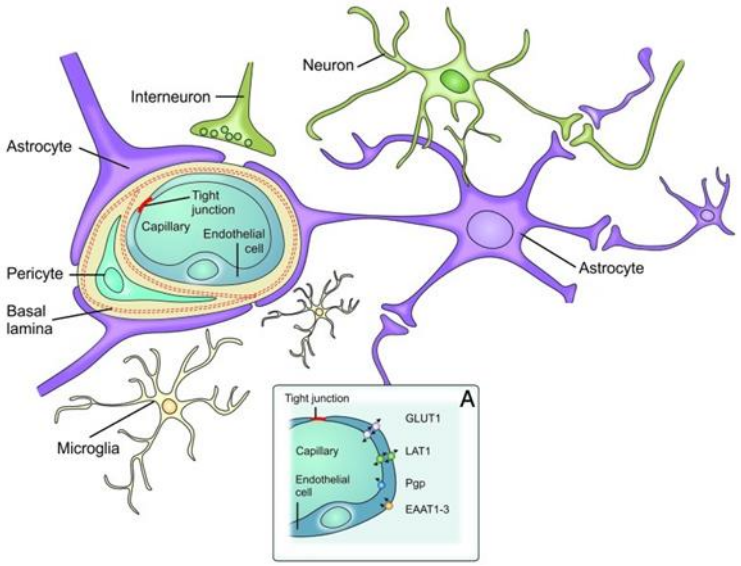

Figure 2.1 Schematic diagram representing (A) The BBB as a component of the NVU (refer to section 2.2). The circumference of the capillary lumen is lined by a single of specialized BMECs connected by TJ. The Pericytes are connected to the endothelia (at the abluminal surface) forming continuous BM with astrocyte end-feet processes connected to BM through the plasma membrane (Feustel *et al*., 2012).

2.2 The NVU: Origin and composition

The BBB is enforced by an amalgamation of cells types whose structural components and intricate interactions function to form the NVU (Figure 2.2) (Hawkins and Davis, 2005). The NVU comprises four main cell types: endothelia, pericytes, astrocytes and neurons all interacting with an extracellular matrix (Begley *et al*., 2004; Zlokovic *et al*., 2008). The intimate relationship between the cell types is a result of neuronal and vasculature coupling-brought about by a cascade of genetically programmed events during embryogenesis (Shima and Mailhos, 2000.). During this period, juxtaposition occurs between the neuronal progenitor cells (stemming from the neural tube) and vascular progenitor cells (stemming from the neural crest) which is then stimulated by endothelial growth factor (VEGF) and nerve growth factor (NGF) (Bagnard *et al*., 2001). Hence, during the period of embryonic vascularization of the brain, the formation of the BBB occurs alongside the development of cerebral blood vessels. The establishment of a fibronectin-rich extracellular matrix initiates the migration and proliferation of the endothelia thus forming a BM. The progression of embryonic development allows for a deep anatomical and chemical connection between these two components. This denotes the formation of phenotypically defined cell types with anatomical and functional interactions (Bagnard *et al*., 2001; Muoio *et al*., 2014). Over the last few decades, it has been shown that there is significant intercellular communication between neurons, non-neuronal supporting cells and the vasculature. This signifies the collective role of each cell type in overall functioning, hence the BBB is a module in a greater context of the NVU (McConnell *et al*., 2017). Here we describe the individual functional components of the NVU; the endothelia, TJs, astrocytes and pericytes.

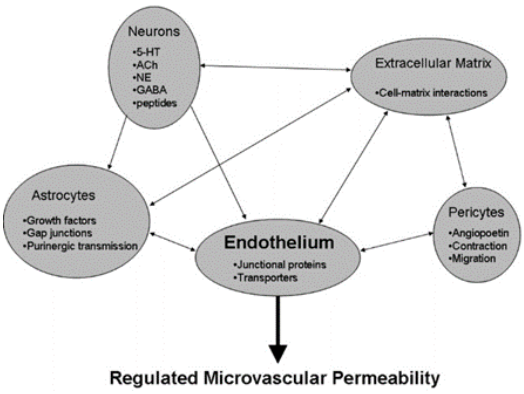

Figure 2.2 illustration showing examples of the various components of the NVU unit contribute to the dynamic regulation of BBB and vasculature properties (Hawkins and Davis, 2005).

2.2.1 Brain microvascular endothelial cells; anatomy, function and extracellular matrix

2.2.1.1 Anatomical consideration and function of the endothelia

The endothelia are the core structural unit of the BBB. They have anatomical nonconformities in comparison to peripheral endothelia in order to support specialized functioning (Figure 2.3). Salient features include tauter tight junctions, thickness, and lack of fenestra with significantly less pinocytic vesicles (Nagpal *et al*., 2013). Moreover, they have a higher expression of γ glutamyl-transpeptidase (γ-GT), monoamine oxidase (MAO) and alkaline phosphatase (AP) enzymes (Ballabh *et al*., 2004; Zeng, 2012) with a greater fraction of mitochondria (which maintains the metabolic pumps that maintain solute concentrations across the BBB) (Ueno *et al*., 2004: Zeng, 2012). The endothelia play a crucial role in the bi-directional movement of solutes across the BBB (Nag, 2003) as well as receptor-mediated signalling, leukocyte trafficking, and osmoregulation (Baeten and Akassoglou, 2011). Membrane transporters include glucose transporter (GLUT-1) on the luminal compartment and sodium and potassium adenosine triphosphate transporter (ATPase) associated with the abluminal compartment. Another barrier property is the formation of an endothelial enzymatic barrier responsible for metabolizing pharmaceutical agents, nutrients and neuroactive blood-borne solutes. These enzymes include γ-GTP, AP, and aromatic acid decarboxylase (Fu *et al*., 2012; Pardridge, 2012; Nagpal *et al*., 2013; Singh *et al*., 2013).

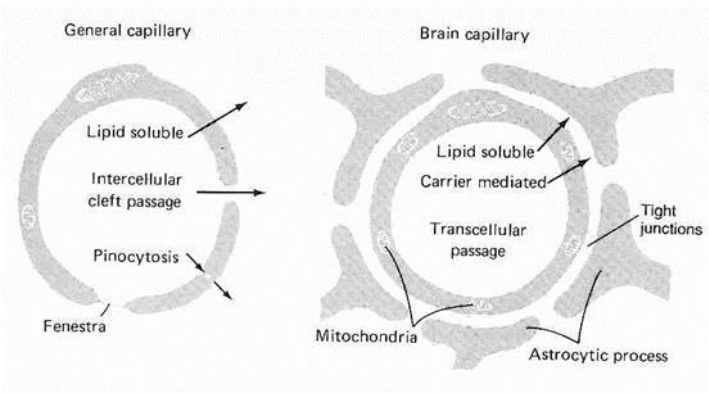

Figure 2.3 Schematic diagram showing the anatomical differentiation between peripheral (general capillary) versus brain capillary (Muoio *et al*., 2014).

2.2.1.2 The extracellular matrix: structural components and function

The production and preservation of the BM is a result of endothelia and astrocytes secreting extracellular matrix proteins. Such proteins include collagen type IV, heparan sulphate proteoglycans, laminin, fibronectin. The matrix functions to provide structural rigidity (Fu, 2012; Pardridge, 2005) as well as provide endothelia spatial orientation by forming the apical (luminal) and basolateral (abluminal) membrane. The apical membrane refers to the side facing the lumen-associated with the endothelia and pericytes (Cardoso *et al*., 2010). The basolateral membrane refers to the endothelial compartment facing the neuronal tissue- mainly consisting of astrocyte end-feet processes attached to the membrane (Pardridge, 2012).

The matrix itself has two main receptors/adhesion proteins, dystroglycan and integrins. These are fundamental in cell-to-cell and cell-to-matrix interactions of the BBB (Baeten and Akassoglou, 2011). Dystroglycan contains a glycosylated extracellular alpha subunit and a transmembrane beta subunit (Hynes *et al*., 2002; Zaccaria *et al*., 2001). Integrins stem from a class of transmembrane glycoprotein heterodimers of alpha and beta chains (Hynes *et al*., 2002). Typically, integrins associate with several endothelia ligands and activate a wide range of signalling pathways (Engelhardt and Sorokin, 2009; Baeten and Akassoglou, 2011). These signalling pathways regulate cellular proliferation, differentiation and migration thus support cell adaptation to microenvironment variations. Moreover, the physical arrangement of these proteins contributes to the physical connection between the endothelia and the cytoskeleton. This fastens the cells in place thus conferring structural rigidity as well as motility (Zaccaria *et al*., 2001; Jensen and Yaari, 1997).

2.2.2 Tight junctions

Between adjacent endothelial cells lie intricate interconnected junctional complexes; TJ and AJ (Figure 2.4 and 2.5) (Liu *et al*., 2012). AJ comprise calcium-dependent cadherin proteins that form extracellular domains between adjacent endothelial cells. The cytoplasmic regions of cadherins are conjugated to beta and gamma catenins (intermediary proteins) which are conglomerated to alpha catenins. Alpha-catenins interact with cytoskeletal actin, where actin interactions are suggested to influence TJ assembly and structural stabilization (Ballabh *et al*., 2003, Matter *et al*., 2003). Although the presence AJs contributes to the tautness of the BBB, it is primarily the TJ that confers high transendothelial resistance (1800 Ω cm2) and thus low permeability (Butt *et al*., 1990; McConnell *et al*., 2017). TJs have three integral membrane proteins namely the claudins, occludins, and junctional adhesion molecules (JAMs). The cytoplasmic accessory protein structural components are Zona occludin-1 (ZO-1), Zona occludin-2 (ZO-2) and Zona occludin-3 (ZO-3) with cingulin and other proteins (Ballabh *et al*., 2004; Abbott *et al*., 2006). Collectively, the structures of the tight junctions establish a paracellular diffusion barrier. This mediates the permeation of substances into brain microenvironment based on their physical-chemical configuration (polar, lipophilic, ionization nature of blood-borne substances) (Jouyban *et al*., 2012).

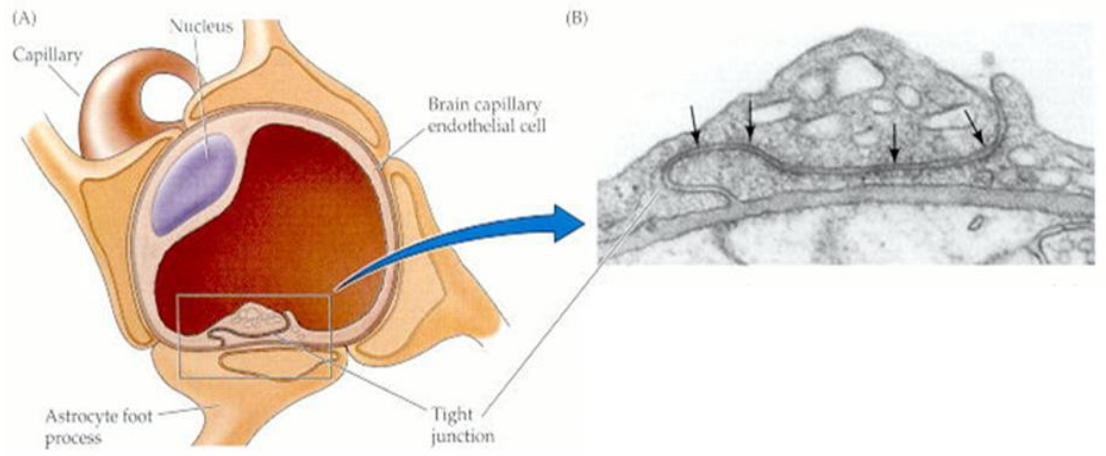

Figure 2.4 Schematic diagram of (A) brain capillary in cross section and showing endothelial TJ and the support of the capillary by astrocytic end feet processes. (B) Electron micrograph of the boxed area showing the appearance of tight junctions between neighbouring endothelial cells (arrows) ((A) Goldstein *et al*., 1986; (B) Peters *et al*., 1991).

2.2.2.1 Integral membrane proteins: claudins, occludins,

Claudins belong to a family of 24 proteins that entail 20-24 kDa phosphoproteins all expressing four trans-membranous domains (two extracellular loops and carboxyl intracellularly located end tail) (Figure 2.5) (Morita *et al*., 1999). Claudin extracellular loops bind homotypically to protruding extracellular loops of adjacent endothelial cells thus forming the primary seal of tight junctions (Ballabh *et al*., 2003; Abbott *et al*., 2006). Brain endothelial cells typically express Claudin-1, -2, -3, -5, -11, and -12, with a high expression of claudin-3 and claudin-5 (Luissint *et al*., 2012; Liu *et al*., 2012). The occludins, however, are significantly larger than claudins, they comprise 60 kDa phosphoproteins also with four trans-membranous loops (two extracellular loops, a short NH2 and a longer COOH-terminal cytoplasmic domain), the amino acid sequencing of the integral membrane proteins is heterogeneous to each other (Tsukita and Furuse, 1999; Hawkins and Davis, 2005; Abbott *et al*., 2006; Liu *et al*., 2012,). Both cytoplasmic terminal components of claudins and occludins are stabilized to zona occludins (ZO) at a specific region, where claudin terminals link directly to PDZ1 domains (Protein interaction domains (approximately 70-90 amino acid residues), named after a common structure found in PSD-95, Discs Large, and Zona Occludens 1 proteins) of ZO1 to 3 and the occludin terminals interrelate with guanylate kinase (GUK) domains of ZO-1 (Luissint *et al*., 2012). Subsequent interactions of zona occludins with primary cytoskeletal actin protein infer the structural support of the integral membrane proteins to endothelial cells thus maintaining the functional integrity and the tautness of the BBB (Abbott *et al*., 2006). Furthermore, it has been suggested that the ZOs are vital in the assembly of claudin proteins (Luissint *et al*., 2012). The heteropolymer formation of occludin and claudin extracellular loops interconnections have been proposed to possess oscillating channels that facilitate the movement of hydrophilic molecules across the paracellular junction. The high impedance of charge molecules, in turn, establishes a high electrical resistance across the BBB (Abbott *et al*., 2006).

2.2.2.2 Junction adhesion molecules

The third member of the integral membrane proteins is the intermediate size, Mwt of 40 kDa JAM's (Abbott *et al*., 2006). JAM's have extracellular segment with two immunoglobulin loops that are conjoined via disulfide bonds, a singular transmembrane component and an intracellular tail (Figure 2.5) (Liu *et al*., 2012). JAM's form part of the immunoglobulin family and facilitate in transmigration of monocytes through the BBB alongside the adhesion of adjacent endothelial cells (Martin-Padura *et al*., 1999).

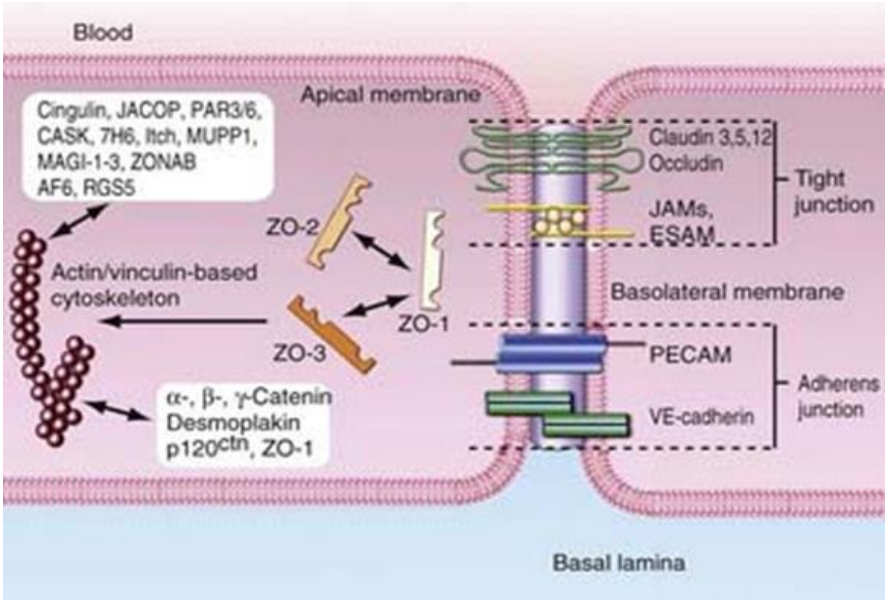

Figure 2.5 Schematic diagram of TJ between adjacent endothelial cells. Claudins make up the backbone of the tight junction strands and bind homotypically to claudins on adjacent cells to produce the primary seal of the TJ. Occludin functions as a dynamic regulatory protein which is associated with increased transendothelial electrical resistance and decreased paracellular permeability. JAMs are associated with platelet endothelial cell adhesion molecule-1 (PECAM), regulate leukocyte migration across the BBB. Several accessory proteins also contribute to its structural support, such as zona occludins-1 (ZO-1) to ZO-3, cingulin, and 7H6. AJs are located near the basolateral side of the endothelial cells (Abbot et al., 2006)

2.2.3 Astrocytes

Astrocytes are glial cells (non-neuronal cells) that physically, metabolically and biochemically support the CNS by inducing and maintaining the unique characteristics of the BBB. Anatomically, they are star-shaped, branched heterogeneous cells ubiquitously disseminated throughout the neuronal vasculature (Figure 2.6) (Agulhon *et al*., 2008). Neighbouring astrocytes touch through gap junctions (which confers long-range signaling), individual astrocytes are medial to neurons and endothelia but extend their end-feet processes to the wrap the surface of the cerebral blood vessels (Baeten and Akassoglou, 2011; Nagy and Rash, 2003). Hence, the end-feet cover approximately 98% of the abluminal compartment (Filosa *et al*., 2016; Sosunov *et al*., 2014). The anatomical consideration of the astrocytes within the NVU promotes responses to synaptic activity and neuronal metabolism by maintaining an equilibrium of fluids, electrolytes, amino acids and neurotransmitters through the expression of water-protein channel aquaporin 4 and the potassium channel, Kir4.1 (Wolburg *et al*., 1994; Ballabh *et al*., 2004; Hawkins *et al*, 2005; Muoio *et al*., 2014). This is rudimentary to maintaining the homeostatic environment required for optimal neuronal functioning. (Rubin and Staddon, 1999).

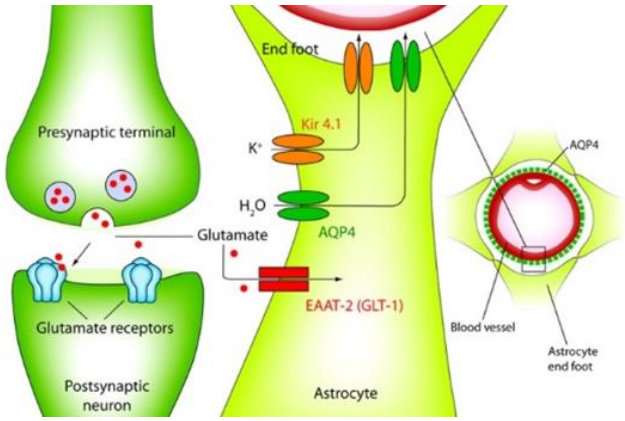

Figure 2.6 Schematic diagram showing the role of astrocytes in the NVU, the astrocyte end-feet reach to wrap the cerebral blood vessels. They also express water protein channel aquaporin 4 and the potassium channel, Kir4.1 that function in homeostatic regulation (Chen and Liu, 2012).

2.2.4 Pericytes

Pericytes are mural cells localized within BM. Their assimilation confers the structural support and 'vasodynamic capacity' of microvasculature (Lindahl *et al*., 1997). The main role of pericytes is angiogenesis and subsequent differentiation of endothelial cells. In addition, pericytes play a role in the maintenance of the structural integrity of the microvessels Also,

they express receptors for mediators such as catecholamine's, endothelial-1, vasoactive intestinal peptides and vasopressin for cerebral auto-regulation (Ballabh *et al*., 2003).

2.3 Transportation across the BBB

2.3.1 Mathematical model for solute flow

Synergistically the structural components of the BBB confer its rate-barrier properties, in this respect, the BBB is the epitome of a dynamic, multifunctioning physiological interface. Firstly, as a physical barrier, it limits paracellular movement of proteins and water-substances across the membrane. Secondly, as a transportation barrier, it modulates nutrient supply and waste removal to the brain through specific transport systems. This house-keeping effect ensures the retention of ionic concentrations (sodium, potassium, and calcium) within narrow ranges required for neuronal signalling. (Ballabh *et al*., 2003; Abbott *et al*., 2005). Lastly, as a metabolic barrier, it contains enzymes that metabolize ATP and neuro-active compounds. This mediates the exposure of the CNS to neuro-active hormones (i.e. glutamate, glycine, norepinephrine, and epinephrine) which can increase with physiological changes (e.g., diet and stress) and pathological changes (e.g., injury and diseases) (Pardridge, 1998).

Mathematically, the membrane transport properties of the BBB can be defined by the Kedem-Katchalsky equation which is derived from the theory of irreversible thermodynamics (Curry *et al*., 1986):

$$Jv = Lp\ (\Delta p - \sigma d\ RT\Delta C)$$

$$Js = PRT\Delta C + \bar{c}\ (1 - \sigma f)\ Jv$$

Js and Jv represent solute and volumetric flux respectively. ΔC and Δp denotes the concentration and pressure differences respectively. The hydraulic conductivity is described by Lp which accounts for the membrane permeability to water. P describes the permeability to solutes. The two coefficients represented in this mathematical model are: the reflection coefficient, σd, which pertains to the selectivity of the membrane to molecules. As well as, σf solvent drag, for the constraint of molecules due to membrane restriction (Fu, 2012).

However, the Kedem-Katchalsky equation only accounts for the volume flow Jv and the solute flow Js for non-electrolytes across the membrane. The selectively permeable nature of the BBB is also due to intrinsic solute properties such as Mwt, lipid solubility, and electrical charge in conjunction with membrane transport pathways (Squire *et al*., 200; Ueno *et al*., 2004).

2.3.2 Influx mechanisms

2.3.2.1 Passive transportation: passage of small molecules into the brain parenchyma with consideration to Lipinski's "rule of 5"

Naturally, small lipid-soluble molecules (gasses: oxygen and carbon dioxide, and alcohol) have free transmembranous diffusion along their concentration gradients across the BBB (Ballabh *et al*., 2003). The notion of passive diffusion is underlined by Lipinski's "rule of five" which is supported by experimental and computational Quantitative Structure-Activity Relationship (QSAR) equations (in silico approach for CNS active drugs alongside their analogues established throughout 1988) (Ma *et al*., 2005; Mikitsh and Chacko, 2014).

Lipinski's "rule of five" correlates the permeability of the BBB to Mwt, lipophilicity (Log P), polar surface area, hydrogen bonding and charge (Lipinski *et al*., 1997). In order for free diffusion to occur small molecules or drugs must have no more than 5 hydrogen-bond donors (expressed as the sum of OHs and NHs), 10 H-bond acceptors (expressed as the sum of Ns and Os), the calculated log P (clogP) (Nagpal *et al*., 2013) must be greater than 5 (or MlogP > 4.15) (Pajouhesh and Lenz, 2005; Pardridge, 2012) and Mwt threshold of 500 Da (Misra *et al*., 2003).

The transport of drugs across the BBB based on Mwt was one of the first parameters to be well established. Work by Fischer *et al* (1998) to physiochemically classify 53 clinically significant compounds demonstrated the correlation between Mwt and BBB permeation. It was shown that BBB permeation decreased 100-fold when the size of the drug increased from 300 Da to 450 Da. It is thought that the Mwt threshold results from finite, temporary pores being formed within the phospholipid bilayer due to free fatty acyl side-chain links of the solute. Molecules or lipophilic drugs that supersede this small-sized pores therefore cannot cross the BBB (Pardridge, 2005; Nagpal *et al*., 2013; Singh *et al*., 2013). Interestingly, almost all CNS drugs currently in clinical practice are lipid-soluble small molecules with a Mwt no greater than 400 Da. Based on Lipinski premise, theoretically, these drugs should be able to 'freely' permeate the BBB. However, the Comprehensive Medicinal Chemistry database shows that of 6,000 CNS drugs only 6% are practically applicable (Lipinski *et al*., 2000).

Another key parameter for BBB permeation is Log P. In order for a small molecule to permeate the hydrophobic phospholipid bilayer by passive diffusion, it has to be lipophilic (Sangster, 1989; Mikitsh *et al*., 2014). The relationship between lipophilicity and permeability is thought to be linear; the greater the log P value, the higher the permeability. The log P value for most CNS drugs is between −0.05 and 6.0 (Begley *et al*., 2004). However, the optimum range for

BBB permeability has been found to be 1.5–2.5 (Misra *et al*., 2003). A classic example of the relationship between log P and BBB drug permeability is morphine, codeine, and heroin. Changing the 3-hydroxy moiety of morphine to methoxy to form codeine, increases the log P from 0.99 to 1.2, respectively. The acetylation of 3- and 6-hydroxy groups of morphine results in heroin with a log P value of 2.3. Studies showed that, in relation to their permeability, increasing the log P, resulted in a 100-fold increase in their relative rate of brain uptake index from 10% to 30% to 70%, respectively (Oldendorf *et al*., 1972).

The dependency of free diffusion is also attributed to the octanol/water partition coefficient of a solute. Initially, the quantification of the partition coefficient (between n-octanol and water) is rudimentary in ascertaining log P (Levin, 1980; Sangster, 1989; Sawchuk and Elmquist, 2000). Presently there are a variety of readily available computational procedures that have been set for extrapolation of log P (Tute *et al*., 1990; Halnes *et al*., 2016). Nevertheless, a static depiction of partition coefficient is true when comparing drugs such as diphenhydramine and loratadine. Diphenhydramine has a relatively high partition coefficient and thus easily crosses the BBB, whereas water-soluble claritin has a lower value and therefore does not have free diffusion into the CNS (Kay *et al*., 2000). However, now it is thought that the octanol/water partition coefficient is not a true representation of BBB permeability to solutes (Pajouhesh and Lenz, 2005). The BBB permeation can essentially be enhanced by merging the octanol-water partition coefficient with Mwt and the number of H-bond acceptors and donors. In practice, however, most drugs are excluded by the cut off rules (singular or in combination) presented by Lipinski rule for small molecules (Nagpal *et al*., 2013).

2.3.2.2 Facilitated transportation of molecules across the BBB

In contrast to free diffusion, BBB flux of molecules can be facilitated by a more active route. This type of transportation is governed by carrier-mediated transport (CMT), receptor-mediated transcytosis (RMT) and adsorptive endocytosis (AE) (Figure 2.7) (Ballabh *et al*., 2004; Pardridge, 2005).

CMT is an energy independent method for small hydrophilic molecules to enter the BBB within milliseconds. It entails pore formation by the transmembrane domains of transporter proteins in response to respective complementary molecules (such as hexoses, amino acids, nucleoside, and vitamins) (Malhotra and Prakash, 2011; Umut, 2013). An estimated 20 CMT-proteins have been categorized on both the luminal and abluminal compartment of the endothelia. (Abbott *et al*., 2006; Hawkins *et al*., 2006). For example, transporters involved in nutrient supply to the brain include the L-system for (1) neutral amino acids, i.e. L-phenylalanine, encoded by the SLC7A5 gene (solute carrier family) and (2) basic amino acids, i.e. L-arginine, encoded by the SLC7A1 gene (Nag, 2003; Pardridge, 2012). The kinetics of substrate permeability across a transporter is determined by the endothelial permeability surface area. Characterization of CMT typically pertains to substrate affinity, saturability, selectivity and stereoselectivity. The most notable is saturability which is the maximal transport capacity (represented by Vmax) as well as substrate affinity (represented by Km) (Nag, 2003).

Generally, molecules are selectively taken up according to the capacity and frequency of the complement transporter according to the functional requirements of the CNS. For example, there is an overexpression of the hexose uniporter GLUT1 in order to meet the high metabolic demands of the CNS. GLUT1 is a gene product of *SLC2A1* for d-glucose, 2-deoxy-d-glucose, mannose, and galactose substrates and represents more than 90% of all the BBB glucose transporters (6×10^6 molecules per brain endothelial cell) (Tsuji and Tamai, 1999). Although ubiquitous, transportation of glucose molecules is still defined by certain intrinsic parameters. There is an inversely proportionate relationship between substrate affinity and transport capacity, as the substrate affinity increases, the transport capacity decreases (Pardridge, 2012). This has been well illustrated in literature; Km for most transporters GLUT1 is 11.000 ± 1.400 µM, MCT1 1.800 ± 600 µM, neutral amino acids 26 ± 6 µM and basic amino acids 40 ± 24 µM. The Vmax turnover number (per second) by a single transporter molecule was shown to be 600, 2300, 3000, 270 (respectively, for each receptor type) (Mikitsh *et al*., 2014). The outstanding performance of GLUT1 to substrate affinity, as well as its differential expression

on the luminal and abluminal compartments of the BBB attracted significant pharmaceutical interest for prodrug delivery. However, the conjugation of drug to glucose forming a prodrug shows poor BBB permeability due to prodrug size and a decrease in GLUT1 affinity (Pardridge, 2012). One such approach is the GLUT1-mediated transport of chlorambucil-glucose conjugate utilized in the treatment of chronic lymphocytic leukaemia (Halmos *et al*., 1996). Consequently, the clinical significance of GLUT1 properties has been left up for dispute (Cardoso *et al*., 2010; Wilhelm and Krizbai, 2014).

RMT is facilitated by luminal receptors where conformational changes occur due to ligand-receptor interaction with complement molecules (Busquets *et al*., 2015; Upadhyay, 2014). Subsequently, the formed complex is transported within endosomes/lysosomes or transcytosis across the cell interior and exocytosis from the abluminal surface of the capillary endothelium. This is inclusive of proteins such as transferrin, insulin and low-density lipoproteins (Nagpal *et al*., 2013).

Adsorptive endocytosis (AE) accounts for molecules such as albumin (cationized) and plasma proteins. The process relies on the electrostatic interaction between a positively charged substrate and the negatively charged plasma membrane (Abbott *et al*., 2006).

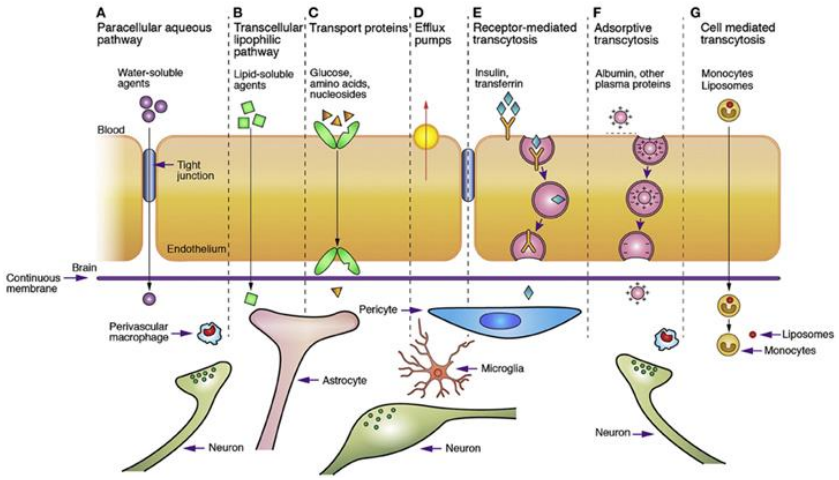

Figure 2.7 Transport routes across BBB. Pathways "a" involves paracellular movement across TJ, "b" to "f" are the typical transcellular routes for different types of solute molecules, "g" involves monocytes, macrophages and other immune cells (Ohtsuki and Terasaki, 2007).

2.3.3 Efflux mechanisms

Another functionality of BBB impendence that contributes to it being a therapeutic challenge is the presence of active efflux transporters. These transporters, establish a molecular barrier that expels xenobiotics (foreign substances such as drugs or drug metabolites) from the endothelia to the blood (Jouyban *et al*., 2012). Generally, the efflux transporters are characterized into families according to their molecular and functional similarities. ATP-binding cassette transporters (ABC transporters) are a family of P-glycoprotein (P-gp), multidrug resistance proteins (MDR) and multidrug resistance-associated proteins (MRP), which are expressed on the luminal compartment of the BBB (Pardridge, 2005; Gao and Jiang, 2006; McCarthy *et al*., 2015). Other members include organic cation transporters (OCT), organic anion transporters (OAT) and organic anion transporting polypeptide (OATP) (Nagpal *et al*., 2013). Mostly functionally, the MRP1, MRP2 and MRP4 are associated with anionic xenobiotics. The effect of transporters allows for the removal of neurotoxins, metabolic by-products and xenobiotic compounds from the brain interstitial fluid to the circulatory system (Figure 2.8) (Wilhelm and Krizbai, 2014). The most prominent of these transporters is P-gp which is encoded by the MDR1 gene in humans and MDR1a, MDR1b, and MDR2 isoforms in rodents. (Gao and Jiang, 2006: Neuwelt *et al*., 2011). P-gp is a 170 kDa transmembranous protein with two analogues embedded in the endothelial membrane. Specifically, it recognizes organic cations and uncharged xenobiotics as well as amphiphilic or lipophilic compounds with a molecular threshold of 300-2000 Da (Ma *et al*., 2005; Fu, 2012; Saunders *et al*., 2014). The clinical significance of P-gp properties denotes its recognition of opioids, steroids, antibiotics, immunosuppressant, chemotherapeutics, and anti-HIV drugs. Hence, over the last decade, a considerable amount of attention has been focused on the counter-therapeutic role of P-gp on CNS infections (Nau *et al*., 2010; Nagpal *et al*., 2013). Fellner *et al* (2002) showed that chemically knocking out P-gp (using P-gp specific inhibitor (PSC833)) in mice increased levels of chemotherapeutic paclitaxel within the brain parenchyma. This was also noted by a significant therapeutic effect on paclitaxel-susceptible, intracerebral implanted human glioblastomas. Notably, the study showed that the coupling of PSC833 with paclitaxel enhances the therapeutic outcome as decreased tumour volumes by 90%-whereas paclitaxel alone had no effect on tumour size. Consequently, P-gp prevents the accumulation of therapeutics into the cytoplasm of the endothelia. This accounts for most clinically significant therapeutics as P-gp has a high selectivity and recognition for a broad spectrum of substrates (Gao and Jiang, 2006; Saboktakin *et al*., 2011).

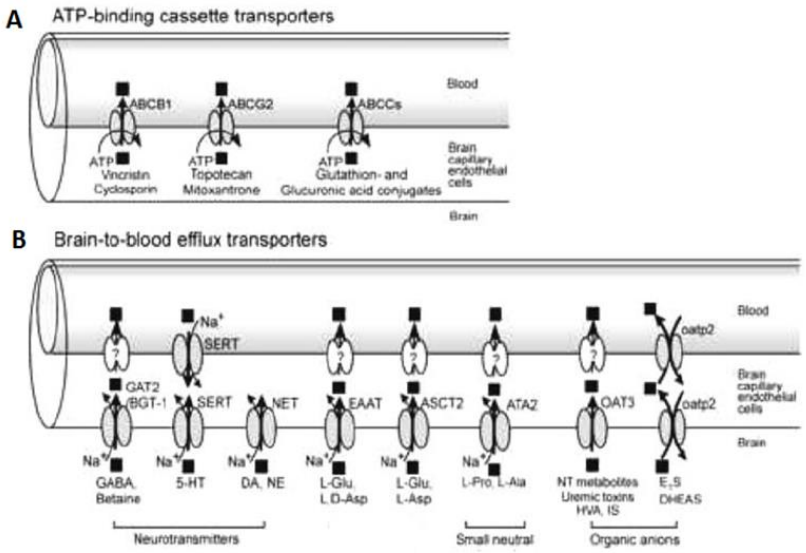

Figure 2.8 Schematic diagram of the efflux transporters present on the endothelia of the BBB with reference to (A) ABC transporters and (B) brain to blood transporters including OAT members (Chen and Liu, 2012).

2.4 Methods of overcoming the BBB

BBB involves an anatomic and biochemical complex that allows for wide range of cellular cross-talk (Ballabh *et al*., 2004; Salama *et al*., 2006). As a transport barrier, it controls nutrient supply and waste removal to and from the brain. As a metabolic barrier, it comprises enzymes that break down ATP and neuroactive compounds thus establishing a demarcation between central and peripheral pools of neurotransmitters (Abbott *et al*., 2006). Therefore, the BBB is neither an absolute barrier nor is it static (Carvey *et al*., 2009; Neuwelt *et al*., 2011). However, it has a rather dynamic structure that has continuous interactions with underlying cellular and extracellular components to establish a highly specialized structure that is essential to neuronal functioning (Baeten and Akassoglou, 2011).

Clinically significant drugs that are BBB permeable only include opiates (morphine and meperidine), anxiolytics (diazepam family) and antipsychotics (chlorpromazine). Unfortunately, this specificity only serves a select few of CNS disorders by excluding the majority of chemotherapeutic antibiotics and neurodegenerative therapeutics (Masserini, 2013; Busquets *et al*., 2015). In order to enhance drug permeation across the BBB, some approaches focus on targeting the plethora of luminal influx transporters on the endothelial cell membrane. In this case, only a few have been shown to achieve successful penetration of therapeutic compounds into the brain parenchyma (Aggarwal *et al*., 2009; Jain, 2012). The earliest and notorious is the therapeutic agent L-3,4-dihydroxyphenylalanine (L-DOPA) for the treatment of Parkinson's disease-although prolonged use associates with clinical limitations (Pardridge, 2005). Innovative strategies involve the targeting of endogenous RMT pathway in drug delivery systems. BBB impermeable substances would be conjugated to ligands or antibodies that activate the RMT pathway thereby effectively acting as a "molecular Trojan horse". In light of this numerous RMT have been elucidated for this function including insulin receptor, transferrin and low-density lipoprotein receptor. Studies have shown that monoclonal antibodies against transferrin successfully delivered gene constructs across the BBB. Whilst other studies suggest that only 1% substrate accumulation in the brain parenchyma when using insulin receptor occurs (Liu *et al*., 2012; Fu, 2012).

Low-density lipoprotein (LDL) receptors, on the other hand, have seen their way into Phase I clinical trials utilizing paclitaxel for recurring malignant gliomas. However, there have been reports of toxicities including neutropenia, fatigue and mucositis (Faraji and Wipft, 2009; Tian *et al*., 2012). Although ubiquitous, influx transporters have limited transport capacity into the

brain. Moreover, efflux transporters export most therapeutically significant drugs out of the brain. Thus, mechanical perturbation of the endothelial cells using reverse osmotic opening and focused ultrasound (FUS) becomes the likely option for drug delivery (Martinho, 2011; Shetab and Lamprecht, 2015).

2.4.1 Reverse osmotic opening

Reverse osmotic opening pertains to the use of hypertonic and non-electrolyte solutions to transiently open the BBB (mannitol, urea and arabinose). Initially, Brightman *et al* (1977) displayed the permeability of the BBB to horseradish peroxidase due to TJ opening. Rapoport *et al* (1980) showed that exposure to osmotic agents' increases brain water by 1.5. A surplus of animal and patient imaging techniques which facilitate discrete observations of TJ opening due to hypertonic solutions has been established (Williams *et al*., 1995; Neuwelt *et al*., 1991) Although osmotic agents display an array of TJ modulation mechanism, primarily, administration of electrolyte solution shrinks the endothelia by drawing water out of the cells and into the luminal interface (Salama *et al*., 2006) allowing for a therapeutic window of several hours (Rapoport and Robinson,1980). The overall movement of water into the lumen facilitates vasodilation hence stretching the endothelial cell membrane. Ultimately, the endothelial cytoskeleton contracts due to cadherin-actin interactions-which endorse TJ stress thus increasing paracellular permeability (Nag, 2003). Various agents have been used but the most common is mannitol (Bellavance *et al*., 2008; Blanchette *et al*., 2009). There is a debate about the effectiveness of this method due to non-selective opening of the BBB. Several animal model studies have shown non-selective opening of the BBB (Groothuis *et al*., 1990; Nakagawa *et al*., 1984; Zünkeler *et al*., 1996). However, there is a concern that this non-selectivity could cause widespread toxicity in the CNS (Kemper *et al*., 2004).

2.4.2. FUS

FUS is a combination approach that utilized intravenous injection of gas bubbles enhanced with focus ultrasound (Figure 2.9). Initially, FUS was eliminated largely due to beam distortion and attenuation during interaction with skull bone. However, FUS in combination with other technologies like gas bubbles as well as magnetic resonance (MR) thermometry has renowned its use (Nau *et al*., 2010). Currently, MR thermometry has seen its way to Phase I clinical trials in the treatment of Parkinson's disease. In these studies, it has been shown that the acoustic energy can be effectively intensified at a focal point with high spatial intensity and energy deposition. However, FUS also yielded mechanical effects including acoustic streaming and

cavitation (Masserini, 2013). Although the exact mechanism of action between the bubbles and ultrasound has not yet been fully elucidated, succeeding studies have assessed the safety of the procedure alongside its effects with varying anaesthetic agents and its practicability. Irrespectively so, FUS compared to the osmotic opening is a little less invasive, can be discretely directed to the tumour region and as of yet shows no evidence of post-surgical complications (apoptosis, disruption of cognitive dysfunction or ischaemia) (Martinho, 2011).

Primarily these techniques serve to enhance the access of therapeutic agents across the BBB by disrupting barrier properties thus endorsing paracellular influx. Be that as it may, this enhanced influx is non-discriminant thus allows for entry of potentially neurotoxic substances into the brain and more especially the techniques are largely invasive (Upadhyay, 2014). There are, however, alternative strategies that focus on completely by-passing the BBB all together, these include intraventricular and intrathecal routes intranasal and interstitial delivery via biodegradable wafers or convection-enhanced delivery-however most display limited usage (Nagpal *et al*., 2013).

Due to the imperative function of the BBB to the brain microvasculature, its presence demands innovative therapeutic methods for treatment of CNS diseases that are not only non-invasive but biocompatible (Jain, 2012). Given the ageing population and increasing occurrence of neurological disorders, the requirement for biocompatible CNS focused therapeutics will surely increase with time. The arena of drug delivery systems is then challenged to focus on potential therapeutic agents that protect barrier properties whilst minimizing CNS toxicity (Sarvaiya and Agrawal, 2015).

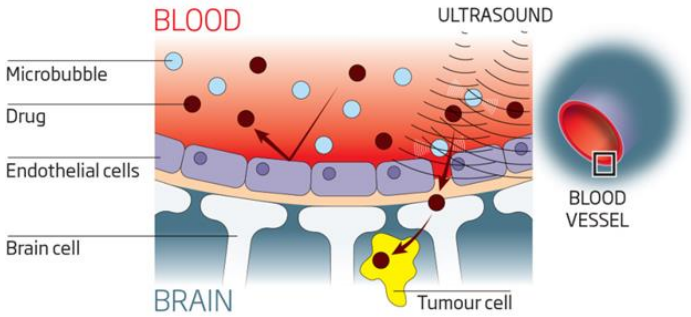

Figure 2.9 Schematic diagram showing microbubbles in combination with ultrasound waves opening the paracellular space between adjacent endothelial enabling drugs to cross the BBB (https://www.newscientist.com/article/mg22229742-400-human-brains-ultimate-barrier-to-open-for-first-time)

2.5 The issues of CNS diseases and their economic significance

Within the realm of neurological disorders, there are 600 estimated conditions. These have been sub-classed into neurodegenerative diseases (Alzheimer's, Parkinson's and Huntington's), cerebrovascular disorders (brain tumours and strokes), central nervous system infections and/or neuro-inflammation (Mc Carthy *et al*., 2015). The pathological outcome includes neurological degeneration of the affected area(s), a decline in cognition, morbidity and consequently mortality (National Institute of Neurological Disorders and Stroke (NINDS), 2012). An estimated 35.6 million people worldwide suffer from dementia, with Alzheimer's underlined as a predominant cause (60–70%of the cases) (Olesen *et al*., 2012). Not only do these pose a significant effect on patient's health but also have large global economic cost. Considering that over a billion people have suffered from a CNS infection, which is double the number of people with cardiovascular diseases, the market for CNS drugs is only half the size (70 billion vs. 33 billion USD, respectively) (Pardridge, 2002). For CNS infections, MDR infections account for over 27,000 deaths per annum with an economic impact of €1.5 billion in Europe (Olesen *et al*., 2012) and 14-22 billion USD in the USA per annum (Kowal *et al*., 2003). Alarmingly, this is projected to be 100 trillion USD by 2050, with staggering 10 million deaths per annum (Review on Antimicrobial Resistance, 2016). Besides the impedance effect of the BBB, difficulties in treating CNS infections are exacerbated by a continuous decline in the production of novel antimicrobials within the pharmaceutics industry (Wallace *et al*., 2010) as well as a lack of commercial investment incentives and public health requirements. The total venture capital investment in pharmaceutical research and development was 38 billion USD between 2003 and 2013, yet, only 5% was dedicated to antimicrobial development (Review on Antimicrobial Resistance, 2016). Is it possible that the investment in antimicrobial development may not be seen as profitable until widespread MDR has emerged? In the meantime, gram-negative infections are still underrepresented in antimicrobial development although they are a looming global health concern (Horton, 2009; Talbot, 2008). Evidently, CNS infections are now being treated using an old, last line of defence antibiotic (colistin) (Wallace *et al*., 2010). Even though efforts have been made to support 'early-stage and non-commercial research', i.e the Global Innovation Fund secured with 2 billion USD, drug candidates in the pipeline still face the challenge of acquiring clinically significant doses across the BBB (Review on Antimicrobial Resistance, 2016). Therefore, difficulties in treating CNS infections is a complex multifactorial process that has significant effects on the greater population.

2.5.1 Infections of the CNS

2.5.1.1 Susceptibility to CNS infections

The cause of CNS infections may vary; however, it is enhanced by CNS vulnerability due to BBB insult. Insult to the BBB is associated with a decline in its structural integrity thus impeding its natural barrier properties-which can favour the migration of pathogens into the CNS. Clinically significant scenarios include hypoxia-ischaemia, brain tumours, cerebral Human Immunodeficiency Virus (HIV) and those of idiopathic and iatrogenic nature (Cardoso *et al*., 2010; Muoio *et al*., 2014). Significantly, these are exacerbated by but not limited to age, immune status (HIV or immunosuppressant therapy) and epidemiological trends (Nau *et al*., 2010). Although each scenario pertains to its own pathology, the outcomes are still detrimental to the structural integrity of the BBB. Hypoxic-ischemia entails a cascade of events (mediated by VEGF and nitric oxide cytokines) that subsequent lead to TJ disruption thus increasing BBB permeability (Fu, 2012). In astrocytoma and metastatic adenocarcinoma (brain tumours), there is a downregulation of occludin proteins thus rendering the TJ vulnerable to permeation. Cerebral HIV involves leukocyte migration into the brain microvasculature thus disrupting occludin and zona occludin function (Ballabh *et al*., 2004). In iatrogenic, the insertion of ventriculoperitoneal shunts potentiates post-neurosurgical complications and nosocomial infections. The current estimated HIV prevalence in the South African population in 2017 was 12.7%, approximately 7.03 million. This suggests that an estimated 18.9% of the adult population between the ages of 15–49 is HIV positive. As it stands, neurocognitive complications account for 53% of neurological manifestations in HIV-positive patients- which a sizeable percentage is considering the progressing of HIV-AIDS epidemic in South Africa (Statistics South Africa, 2016). Therefore, there is a significantly large margin of South African individuals who are susceptible to opportunistic neurological infections.

2.5.1.2 Etiological agents responsible for CNS infections and treatment

The bacterial etiological agents responsible for acute CNS infections include Gram-negative bacilli groups; *Haemophilus influenzae, Neisseria meningitidis*, *Streptococcus pneumoniae* and *Listeria monocytogenes*. The clinical manifestation includes acute meningitis, encephalitis focal lesions (brain abscess and subdural empyema) and even spinal cord infections (Roy *et al*., 2014). The most common biological point of entry is through the nasopharyngeal region leading to colonization, systemic invasion, high-grade bacteremia and CNS invasion (Somand and Meurer, 2009).

Empiric therapy is usually the option of choice hence treatment is given based on a summation of clinically relevant symptoms the classical triad of symptoms (fever, neck stiffness, and altered mental status) (Karlowsky *et al*., 2002). Subsequent treatment is according to the patients' immune status either being immunocompromised or immunocompetent. In the former, patients suspected with *H.influenzae* or *N.meningitidis* are given cefepime or vancomycin. Patients with post-neurosurgical complications due to MDR *Staphylococcus aureus* or *N.meningitidis* are given cefepime or meropenem (Roy *et al*., 2014). In the latter, penicillin or ceftriaxone is used for *N.meningitidis*, ampicillin for non-beta lactamase producing H. influenza and ceftriaxone for beta-lactamase producing *H.influenza* (Bodilsen *et al*., 2014). However, due to the emergence of MDR gram-negative bacteria to these classes of antibiotics (Auburtin *et al*., 2006), hence there has been a surge in the utilization polymyxin, cyclic antibiotic colistin as the last line of defence (Wallace *et al*., 2010).

2.6 Colistin

2.6.1 Historical use

Polymyxins are a group of cationic peptide antibiotics with 5 chemical deviant compounds, Polymyxin A to E, which were discovered in 1947 (Benedict and Langlykke, 1947; Stansly *et al*., 1947; Ainsworth *et al*., 1947). Colistin discovery started its therapeutic use in Japan, Europe (the 1950s) and in the United States (1959) (Spapen *et al*., 2011). However, by 1980 there was a steady decline in its intravenous administration as a result of high incidences of nephron-and neurotoxicity (Zhang, *et al*., 2013; Levin *et al*., 1999). In the interim, the utilization of colistin was limited to the treatment MDR lung infections such as those in cystic fibrosis (Radhakrishnan *et al*., 2015).

2.6.2 Chemical structure

Colistin is a multicomponent 1750 Da antibiotic that is non-ribosomally synthesized by Bacillus polymyxa sub-species. Colistinus (Bai *et al*., 2011; Choosakoonkriang *et al*., 2013). It has a variety of similar decapeptides, nearly 13 analogous components that differ by their amino acids and fatty acid. The two main components of colistin are colistin A (polymyxin E 1 ± 85%) and colistin B (polymyxin E 2 ±15%) each with a log P value of -3.15 and -3.68, respectively. The general structure is a cyclic peptide head associated with a hydrophobic side chain that is acetylated at the N-terminus by three fatty acids-homologous structure of cyclic decapeptide conjugated to the fatty acid chain via amide group (Jin *et al*., 2009; Choosakoonkriang *et al*., 2013). The amino acid group within the structure has D-leucine, L-threonine and L-α–γ diaminobutyric acid (Dab). The L-α–γ Dab is joined to 6-methyl-octanoic acid creates a deviant colistin A, versus a sole 6-methyl-heptanoic acid which is colistin B (Wallace, 2017). Colistin A and B exhibit pentacationic decapeptides with five Dab residues that have a positive charge at physiological pH (Nidhi *et al*., 2011). However, colistin A contains an octanoic acyl hydrophobicity moiety (Figure 2.10).

The production of colistin yields to two commercially available forms: colistin and colistin methanesulfonate (CMS) (Zhang, *et al*., 2013). CMS is synthesized from the reaction between formaldehyde and bisulfite (Nidhi *et al*., 2011). Typically, this is via the derivation of the primary groups on five of the colistin Dab residues using methane sulfonate moieties. *In vivo*, CMS is hydrolyzed into a complex mixture of sulphomethyl derivatives plus colistin (Spapen *et al*., 2011). CMS is viewed as the non-active prodrug as all five sulphomethyl groups have to

be cleaved from the main peptide structure to form active colistin. Although it is less toxic, the clinical use of the non-active form reduces antibacterial potency (Jin *et al*., 2009; Bai *et al*., 2011; Nidhi *et al*., 2011; Chemmangattu *et al*., 2015).

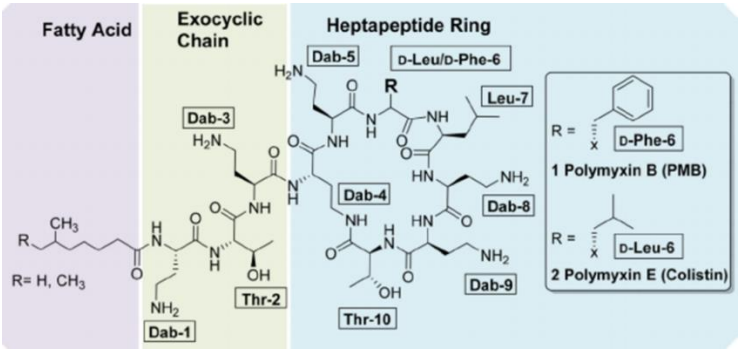

Figure 2.10 Chemical structure of colistin showing cyclic heptapeptide head ring (mainly D-leucine, L-threonine and L-α–γ diaminobutyric acids) that is acetylated at the N-terminus by three fatty acids (Gallardo-Godoy *et al*., 2016).

2.6.3. Mechanism of microbial action

The site of antimicrobial action of colistin is the bacterial cell wall. The initial interaction is conferred through electrostatic interactions between the anionic lipopolysaccharide (LPS) molecules situated on the gram-negative cell membrane and cationic polypeptide segments of colistin (Figure 2.11) (Morrison and Jacobs, 1976; Vaara and Viljanen, 1985). In turn, the localization of colistin on the cell membrane yields to alterations in membrane structural integrity. Subsequently, intracellular calcium and magnesium ions, which function in LPS stabilization, become displaced resulting in further destabilization of the cell membrane. Ultimately, the cell membrane becomes permeable thus expelling its intracellular contents subsequently leading to cell death (Koczulla *et al*., 2000).

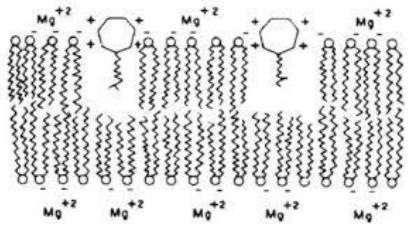

Figure 2.11 Schematic diagram showing the proposed mechanism of action of polymyxin E colistin antibiotic on the cell membrane of gram-negative bacteria. Colistin neutralizes the negative moieties on the bacterial outer membrane thus destabilizing the membrane (https://www.atsu.edu/faculty/chamberlain/Website/Lects/Metabo.htm

2.7 Nanoparticles

2.7.1 Introduction to nanoparticles

The word 'nano' originates from Latin word 'dwarf', hence NPs are small particles in the nanometer scale-one thousand millionth of a meter (10^{-9} m) (Satalkar *et al*., 2016). Classically, NPs are defined as particles between 1 and 100 nm range-with physicochemical properties that differ significantly from those of bulk materials (particles below 1 nm are omitted from this range to avoid classing clusters of atoms as particles) (Aggarwal *et al*., 2009). Structurally, NPs exist either as one, two or three-dimensional configurations with at least one dimensions between 1 – 100 nm. NP size seems to be inherent to the type of material, i.e. metallic NPs like gold and silver seems are generally lower than 100 nm, whereas polymeric NPs tend to supersede this spectrum and size up to 1000 nm is acceptable (Burgess *et al*., 2004). Be that as it may, NP size influences cellular interactions such as the mechanisms of cellular uptake (Wagner *et al*., 2010). For example, NPs less than 200 nm have a greater inclination to be internalized via clathrin-mediated endocytosis, whereas larger particles utilize caveolae-mediated endocytosis. Other studies have shown a greater CNS accumulation of NPs in 10-50 nm range versus NPs greater than 200 nm (Saptarshi *et al*., 2013).

The ability of NPs to overcome some of the limitations posed by conventional drug delivery mechanisms catapults their use for CNS diseases and infections (Chen and Liu, 2012; Masserini, 2013; Wilhelm and Krizbai, 2014). The majority of their attraction relies on remarkable innate physicochemical properties such as small sizes, surface charge and ability to encapsulate active hydrophilic or hydrophobic therapeutic agents (proteins, vaccine, drug deliveries) which otherwise have poor solubility (Berger *et al*., 2013). The large surface area to volume ratio of NPs allows for therapeutic agents to be adsorbed onto, dissolved into or covalently attached to the NPs (Faraji and Wipft, 2009; Masserini, 2013). Moreover, NP administration has a variety of routes including oral, inhalation and parenteral (Faraji and Wipft, 2009; Sarvaiya and Agrawal, 2015). In such a regard an exemplary NP is one which displays effective and efficient therapeutic delivery across the BBB devoid of enzymatic degradation, facilitates self-regulated drug release, avoids efflux transporters (P-glycoproteins) and is biocompatible (Mc Carthy *et al*., 2015). Although drug encapsulation is one of the most significant characteristics of NPs, it is also the notion of achieving high drug concentrations into the CNS microenvironment. Another attractive feature is the ability to modify the NP

surface with surfactants or coating agents to enhance cellular uptake via cell membrane-receptor specific targeting (Nguyena and Paika, 2012; Honary and Zahir, 2013a; Umut, 2013).

2.7.2 Types of NPs

There are two categories of NP, namely inorganic and organic. Inorganic NPs are those comprising metallic, magnetic or ceramic counterparts such as gold, silver or platinum. Organic NPs, on the other hand, include carbon nanotubes (CNs), liposomes, dendrimers and polymerics (Figure 2.12) (De Rosa *et al*., 2012; Kesharwani *et al*., 2012; O'Mahony *et al*., 2013). CNs are composed of graphite sheets that have been rolled into single or multi-walled tubes (Lynch and Dawson, 2008). Therapeutically, CNs are used for cell-specific targeting for drug delivery in thermotherapy of tumours (Eng, 2011; Upadhyay, 2014; Khanna *et al*., 2015). Liposomes are enclosed spherical formations made of an amphipathic phospholipid bilayer. Mainly they contain an aqueous core encircled by concentric layers of a phospholipid bilayer (Chen and Liu, 2012; Yang *et al*., 2014). Liposomes vary in size ranging from small (less than 100, mainly unilamellar) to larger structures (less than 500 nm, mainly multilamellar) (Korting *et al*., 2010). Interestingly surface functionalized liposomes with transferrin have been found to increase the delivery of 5-fluorouracil to the brain, by 17 folds, in albino rats when administered systemically (Soni *et al*., 2008). Other functionalized liposomes have included PEG which showed higher uptake of methylprednisolone in rat models with multiple sclerosis (Gaillard *et al*., 2012). Even for specific targeting, liposomes functionalized for LDL receptors have shown to deliver mitoxantrone to the brain, significantly reducing tumour sizes in rat models (Orthmann *et al*., 2012). There are however significant disadvantages to liposome utilizations. Some reports suggest that liposomes may be physicochemically unstable when in a biologically active environment. Furthermore, the ester bond contained in the bilayer becomes vulnerable to hydrolysis during agglomeration resulting in leaking of the encapsulated agent (Van Thienen *et al*., 2007). Due to their variances in size, liposomes are also subject to clearance from circulation by the reticuloendothelial system. Lastly, due to their innate chemical composition, in thermotherapy liposome sterilization may pose significant challenges as the phospholipids' bilayer is heat sensitive (Martinho, 2011; Masserini, 2013).

Polymeric NPs are those comprising of natural or semi-synthetic materials (forming structures 60 nm to 200 nm) with a core polymer matrix in which drugs can be encapsulated (Figure 2.13) (Masserini, 2013). In recent years, polymers have been primarily designed with the intent of controlled release of active therapeutic compounds (Liu *et al*., 2013; Shetab *et al*, 2015). The

most common materials utilized in the polymeric design include synthetic and semi-synthetic polylactides (PLA), poly (lactide-co-glycolic acid (PLGA), polyanhydrides as well as natural polymers such as CS (Madan *et al*., 2013; Zhang *et al*., 2013). It has been established that the construction of polymers into NPs improves stability in biological milieu, increases therapeutic biodistribution, drug loading, release and drug targeting (due to the high availability of reactive functionalized groups on the polymeric surface) (Kumar *et al*., 2013; Dodane *et al*., 2013). Due to these noteworthy qualities, several reports have described enhanced drug delivery into the brain parenchyma due to polymeric conjugation, functionalization or sole NPs. For example, PLGA NPs containing anti-tuberculosis agents (rifampicin, ethambutol and isoniazid) maintained high drug content in plasma (5-8 days) and in the mice brain (9 days) in comparison to free drug (Choonara *et al*., 2011). Although the majority of polymeric NPs are thought to be inherently biodegradable and biocompatible, the use of some has been limited due to their metabolic byproducts being toxic to the CNS. One most common example is polysorbate 80 functionalized poly (butyl cyanoacrylate) (PBCA) NPs, these were taken up by brain endothelial cells via LDL receptors.

However, PCBA NP degradation leads to toxic byproducts; polycyanoacrylate and alcohol (Kreuter *et al*., 2004). Hence natural material-based NPs like CS NPs have become the preferred source for NP synthesis although their biocompatibility has not been established in all experimental conditions.

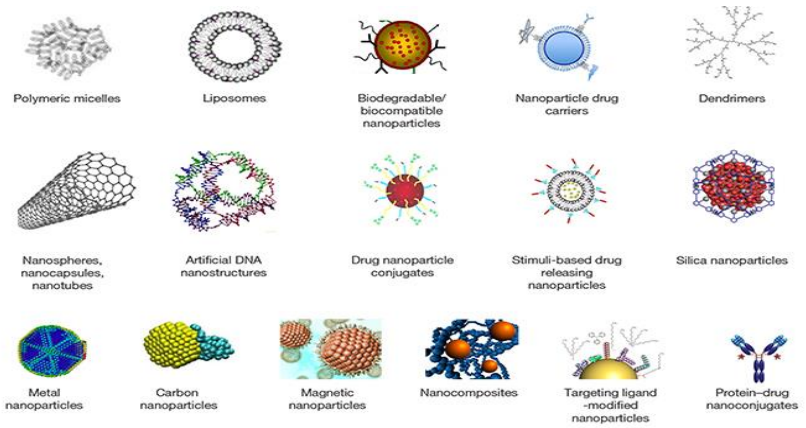

Figure 2.12 Schematic diagram showing different types of NPs (Elsabahy and Wooley, 2012).

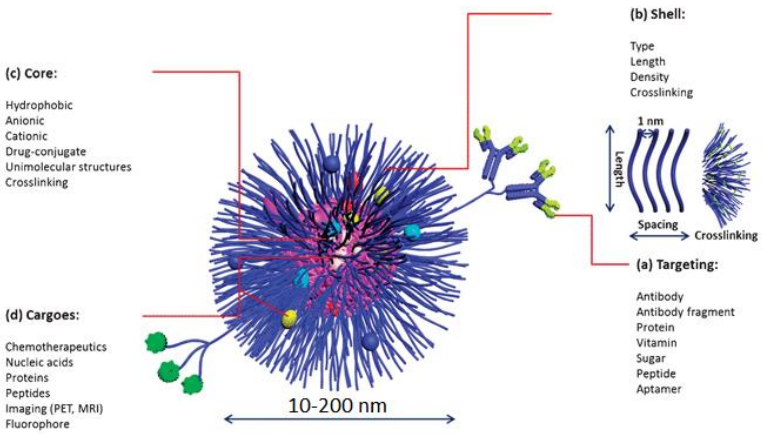

Figure 2.13 Schematic diagram illustrating the functional structural components of polymeric NPs (Iravani *et al*., 2011).

2.7.3 Physicochemical properties of NP

2.7.3.1 ζ-potential

ζ -potential is the net charge that particles obtain within their dispersive medium (Nafee *et al*., 2009) as charged species adsorb onto the interfacial layer surrounding the NPs during synthesis (Kulkarni and Feng, 2013). When particles are suspended within a medium they are encompassed by a liquid layer which exists as two parts. Primarily, the Stern layer, which refers to an inner region where ions have a strong association to the particle surface. Secondary, a diffuse layer, which refers to the outer layer with fewer associations. Within this regard, the ζ-potential is measured as the average electrostatic potential contained within the hydrodynamic shear existing between the Stern layer and the end of the diffuse layer (approximately 0.2 nm from the surface) (McNaught, 1997; Delgado *et al*., 2005).

The measurement of ζ-potential does not occur directly at the hydrodynamic shear; however, ζ-potential is expressed as a function of theoretical models. An electrokinetic phenomenon is observed when applying an electric field across particles contained within a dispersive medium (classically observed during NP characterization using dynamic light scattering, (DLS)) (Honary and Zahir, 2013a). In response to this electrical field, particles in suspension become attracted to and subsequently migrate to an electrode of opposite charge. Viscous forces arising from the medium oppose the movement of particles within the suspension, however, reaching of equilibrium between these opposing forces results in the particles moving with constant velocity. Consequently, the velocity of the migration is directly proportional to the magnitude of the ζ-potential. The velocity, in turn, is influenced by the strength of the applied electric

field/voltage gradient and the dielectric constant of the medium. Electrophoretic mobility refers to the velocity of the particle relative to the unit of electric field. The ζ-potential and electrophoretic mobility are correlated by the Henry equation (Figure 2.14) (Everett *et al*., 2007). The magnitude of the ζ-potential is an inference to the potential stability of the colloidal system. The general separation of potentially stable and unstable suspensions is expressed as either +30 or -30 mV. Hence, colloidal systems possessing ζ-potential values greater than +30 mV or less than (more negative) -30 mV are considered to stable (Gref and Couvreur, 2006)

$$(UE= 2\ \varepsilon\ z\ f(ka)/\ (3\ \eta)$$

UE refers to the electrophoretic mobility, z is the ζ-potential, ε is the dielectric constant, η is the viscosity and f (κa) is Henry`s function

The colloidal stability of a suspension is concerned with the DLVO (Derjaguin, Landau, Verwey and Overbeek theory) theory; this theory refers the stability as a factor of the total potential energy function (VT) (Toman, 2012). VT, in turn, is a balance of several competing factors:

$$VT = VA + VR + VS$$

VS refers to the potential energy due to the solvent, which does not entail a significant contribution to the total potential energy as VA (attraction forces) and VR (repulsive forces). The DLVO theory attributes the colloidal stability of particles in suspension to be a collective contribution of the innate van der Waals attractive (VA) and electrical double layer repulsive (VR) forces present between particles. These forces continually act on particles approaching each other moving in Brownian motion. Hence, particles in suspension are encompassed by an energy barrier created by the repulsive forces of two systems in approximation. However, the collision between particles in a manner that possesses sufficient energy to overcome the innate energy barrier, would lead to strong, potentially irreversible agglomeration (Malvern Zetasizer, 2013).

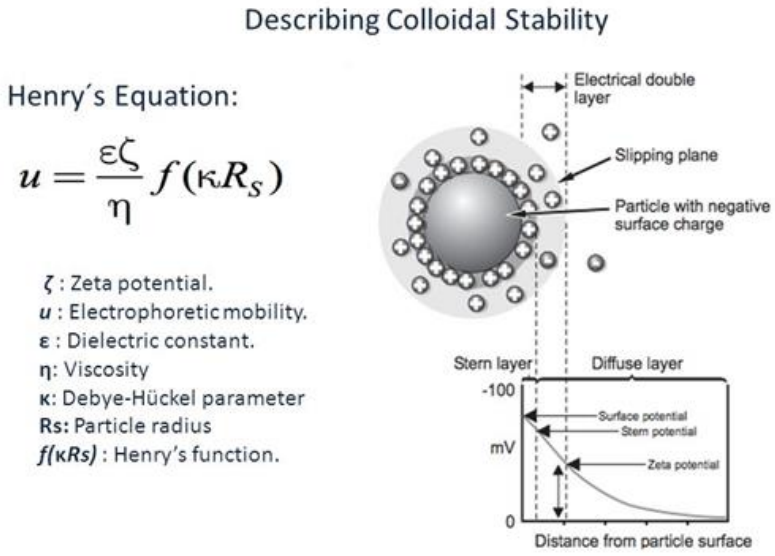

Figure 2.14 Schematic diagram of particle surface charge, ζ-potential, with reference to the Stern and diffuse layer with Henry´s equation (https://commons.wikimedia.org/wiki/File%3AGold_nanoparticle_Zeta-potential.png).

2.7.3.2 The role of ζ-potential on cellular uptake

NP size, composition (Gojova *et al*., 2007; Sohaebuddin *et al*., 2010), hydrophobicity (Turci *et al*., 2010) and charge are amongst the common properties that influence how NPs will inherently interact with cells (Wagner *et al*., 2010). Although ζ-potential is an inference to colloidal stability, its charge also determines the probability of cellular uptake (Yin *et al*., 2005). Inherently cells prefer cationic NPs due to possible electrostatic interaction with the negative residues found on the cell membrane. However, the use of cationic NPs has been significantly limited due to cell membrane damage leading to toxicity (Song *et al*., 2011; Honary and Zahir, 2013a). Toxicity can also be enhanced by the charge density, for example, the toxicity of poly (amidoamine) dendrimers was shown to be associated with the concentration of the surface primary amino groups available. Subsequently, the toxicity decreased when these groups were neutralized with acetyl groups (Fröhlich, 2012). Nevertheless, it is becoming clear that NP-induced toxicity is based on an intricate relationship between inherit physicochemical characteristics and biological factors i.e. cell type and morphology, *in vitro* conditions (cell density, culture media, composition and incubation temperature etc.), *in vivo* conditions as well as NP properties (charge, concentration, structure, size) (Khanna *et al*., 2015; Rizzello *et al*., 2012). For example, in non-phagocytic cells, the toxicity was shown as higher toxicity to smaller sizes- in contrast to phagocytic cells such as

macrophages and monocytes. However, some literature argues that in fact toxicity based on size is inconclusive (Masserini, 2013; Saptarshi *et al*., 2013).

2.7.3.3 Formation of the protein corona

'Bare' NPs do not remain so *in vivo*, as they immediately adsorb plasma proteins (Lynch and Dawson, 2008). NP-protein interactions lead to the formation of a 'protein corona' on the surface of the NP, depending on the affinity of the protein to the NP. The corona consists of a primary layer of tightly bound proteins called the hard corona followed by a weakly associated soft corona layer (Casals *et al*., 2010). NP's physiochemical properties may influence their protein binding potential; some studies have demonstrated that anionic NPs (COOH functionalized) and cationic charged (amine functionalized) had a greater degree of protein binding than their neutral counterparts (Saptarshi *et al*., 2013). Other studies have suggested that the size of the NP determines protein binding, it has been shown that 12 nm negatively charged poly acrylic NPs bound to fibrinogens at a higher degree than their 7 nm counterpart (Deng *et al*., 2012). It is also thought that the NP themselves can induce conformational changes to the structure of the subsequently bound protein. It has been demonstrated that gold NPs induced structural conformational changes to bovine serum albumin in a dose-dependent manner (Wangoo *et al*., 2008). The ability of NPs to induce structural modifications not only has implications on the bio-reactivity of the NP-protein complex but signifies the importance of understanding the relationship between NP-protein and cellular component. Most importantly there also the question of how protein surface modification of NP inside the blood may influence NP crossing the BBB (Honary and Zahir, 2013a).

2.7.4 Nanoparticles synthesis, cross-linking of polyelectrolytes

Generally, there are two approaches used for NP synthesis either top–down or bottom–up techniques. The former of which, focuses on the construction of NP by deconstructing larger materials with bulk properties. The latter focuses on the molecular construction of NPs by rearranging smaller materials into complex structures (Rosa *et al*.,2013). Either method is determined by the desired properties for each type of NP. The physicochemical properties such as size, chemical stability, toxicity and drug-release kinetics are consequential to the synthesis technique. For the synthesis of NPs using naturally occurring polymers such as CS, size can be largely influenced by Mwt (generally, the higher the Mwt the larger the NP size), innate polymer structure and degree of deacetylation (Goycoolea *et al*., 2007). Incorporation of the therapeutic agent into CS NPs can be accomplished either during synthesis or after the formation of NP. During synthesis, the therapeutic agent is integrated and embedded in the CS matrix versus the latter where the therapeutic agent is adsorbed onto the NP surface (Rosa *et al*., 2013).

Polyelectrolyte (PE) refers to a group of macromolecular compounds with an elementary charge dispersed on its backbone (obtained spontaneously or deliberately) (Dakhara and Anajwala, 2010). In an aqueous state, ionic fractions are solubilized thus denoting a looser association-although most moieties are still confined to the polymer domain via the electrostatic attraction inherent to the PE. Overall, PE's either cationic i.e. CS, gelatin and alginate, or anionic semisynthetic cellulose and DS (Ko *et al*., 2002; Schönhoff *et al*., 2003). Molecular chain conformations, viscosity, polarizability and miscibility are affected when PEs interact with ion moieties during a reaction. Hence PEs are vulnerable to phase transition (based on temperature, electric potential, pH, ionic strength manipulation) (Berger *et al*., 2004; Szymańska and Winnicka, 2015). Polyelectrolyte complexes (PECs) are formed as a result of intermolecular interactions between polyelectrolytes/polymers of opposing charges (Figure 2.15) (Mahmoud *et al*., 2010). For a complex to be formed, both polymers must undergo ionization, therefore, the pH value of each polymer must be in the same pKa range (Lee *et al*., 1999). Although electrostatic interactions are the main forces of attraction, hydrogen bonding, hydrophobic interactions and ion-dipole forces also contribute to the type of structure being formed (Berger *et al*., 2004).

Naturally, complexation occurs spontaneously without additional cross-linking agents between the oppositely charged polymers within a polar solvent. Before thermodynamic equilibrium is

reached there is a loss in the translational and conformational entropy of each polymer chain-which has to be compensated to confer complexation (Jafar *et al*., 2014). The greatest loss in entropy is during the formation of the first bond between the two polymers. Although in smaller amounts, secondary losses in entropy occur during bond formation. The overall change in enthalpy per bond (owing to the electrostatic interaction of each monomeric unit) remains constant (Andrianov *et al*., 2006). Hence, the formation of PECs has three main phases; primary complex formation, formation process within intra-complexes and lastly inter-complex aggregation process. Primary complex formation pertains to secondary binding sources (i.e. Coulomb forces) and occurs rapidly between oppositely charged polyelectrolyte solutions. Formation process within intra-complexes mainly refers to the formation of new bonds and/or the linearization of the polymer chains-which occurs over a longer period of time. The latter process involves hydrophobic interactions in the aggregation of the secondary complexes (Prokop *et al*., 1998; Kaibara *et al*., 2000).

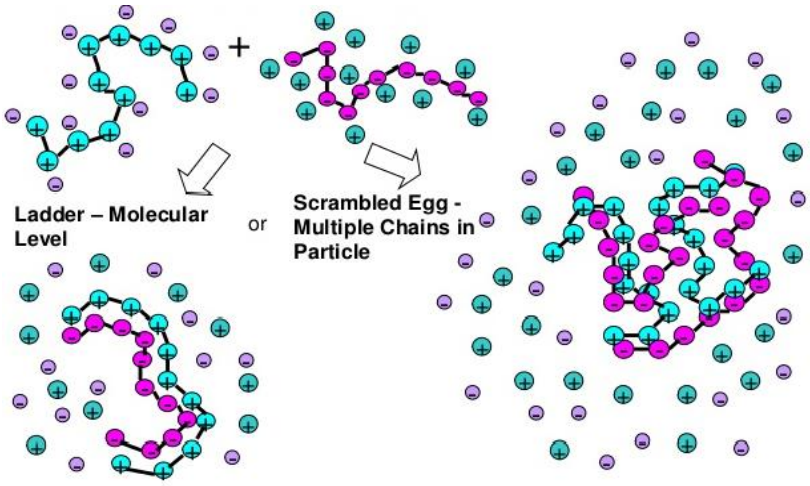

Figure 2.15 Schematic diagram showing self-assembling aggregates of oppositely charged polymers (https://www.slideshare.net/DavidScheuing/phase-behavior-and-characterization-of-polyelectrolyte-complexes).

2.7.5 Chitosan: properties of cationic polyelectrolyte

2.7.5.1 Structure

CS is the most frequently utilized polymer in the design of drug delivery systems (Goycoolea *et al*., 2007). This attraction is due to its remarkable structural and biological properties inferred by its cationic nature (De and Robinson, 2003), aqueous solubility (Mahmoud *et al*., 2010), biocompatibility, biodegradability (George and Abraham, 2006; Gan and McCarron, 2005) and mucoadhesive properties (Bernkop-Schnürch *et al*., 1998; He *et al*., 1998). CS is a linear polymer consisting of a high ratio, of an alternating sequence of glucosamine to N-acetyl glucosamine (NAG's) monomers linked together by β -glycosidic bonds (1→4) (Saboktakin *et al*., 2011; Alameh 2012; Hoemann *et al*., 2013; Yang *et al*., 2014). A significant feature of CS is the relative ease of structural chemical modifications, particularly in the C-2 position, which yields CS derivatives with diverse characteristics (Figure 2.16) (Yang *et al*., 2014).

CS is derived from chitin which is the second most abundant natural polysaccharide after cellulose (Goycoolea *et al*., 2007; Toman, 2012). Chitin, a nitrogen-bearing compound, is naturally found in the exoskeleton of crustaceans: crabs and shrimp (Berger *et al*., 2004; Sadeghi *et al*., 2008; Mahmoud *et al*., 2010; Saboktakin *et al*., 2011). Interestingly, the food industry alone produces an excess of approximately 60 000 to 150 000 metric tons of chitin byproducts. The readily available supply created by this naturally occurring market has significantly substantiated the utilization of CS in biomedical applications (Ahing and Wid, 2016).

The commercial synthesis of CS has four integral steps; deproteinization, demineralization, discolouration and deacetylation. Briefly, protein constituents are removed from crustacean shells using sodium hydroxide under high temperature (Mahmoud *et al*., 2010). Subsequently, the solid mass is demineralized via a series of wash cycles using hydrogen chloride followed by discolouration. Finally, a deacetylation step (determines the percentage of monomers existing within the CS chain), which is the chemical removal of acetyl groups typically in 40% sodium hydroxide for 1-3 hours at 120 (Ahing and Wid, 2016).

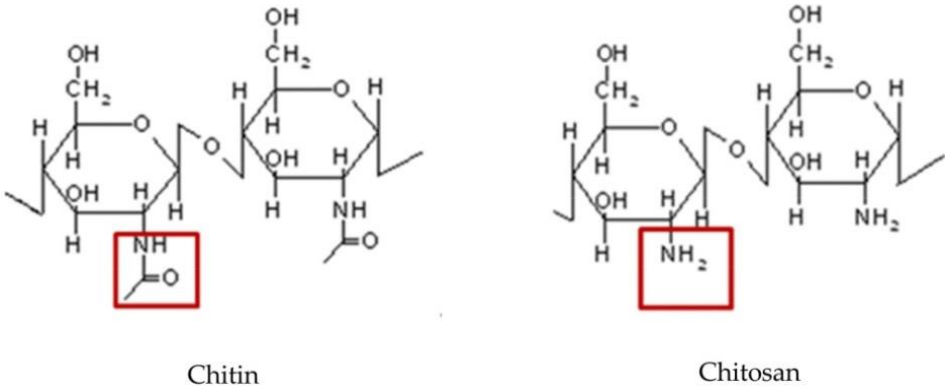

Figure 2.16 Chemical structure of chitosan in comparison to chitin (Stamford *et al*., 2013).

2.7.5.2 Degree of deacetylation

Essentially chitin and CS are structurally differentiated due to the degree of deacetylation (DD) (Berger *et al*., 2004; Saboktakin *et al*., 2011). There is a symbiotic relationship between the DD of and inherent physiochemical properties. Generally, CS is a weak base that can be solubilized in a slightly acidic aqueous environment, with pKa of approximately 6.5 (Chen *et al*., 2003; Alameh, 2012). However, the greater the DD, the greater the number of unrestricted amino groups available for protonation into cationic amine (NH2) groups (Mahmoud *et al*., 2010). This, in turn, determines the solubility of the cationic sites and the intermolecular hydrogen bonding within the CS polymer (Berger *et al*., 2004; Faraji and Wipft, 2009). In this respect, high DD (± 85%) yields greater aqueous solubility, as the DD decreases, so does the solubility (Hoemann *et al*., 2013). Moreover, higher DD provides stronger cationic charge for interaction with negatively charged residues (like sialic acid on mucous membranes) thus higher mucoadhesion. In fact, high DD is utilized for targeting negative cell membranes for delivery systems (Yang *et al*., 2014; Szymańska and Winnicka, 2015).

2.7.5.3 Biocompatibility and biodegradation

Biocompatibility is the ability of a biomaterial to achieve its intended function devoid of negative local or systemic effects, *in vivo*. Instead, the biomaterial should enhance beneficial cellular responses within each unique cellular environment (Rodrigues *et al*., 2012). The biocompatible nature of CS is due to its structural components resembling the mammalian glycosaminoglycans (GAGs) - a group of heteropolysaccharides residing in the extracellular matrix as well as cell surface membrane (Griffon *et al*., 2006). *In vivo*, under normal physiological conditions, CS degradation is initiated by its transformation to an oligomer. This process is facilitated by proteolytic lysozymes, chitinase, chitin deacety-lase, beta-N-

acetylhexosaminidase and chitosanase enzymes (Köping-Höggård *et al*., 2001; Sarvaiya and Agrawal, 2015). Notably, lysozyme and chitinase enzymes are ubiquitous in the brain and the body, hence the clinical significance of CS-based NPs (Berger *et al*., 2004; Katas *et al*., 2013). CS biodegradation rate has also been associated with the DD, that it is faster when the DD is less than 70% (Hoemann *et al*., 2013; Szymańska and Winnicka, 2015). Biocompatibility may, in fact, be specific to the biological system to which it is applied. FDA regulation of CS as a dietary supplement and wound dressing does not necessarily potentiate its biocompatibility in all biological systems. (Rodrigues *et al*., 2012; Hoemann *et al*., 2013; Ahmed and Aljaeid, 2016). In this manner it is imperative to assess biocompatibility CS based NPs on its intrinsic characteristics (i.e. DD, Mwt etc.) within discrete biological environments (*in vitro* cell type and culture conditions). It is known that, as a cationic molecule, CS has a high affinity and interaction with negatively charged cell membranes, however, when in a formulation as a carrier the number of available positively charged amino groups decreases comparatively. As such, the lower number of amino groups significantly affects its ability to interact with the cell membrane and its environment ultimately affecting cellular uptake and potentiating toxicity (Dodane *et al*, 1999; Goycoolea *et al*., 2007; Szymańska and Winnicka, 2015).

2.7.6 Dextran: properties of anionic polyelectrolyte

2.7.6.1 Structural characteristics, synthesis and properties

One of the most promising molecules for complexation with CS is DS. DS is an anionic anhydroglucose polysaccharide consisting of a high concentration of glucose molecules formed in chains of varying lengths (Figure 2.17) (Tiyaboonchai and Limpeanchob, 2007; Mahmoud *et al*., 2010). The main chain has an extensive number of (1→6) glycosidic units with (1→2), (1→3) and (1→4) branched linkages. Innately, DS possesses 17% sulphur: approximately 2.3 sulphate groups per glucosyl residue (Tiyaboonchai and Limpeanchob, 2007). Notably, DS is a biocompatible and biodegradable water-soluble polymer which has resulted in its usage in the formation of NPs (Mitra *et al*., 2001; Chaiyasan *et al*., 2013). Its negative charge allows for its interaction in ionic gelation of polyelectrolytic complexation in with cationic charged molecules like CS (Pajouhesh and Lenz, 2005; Katas *et al*., 2013). The water-soluble nature of DS allows for its utilization devoid organic solvents denoting the NP synthesis process relatively easy and eco-friendly (Qi *et al*., 2010; Saboktakin *et al*., 2011). DS is synthesized by a wide variety of bacterial strains using different substrates. For example, *Leuconostoc mesenteroides* and *Streptococcus mutans* synthesize DS from sucrose whereas *Gluconobacter oxydans* produces DS from maltodextrin (Hornig and Heinze, 2007). Alternatively, it is derived enzymatically from cell-free culture supernatant (Wang *et al*., 2011) as well as chemical synthesis (Hornig and Heinze, 2007). The physiochemical features of DS depend on its Mwt, type of glycosidic branches and the degree of branching- depending on the bacterial strain utilized during synthesis or post-synthesis reactions and modifications.

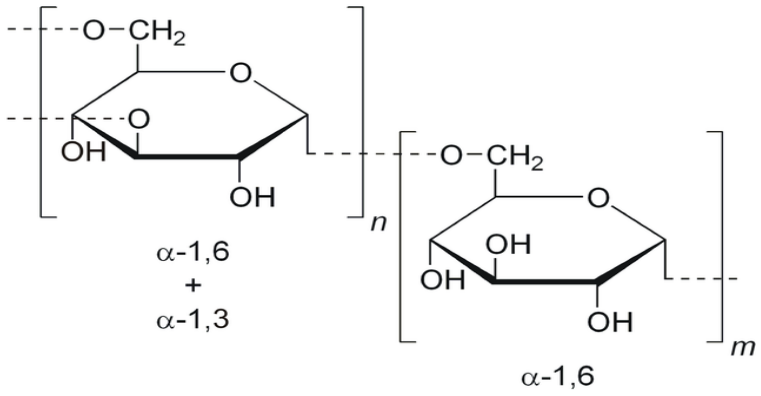

Figure 2.17 Chemical structure of DS (https://en.wikipedia.org/wiki/Dextran).

2.7.7 Advantages of CS-DS NPs

Drugs that are covalently linked to polymers generally have decreased toxicity, increased solubility and lengthy circulation in plasma in comparison to free drug (Zhang *et al*., 2008). PEG and N-2-hydroxypropyl methacrylamide (HPMA) have commonly been conjugated to hydrophobic DOX to increase solubility and circulatory system retention, *in vivo*. However, due to few terminal end groups, PEG allows limited drug loading (Van *et al*., 2007). DS, on the other hand, has shown controlled release of DOX (Mitra *et al*., 2001; Qi *et al*., 2010; Siddharth *et al*., 2017). Due to its high charge density, DS effectively neutralizes the cationic charge of DOX thus increasing drug loading capacity (Yousefpour *et al*., 2011). Other reports have shown that when in a formulation, DS significantly reduces cationic charge-based cytotoxicity (Tiyaboonchai *et al*., 2003b). The first edition of CS-DS NPs was for the encapsulation and controlled release of an anti-angiogenesis hexapeptide (Chen *et al*., 2003). The advantages of CS-DS complexation were greater stability and increased mechanical strength in comparison to other popular CS based NPs such as CS- tripolyphosphate (TPP) NPs (Agnihotri *et al*., 2004). Other inherent benefits of DS and CS are that they are suitable for mild synthesis processes in a pure aqueous environment such- most commonly PEC (Chen *et al*, 2007; Saboktakin *et al*., 2011). CS-DS NPs have shown to be stable in their innate synthesis environment devoid of the use of stabilizers, organic solvents and or heat, as well as being lyophilized for long-term storage. Moreover, for encapsulating hydrophilic biologically active molecules such as proteins and peptides, this complexation has proved advantageous in maintaining the molecular structural integrity of the drug (Goycoolea *et al*., 2007; Mahmoud *et al*., 2010). Therefore, it is possible CS and DS may synergistically act to encapsulate large hydrophilic drug like colistin, whilst having biocompatible effects on the BBB.

2.8 Problem statement

CS-based NPs are a proposed mechanism for drug delivery of therapeutic agents. The need to for an alternative non-invasive mechanism is due to the lack of sufficient entry of clinically significant therapeutics owing to the impedance function of the BBB. There has been a surge in the use of 'last-line of defence' drug colistin in the treatment gram- negative CNS infections as a result of the emergence of multi-drug resistant infections arising from species in the likes of *Klebsiella pneumoniea*, *Pseudomonas aeruginosa* and Acinetobacter. Unlike other organs the brain has limited regenerative abilities, therefore in order for CS NPs to be a successful alternative to invasive methods, it is imperative that their biocompatibility to a highly dynamic and specialized barrier is assessed.

2.9 Research question/hypothesis

This study was based on the hypothesis that the manipulation of charge index will influence physicochemical properties of CS-DS NPs. Moreover, the encapsulation of colistin into CS-DS NPs would have a biocompatible effect on the BBB.

2.10 Aim and objectives

1. Chemically characterize the physicochemical properties of CS-DS NP

    a. Assess the influence of charge index on the hydrodynamic diameter, dispersity index and ζ-potential

    b. Stability of NPs in serum free and serum containing media as well as phosphate buffer solution versus deionized water

2. Define the drug encapsulation efficacy of CS-DS NP

    a. Assess the concentration of colistin encapsulated inside the NPS using colistin standard calibration curve

3. Analyze the *in vitro* effects of CS-DS NP on the BBB

    a. Ascertain bEnd5 cytotoxicity using trypan blue cell viability assay

    b. Measure the TEER across the monolayer

CHAPTER THREE: METHODS OF SYNTHESIS AND *IN VITRO* CHARACTERIZATION OF NPs

The purpose of this chapter was to ascertain the physiological response of the BBB to an acute and chronic treatment of CS-DS NPs. This chapter focused on two discrete features of experimental work. The first part dealt with the chemical characterization of the physicochemical properties of CS-DS NPs in solution and in biological media, as well as ascertaining drug encapsulation properties. The second part, detailed the interaction between NPs and the BBB (represented by the immortalized mouse brain endothelial cell, *in vitro*) measured as physiological parameters; cytotoxicity, endothelial permeability as well endothelial morphology in the presence of NPs.

The preparation and characterization of NPs and cell culture was done at the University of the Western Cape (UWC). The NPs were synthesized at the School of Pharmacy and characterization was performed at the Department of Biotechnology. Cell culture studies were conducted at the Department of Medical Biosciences. All work involving scanning electron microscopy was performed that the electron microscopy unit (EMU) at the Department of Physical Sciences.

3.1 Materials

Table 3.1: Materials used in the study

	MANUFACTURER	CATALOGUE NUMBER
TISSUE CULTURE		
DULBECCO' MODIFIED EAGLE'S MEDIUM (DMEM)	Lonza®	12-604-F
FETAL BOVINE SERUM	Gibco®	10500
PHOSPHATE BUFFER SALINE	Sigma-Aldrich®	D8662
NON-ESSENTIAL AMINO ACIDS	Biowhittaker Lonza®	13-114E
PENICILLIN/STREPTOMYCIN AMPHOTERICIN B MIXTURE (1%)	Whitehead Scientific (Pty) Ltd.	17-745E
SODIUM PYRUVATE (1%)	Gibco®	11360
TRYPSIN (0.4%)	Gibco®	25200
TRYPAN BLUE	Sigma-Aldrich®	T-8154
ETHANOL (99.9%)	Kimix	
GLUTARALDEHYDE	Fluka	49626
PLASTIC CONSUMABLES		
TRANSWELL® INSERTS (24 WELL PLATES)	Millipore/MERCK	PIHA01250
96 WELL PLATES	Adcock Ingram	3524
CONICAL CENTRIFUGE (15ML)	Biosmart Scientific	PBIOT15
PETRI DISHES (3MM)	Cell Star	627 160
DISPOSABLE PLASTIC CUVETTE (12MM SQUARE POLYSTYRENE. DTS0012)	Malvern Ltd	Acquired with Malvern instrument
DISPOSABLE FOLDED CAPILLARY CELL (DTS1070)	Malvern Ltd	Acquired with Malvern instrument

OPTISEAL, POLYPROPYLENE. 4.9 ML. 3 X 51 MM TUBES	Beckman Coulter	Gift from nanotechnology department, University of the Western Cape
BEND5 CELL LINE	ATCC	Gift from Medical Bioscience department, University of the Western Cape
MICROSCOPY WORK		
CARBON TAPE	PELCO	16084-1
ALUMINIUM STUBS	Agar Scientific	AGG301
PARTICLE SYNTHESIS		
CHITOSAN (LOW MOLECULAR WEIGHT) (DEACETYLATED CHITIN, POLY(D-GLUCOSAMINE))	Sigma-Aldrich®	**448869**
DEXTRAN	Sigma-Aldrich®	1179708

3.2 Methods

3.2.1 Chemical characterization in of CS-DS NPs in deionized water

3.2.1.1 Theoretical calculation of charge index

Polyelectrolyte complexation was utilized to synthesize CS-DS NPs with the aim of obtaining monodisperse samples with PDI greater than or equal to 0.1 or less than 0.3, a hydrodynamic diameter between 100 nm and 200 nm and ζ-potential ≥ ±30 mV. CS-DS NP preparation was achieved through electrostatic interactions between anionic DS and cationic CS. Polyionic interactions have been detailed by Chaiyasan *et al* (2013) using FTIR, who showed asymmetrical stretching in DS and CS functional groups signifying CS-DS NP formation ( ). The synthesis was in accordance to a previously described method by Chen *et al* (2003). Using polyelectrolyte complexation, the spontaneous interactions between the opposite charges of CS and DS were responsible for the formation of CS-DS NPs. Under experimental conditions (where the pH is 3-4 when CS pH value is below its pKa ∼6.5) theoretically, DS consists of approximately 74 sulfate groups per mole, corresponding to 5.78×10^{-3} negatively charged groups per gram. CS, on the other hand, consists of approximately 2073 amino groups per mole, corresponding to 5.18×10^{-3} positively charged groups per gram. The ratio between the negatively charged sulfate groups (N) in DS and positively charged amine groups (P) in CS was calculated per formulation (Table 3.2) (Chen *et al*, 2007). These charge indices were set to study their effects on the physiochemical properties of the CS-DS NPs formed.

Table 3.2: Theoretical charge contribution of DS and CS functional groups per formulation

DS:CS (w/v)	*DS:CS (Number of charged molecules/g)*	*Charge index (N:P)*
9.1:0.9	$5{,}25X10^{-5}$: $4{,}66X10^{-6}$	11
9.5:0.5	$5{,}49X10^{-5}$: $2{,}59X10^{-6}$	21
9.75:0.25	$5{,}63X10^{-5}$: $1{,}29X10^{-6}$	43.5
0.9:9.1	$5{,}2X10^{-6}$: $4{,}71X10^{-5}$	0.1
0.5:9.5	$2{,}89X10^{-6}$: $4{,}92X10^{-5}$	0.05
0.25:9.75	$1{,}4X10^{-6}$: $5{,}06X10^{-5}$	0.03

DS and CS solutions were 0.1% w/v, calculated to a final volume of 10 mL- pH 3-4. Charge index was calculated using the following equation:

$$\frac{\text{DS mass (g)} \times 5.78E3}{\text{CS mass (g)} \times 5.18E3}$$

**Note: Charge index 21 was found to produce monodisperse samples with the lowest hydrodynamic diameter with a relatively high ζ-potential. This was the charge index to be used for CSS encapsulation and application in cell culture work.*

3.2.1.2 Preparation of DS and CS stock concentrations

The stock concentration was prepared by dissolving each polymer in deionized water (DI) (Mili-Q water purification system 15 Ω.cm). For CS, 0.1 g was dissolved in 100 ml of DI containing 0.175 µl of acetic acid- the acetic acid facilitated the protonation and maintenance of the CS in the solution. Similarly, 0.1g of DS was dissolved in 100 ml of DI to make up a final concentration of 0.1% w/v. The solutions were agitated at 1000 rpm for an hour at room temperature (RT) to enable complete homogenization (Chen *et al*., 2007).

3.2.1.3 Synthesis of empty CS-DS NPs

For each charge index, a specific volume of CS solution (0.1% w/v) was placed into a glass vial which was kept under agitation in anticipation for the addition of DS (0.1%) (Magnetic stirring at 700 rpm at RT). The complementary volume of DS was slowly added to the solution to a final volume of 10 ml, the reaction continued for 10mins (magnetic stirring at 1000 rpm at

room temperature) (Table 3.1). The solutions were stored at 4°C until required. Fresh stock solutions were synthesized every 3 days to prevent contamination. During synthesis, the size of the glass vials, stirrer bars and stirring speed, were kept constant. Before characterization, the pH of the stock solutions and the formulation was measured (*CRISON 058 002000*).

3.2.1.4 Synthesis of CSS loaded CS-DS NPs

The incorporation method was used for CSS encapsulation into CS-DS NPs. This method involved the inclusion of drug during the NP synthesis- before nano-complex was formed (Hirani *et al*., 2009). Herein, 4.8 mg of CSS was dissolved into 9.5 ml of DS anionic solution (0.1% w/v) under agitation for 10 min (1000 rpm, RT) (Chen *et al*., 2007). After which, 0.5 ml of CS (0.1% w/v) was added into the DS-CSS solution thus facilitating the spontaneous formation of CSS loaded CS-DS NP (see *note, Table 3.1).

The physicochemical properties; hydrodynamic diameter (nm), ζ-potential mV and polydispersity (PDI) for empty and CSS loaded CS-DS NPs was characterized using photon correlation spectroscopy.

3.2.2 Chemical characterization of CS-DS NPs in biological milieu

Dulbecco's Modified Eagle Medium (DMEM) was supplemented with 10% FBS, 1% non-essential amino acids (NEAA), 1% sodium pyruvate and 1% *Penicillin* and *Streptomycin* (Reiss *et al*., 1998; Steiner *et al*., 2011). This was to simulate media conditions used during the culturing of bEnd5 cells. DMEM devoid of supplementation (serum-free) as well as phosphate buffer solution (PBS) was set out as a control for the experimental outline. All samples were pH 7.4. The temperature of the DMEM (serum contain and serum-free) was regulated by heating in a water bath to 37°C for 60 mins. This was performed to replicate the temperature of *in vitro* bEnd5 cell incubation.

Freshly synthesized NPs were purified (Section 3.2.6.1). After two consecutive purification cycles, the supernatant was discarded and the NPs were re-suspended in DI. 1 ml of NP was placed into 15 ml centrifuges tubes containing 1ml of biological media. The samples were incubated in the water bath at 37°C for a set timeline of 10, 30, and 60 min. After each timeline, the hydrodynamic diameter (nm), ζ-potential and PDI of the CS-DS NPs were characterized using photon correlation spectroscopy.

3.2.3 Characterization apparatus: photon correlation spectroscopy

3.2.3.1 Operating principle for hydrodynamic diameter (nm) and PDI characterization

Photon correlation spectroscopy uses the principle of DLS. DLS functions as a measure of the Brownian motion of particles in suspension which is then correlated to the particle size. Brownian motion refers to the random movement of particles in suspension due to their relative interactions with surrounding molecules (Lyklema, 2005). Generally, at a fixed temperature, the Brownian motion of a particle is inversely proportional to its size. That is, the larger the particle, the slower the Brownian motion (Shaw and Costello, 1993).

DLS measures the intensity of the light scattering refracted (time-dependent fluctuations) on an illuminated suspension. The system uses a laser to illuminate an incident beam on the particles undergoing Brownian motion; subsequently a 'speckle pattern' is formed representing the position of each particle (Figure 3.1 (a) and (b)). This pattern is seen to be in constant motion due to the constant movement of particles relative to their Brownian motion. A detector positioned at 90° (90° in the Nano S90 and ZS90 and 173 ^{0} NanoS and ZS) measures the light scattering. In the case of too much light being scattered. An attenuator (with a transmission range of 100% to 0.0003%) decreases the intensity of the laser beam thus reducing the intensity

of scattering. Alternatively, in the case where too little light is being scattered due to a small particle size, the attenuator increases the amount of light projected by the later. Finally, the scattering intensity signal is passed from the detector to a correlator which measures the rate at which the intensity fluctuates. This is performed by comparing the intensity of the light signal to the initial light beam passed through the suspension over time (Figure 3.1 c) (Brown, 1996; Pecora *et al*., 2013).

The information obtained from the correlator is passed through to the computer which using Zetasizer software to calculate the hydrodynamic diameter and PDI. Based on the DLS the hydrodynamic diameter is determined using the translational coefficient from the *Stokes-Einstein* equation.

$$d\ (H)\frac{kT}{3\pi\eta D}$$

Where the hydrodynamic diameter d (H) is equated Boltzmann's constant (k) and the absolute temperature (T) divided by the viscosity (η) and the translational diffusion coefficient (D) (Mason, 2000).

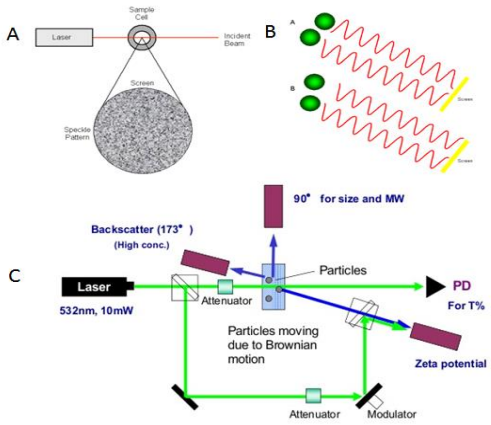

Figure 3.1 Schematic diagram showing the functional parameters of DLS (A) speckle pattern with reference to the laser, sample cells and incident beam, (B) two speckle patterns (example A and B), each signal depends on the phase addition of the scattered light falling on the detector. In example (A), two beams interfere and 'cancel each other out' resulting in a decreased intensity detected. In example (B), two beams interfere and 'enhance each other' resulting in an increased intensity detected, (C) operating principle of photon correlation spectroscopy (adopted from Malvern Zetasizer instrument manual, 2013).

3.2.3.2 Operating principle for ζ-potential characterization

ζ-potential is a physical property pertaining to the net charge that particles acquire within a medium. The presence of the surface electrical charge on the particles results in their interaction with an applied electric field. The Zetasizer utilizes a patented technique called M3-PALS which combines laser Doppler velocimetry and phase analysis light scattering (PALS) to ascertain the particle electrophoretic mobility (Valiño *et al*., 2014). When an electric field is applied to the suspension, the charged particles become attracted towards the electrode of opposite charge (capillary cell fitted with gold electrodes on either side). Initially, viscous forces within the suspension oppose the movement of the particles in suspension. However, the particles move with constant velocity when equilibrium is reached between the two opposing forces. The velocity of the particles relative to the electric field unit is denoted as the electrophoretic mobility. The relationship between mobility and ζ-potential is correlated using the Henry equation (refer to Figure 2.18) (Everett, 2007).

In order to measure the ζ-potential, the light source emanating from the laser is split into an incident and reference beam. The incident laser extends through the centre of the capillary cell, the subsequent scattered light is detected at a 13° angle. Particles moving through the cell result in fluctuations in the light intensity with a frequency proportional to the velocity of the particles. The information on the light intensity is passed through the digital signal processor which is then analyzed using the Zetasizer software (Figure 3.1c) (Malvern Zetasizer instrument, 2013).

3.2.3.3 Sample analysis

The instrument used in this study was the Zetasizer Nano S90° (Malvern Instruments, Ltd., UK.) For the hydrodynamic size and PDI, a 1 ml sample was placed into a cleaned polystyrene disposable cuvette and measured at a detection angle of 90°, at a wavelength of 633 nm with a refractive index of 1.59. The thermostatic sample chamber was selected to be 25 °C for this a refractive index. The measurements were performed at attenuator setting 11 with a measurement range of 0.3 and 200 nm. For, ζ-potential, 700 µl of the aliquot was injected into 12 mm disposable folded Capillary Cell (DTS1070). The sample was read at a detection angle 173° under a voltage of 4 mV at 25 °C.

All samples were prepared and read as triplicates. For each sample, three parallel measurements were reported a cumulative analysis (Zetasizer software, version 6.1) (mean ± SD).

3.2.4 Determining CS-DS NP encapsulation efficacy (EE %)

The aim of this section was to generate a standard calibration curve for CSS as a factor of absorbance versus concentration. The calibration curve was created using serial dilutions of a known concentration of CSS in order to characterize the encapsulation capacity of the CS-DS NPs; the amount of CSS incorporated inside the NPs.

3.2.4.1 Preparation of CSS calibration standards and quality control (QC) samples

Three independent stock solutions were prepared to obtain a series of consecutive calibration curve standards. The stock solutions were prepared by dissolving 4.8 mg CSS in 10 ml DI. Standards were prepared by serial dilution from each stock solution (dilution factor of 2) to achieve the following concentration range: 1.875, 3.75, 7.5, 15, 30, 60, 120 µg/ml (n=3). QC samples were prepared by diluting the appropriate volume of stock solution in DI to achieve 60, 30 and 7.5 µg/ml (n=3).

3.2.4.2 Generation of a calibration curve for CSS quantification using ultraviolet-visible spectroscopy

An aliquot of each concentration was placed in a quartz cell (104.002-QS, with 10 mm light path) for absorbance measurements using UV-Vis at a fixed wavelength of 210nm (Cintra 202; Cintral software version 2.2). The limit of detection (LOD) was defined as the analyte concentration yielding an optical density (OD) greater than 1 (Wallace *et al*., 2010). The specificity of the assay was ensured by analyzing blank samples of DI to check for the presence of interfering peaks against the inherent peak of CSS (no interfering peaks were observed). A linear calibration curve was established using the seven prepared calibration standards (1.875-120 µg/ml).

3.2.4.3 CSS quantification: determining EE %

The indirect method was utilized to calculate CSS encapsulated in or associated with the CS-DS NPs. The concentration CSS encapsulated was expressed as the difference between the total amounts of CSS incorporated during NP formation to that of ‘non-encapsulated’ CSS remaining in the aqueous phase. A high concentration of ‘free’ CSS in the supernatant would be indicative of low encapsulation efficiency in the NPs. After CSS encapsulation, CSS-NPs were centrifuged (15 000 rpm for 15 minutes) and the supernatant was analyzed for CSS concentration (UV-Vis, 210 nm wavelength (n=3)). The CSS concentration was determined using the linear calibration curve and the EE (%) was calculated by the following equation:

$$\text{Entrapment Efficiency (\%)} = \frac{\text{the initial amount of CSS added} - \text{CSS in the supernatant}}{\text{the initial amount of CSS added}} \times 100$$

3.2.4.4 Method validation for CSS calibration curve

Reproducibility was assessed by (1) intra-day assay of QC samples entailing three independently prepared, randomly selected, analyte concentrations measured consecutively within the same day and then stored at 4^0C (2) interday assay with analysis of QC samples analyzed over three days. All samples were analyzed in triplicates using UV-Vis. Linear calibration curves were constructed based on the relationship between CSS peak and the average concentration from each triplicate reading (mean ± SD) (Jian *et al*., 2002).

3.2.5 Characterization apparatus: *ultraviolet-visible spectroscopy*

3.2.5.1 Operating principle

Spectroscopy is based on the fundament of light transmission or absorbance of an analyte as a function of a wavelength in the electromagnetic radiation. The functional components of spectrophotometer include two light sources that produce a spectrum of electromagnetic radiation (Perkampus *et al*., 1992). Generally, the primary light source is a deuterium arc lamp which generates an intensity continuum within the UV region. A secondary light source is usually a tungsten-halogen lamp, which in turn generates a segment of the UV spectrum across the visible range. A source selector facilitates the alteration between the lamps as required, alternatively, combining the light sources thus yielding a single broadband source (Smith and Dent, 2005). The range of the electromagnetic radiation is manipulated using a dispersion device by selecting the desired wavelength that will be illuminated onto the analyte (dispersion device such as prisms and holographic gratings are glass blanks that allows for the diffraction of the wavelengths at different angles) (Krafft *et al*., 2009). Dispersion devices have multidimensional surface functionalized groves that act as reflective sources. The specificity of the dimensions is related to the wavelength of light to be dispersed. Finally, a photodiodes detector converts (with a limit of detection of 170–1100 nm) the light signal obtained from the analyte into an electrical signal. This is produced by electrons from the light source passing through semiconductor on the detector (Figure 3.2). The movement of the electrons drains the charge of the capacitor functioned on the detector. Subsequently, the energy required to replenish the capacitor correlated intensity of light transmitted or absorbed (Thermo Spectronic, 2012). The absorbance and transmittance are denoted as follows:

$$T = \frac{I}{IS}$$

$$A = -\log T$$

Where T is transmittance, I refer to the intensity of incident light, IS is the intensity of transmitted light and A is the absorbance (Thermo Spectronic, 2012).

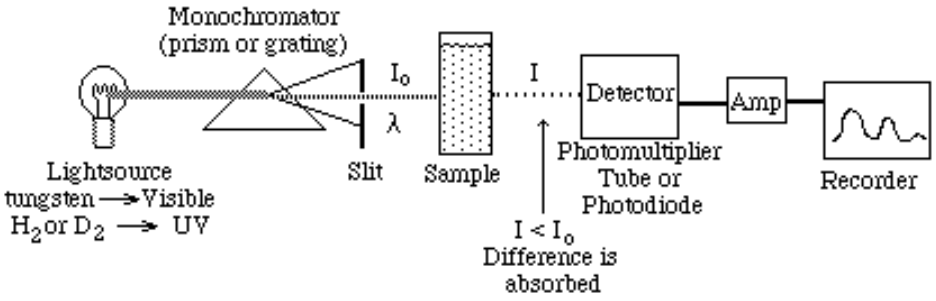

Figure 3.2 Schematic diagram showing the operating principle of UV-Vis (http://www.sci.sdsu.edu/TFrey/Bio750/UV-VisSpectroscopy.html).

3.2.6 CS-DS NP sample treatment: purification and lyophilization

3.2.6.1 Sample purification

CS-DS sample was purified to remove unreacted materials. Samples were transferred into 5 ml Beckman Coulter Optiseal tubes then centrifuged at 65000 rpm for 30 mins at 10°C (ultracentrifugation, Beckman Coulter Optima L-80, Beckman, USA) (modified from Chen *et al*., 2007)

3.2.6.2 Principle of lyophilization

Lyophilization is a water removal process from a substance thus producing a dry powder. This is performed below the triple point under temperature and pressure conditions that allow for co-existing of the three phases, solid, liquid, gas in complete thermodynamic equilibrium. First is the freezing phase which allows for the conversion of water into ice (Nireesha *et al*., 2013). Secondly is drying using sublimation, where substances pass directly from solid state to gaseous state without going through the liquid state. Lastly, a secondary drying to remove unfrozen water by desorption (Kasper and Friess, 2011). Lyophilization is used to maintain the integrity of the physiochemical properties of colloidal systems, for stability and enhanced shelf-life (Abdelwahed *et al*., 2006).

3.2.6.2 Lyophilization procedure

Purified empty and CSS loaded NPs were lyophilized in order to obtain a dry crystalline powder. Washed samples were supplemented with 10% glucose (w/v) as cryoprotectant against freezing and desiccation stresses. The Initiation of lyophilization was marked by the pre-treatment of samples through super-cooling/freezing using liquid nitrogen. Liquid nitrogen was decanted from a Dewar flask into Styrofoam box thus creating a low-temperature bath. Here in, the round bottom flasks were slowly swirled ensured the complete submersion of the samples within the liquid nitrogen. During this process, the samples formed a frozen opaque-like material layering the bottom of the flask. The flasks were then connected to the freeze dryer using the Manifold method. This means that each flask was individually attached to respective ports of the drying manifold/chamber. This step was performed swiftly in order to prevent sample warming (adopted from Abdelwahed *et al*., 2006).

The freeze-drying process was carried out using (VirTis SP Scientific Sentry 2.0) Temperature was kept about - 20 °C and vacuum was kept at 744.24 mTorr. After 24 hours, lyophilized samples were collected, weighed and stored at room temperature for further analysis. Freeze-

drying yielded a white cotton-like crystalline material. The powder was then weighted and used to calculate the % yield.

$$yield\ (\%) = \frac{actual\ weight\ recovered}{(sum\ of\ matrix\ materials\ (DS + CS + Colitin))} \times 100$$

*Note: Before cell culture ensued, lyophilized samples were re-dispersed in distilled water in glass vials under manual agitation. This was performed until complete homogenization was reached. Visual observation indicated aggregate free solutions. The hydrodynamic diameter (nm), ζ-potential and dispersity (PDI) were measured for each sample to ensure that the NPs had the same physiochemical characteristics as before lyophilization.

3. 2.7 Biological characterization of CS-DS NPs

The aim of this section was to establish a comparative analysis of the possible *in vitro* cytotoxic effects of CS-DS NPs (empty and CSS loaded) versus free-drug CSS on the BBB. Additionally, ascertain the paracellular permeability of endothelial cells in the presence of NP and free drug. As well as elucidate the localization of particles on the endothelial surface layer.

The bEnd5 cells were obtained from Highveld Biologicals agents from American Type Culture Collection (ATCC) (The endothelial cells are a subculture from isolates of the cerebral cortex of mice. Immortalization was performed via the transfecting of the primary cells with the retrovirus vector that encodes for polyomavirus middle T antigen. Endothelial characterization was according to the expression of endothelial specific proteins, Platelet Endothelial Cell Adhesion Molecule, PECAM-1, and Panendothelial Cell Antigen Antibody, MECA-32 (Yang *et al*., 2017). The bEnd5 that were stored at -80 °C, thawed at room RT and then centrifuged for 5 min at 1000 rpm. The supernatant was discarded and the pellet was re-suspended in 1ml supplemented DMEM (10% FBS, 1% non-essential amino acids (NEAA), 1% sodium pyruvate and 1% *Penicillin* and *Streptomycin,* as described in Section 3.2.2). 100ul of the cell suspension was transferred into 75 cm^2 flasks containing 10ml media, incubated at 37°C under 95% humidity and 0, 5% CO_2. After 24 hours, bEnd5 monolayer formation (cell attachment) was confirmed using an Inverted Phase Contrast Microscope (Zeiss, South Africa).

**Note: Subsequent experiments were conducted when the cells reached 70-80% confluence. The passage number used was maintained below 40 to prevent using cells that may have reached senescence. Aseptic austerity measures were implemented at all times during culturing and experimental procedures.*

Lyophilized samples were re-suspended in DI to a concentration of 9.6 µg/ml. CSS was prepared separately in 10 ml DI to make 9.6 µg/ml. All samples were prepared in the laminar flow in sterile conditions to avoid bEnd5 cell contamination.

3.2.7.1 The in vitro evaluation of the cytotoxic effects of CS-DS NPs on bEnd5

3.2.7.1.1 Principle of Trypan blue cell viability assay

Trypan blue is an exclusion dye that allows for the differentiation and subsequent enumeration of viable (live) and non-viable (dead) cells within a cell suspension. The principle of which is based on the selectively permeable nature of cell membranes, viable cells possess intact membranes which impede the entry of trypan blue into the cytoplasmic space of the cell. Non-viable cells have diminished structural cell membrane integrity which allows for the entry of the dye into the cellular space. Consequently, viable cells are excluded from being stained thus retain their white colour/incandescent appearance under microscopic observation. Non-viable cells retain the dye thus have a distinctive blue colour (Strober *et al*., 2001).

3.2.7.1.2 BEnd5 cell seeding

When cell-confluency was reached DMEM was decanted; the monolayer was washed with 2 ml of PBS. The monolayer was then exposed to 1 ml of 0.25X Trypsin and left for 2-3 mins in the incubator to facilitate complete detachment. 1 ml of DMEM was then added to the flask to neutralize the trypsin. A cell pellet was collected by centrifuging the cells and re-suspending in an equal volume of fresh media. Cell quantification was performed using the trypan blue assay, this was to assess whether cell numbers within the culture flasks were sufficient for subsequent seeding.

3.2.7.1.3 BEnd5 cell treatment with CSS, empty, and CSS loaded CS-DS NPs

BEnd5 cells were seeded in 3 cm Petri-dishes (Cell Star, Cat no.627 160) at a seeding density of 50 000cells/ml and sample number of 5 dishes per control and experimental set (n=5, seeding day=0). After 24 hours, the cells were independently treated with 9.6µg/ml of CSS (free-drug only), empty and CSS loaded CS-DS NPs - the control was set as cells cultured in DMEM only. The cells were incubated at 37°C under 95% humidity and 0, 5% CO_2 for 24, 48, 72 and 96 hours. Cells treatment was carried out as an acute once-off exposure as well as chronic daily exposure. In the acute exposure; cells were exposed for 24 hours only. Thereafter, cells were replenished with fresh media daily up to and including 96 hours. In the chronic exposure: cells incurred repeat treatment daily up to and including 96 hours.

3.2.7.1.4 Preparation of bEnd5 cells for counting

After each period, the cells were removed from the incubator the media was aspirated from pert-dishes followed by washing with PBS (pH 7.4). Each Petri was trypsinated and incubated

for 2-3 mins to ensure complete detachment. After microscopic confirmation of cellular detachment, the trypsin was neutralized with equal volumes of media. Cells were centrifuged and the supernatant was removed- ensuring not to disrupt the cell pellet. The disruption of the cell pellet could dislodge cells into the supernatant, which could ultimately skew the data as some of the cells would have been lost when the supernatant was discarded. The cell pellet was re-distributed in fresh media after which % toxicity and viability were determined.

3.2.7.1.5 Determining toxicity and viability; cell counting using Neubauer haemocytometer

10 µl of cell suspension and 10 µl of trypan blue dye were mixed in a 96 well plate (1:1). The mixing order was performed where trypan blue was pipetted secondary into the cell suspension in the wells. This creates a concentration gradient where cells are gradually exposed to trypan blue. 10 µl of the mixture was pipetted on the two counting chambers (semi-reflective rectangles) of the hemocytometer (Figure 3.3). Accordingly, the enumeration of live and dead cells in the gridded squares of the chambers ensued under the Inverted Phase Microscope (Zeiss, South Africa).

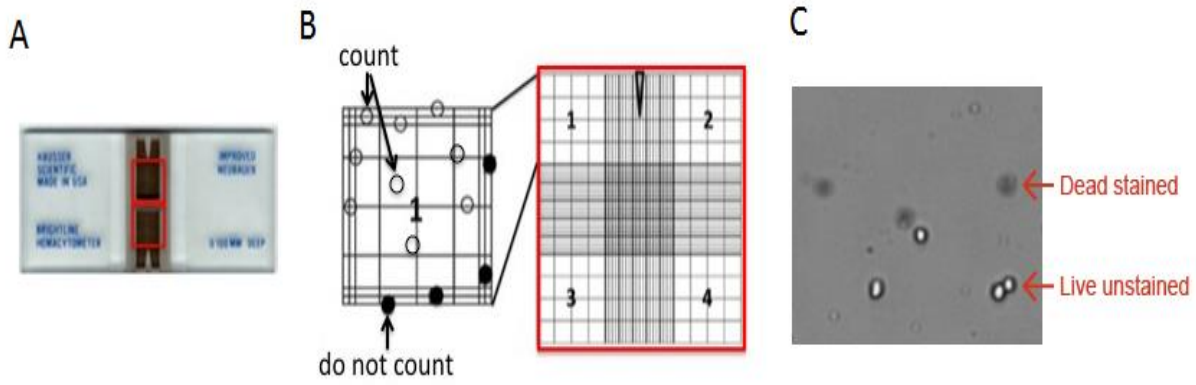

Figure 3.3 Schematic diagram showing (A) hemocytometer with counting two parallel counting chambers in which sample is loaded, (B) grid lines guiding for counting where black cells represent cells outside counting parameters. (C) Trypan blue exclusion method visualized under inverted phase microscope showing white incandescent cells as viable cells versus darkened/blue stained cells as dead cells (http://mityeast.pbworks.com/w/page/67636412/TW%202013%20lab%20manual%20final%202).

**Note: A cell number total (including dead and live) was expressed as the average number counted on both chambers of the hemocytometer. Each cell viewed represented a colony of X* 10^3

Cell viability and toxicity was calculated as follows;

$$\text{Viability (\%)} = \frac{\text{Number of unstained (live) cells}}{\text{total number of cells}} \text{ x } 100$$

$$\text{Toxicity (\%)} = \frac{\text{Number of stained (dead) cells}}{\text{total number of cells}} \text{ x } 100$$

3.2.7.1.6 Cryopreservation

After seeding, the remaining cells were centrifuged and re-suspended in cryomedia (90% FBS and 10% Dimethyl sulfoxide). 1ml aliquots of the cell suspension were placed into cryovials and stored in liquid nitrogen.

3.2.7.2 The Bioelectrical analysis of CS-DS NPs on TEER across the bEnd5 endothelial monolayer

3.2.7.2.1 Principle of TEER

TEER pertains to the electrical resistance across the endothelial monolayer expressed as Ωhms.cm^2 (measured by ohmmeter). It can be used as an inference to the tautness of the paracellular space in between the endothelial cells and hence a measure of permeability across the monolayer. Functionally, TEER is an attribution to the transmembranous tight junction restricting solute permeation through the paracellular space. The bioelectrical resistance obtained across the endothelial monolayer would then be inversely proportional to its permeability (Rempe *et al*., 2011). *In vitro,* a Transwell® system can be established to mimic the *in vivo* BBB model. The aim of the model would be to functionally simulate, as close as possible, the unique features of the *in vivo* BBB model. The *in vitro* model utilizes a Transwell® with a porous membrane situated within a well to physical demarcate and simulate the luminal and abluminal compartments of the BBB (Fu, 2012). This also forms a vertical diffusion system that can be used to assess the physical movements of solutes across the monolayer. The Transwell® system used in the experimental set up resembled the *in vivo* environment in that it comprised of like endothelial cell morphology with a restrictive paracellular pathway maintained by the tight junctions and luminal and abluminal compartments (Chen and Liu, 2012).

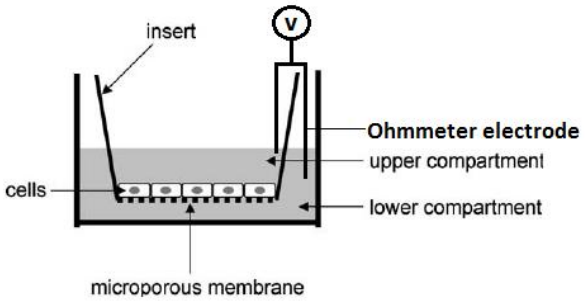

Figure 3.4 Schematic diagram showing TEER operating principle with Transwell® insert set up. Cells cultured on cellulose membrane of the Transwell® insert, which is fitted into the 96-well plates to form a luminal and basolateral lower compartment. Each hand of the electrode is inserted into the insert with the shorter electrode in the luminal compartment and the longer into the basolateral compartment (Benson *et al*., 2013).

3.2.7.2.2 Establishing transendothelial electrical resistance base-line readings as a control

In order to ascertain the true resistance across the monolayer, TEER readings were performed on Transwell® plates devoid of cells. This experimental outline included treating the Transwell® inserts with the appropriate empty and CSS loaded CS-DS NPs. This was performed as an austerity measure in assessing whether the experimental conditions would affect the resistivity of the media. If so, then the effect of the treatment on the cells would be in fact an attribution of the resistivity of the media onto the cells-which would not be a true representation of the effects of the sole treatment on the cells. Transwell® insert with a pore size of 0.45µm, filtration diameter of 12mm and an effective filtration area of 0.6cm^2 were placed in a 96 well plate (Figure 3.4). DMEM was added to both luminal (300 µl) and basolateral compartments (500 µl) and incubated at 37°C under 5% CO2 devoid of bEnd5 cells (n=5, day=0). After which, 9.6 µg/ml of CSS, empty and CSS-loaded NPs was added to the luminal compartment of the insert. TEER readings were conducted using the electrical resistance system (Millipore, Cat no MERS 000 01). Sample readings were obtained every day (in triplicates, two times a day) for 24-96 hours.

3.2.7.2.3 Seeding bEnd5 cells for treatment and transendothelial resistance readings

BEnd5 cells were seeded on filter membrane at a density of 500 000 cells/cm^3. DMEM was added to both luminal (300 µl) and basolateral compartments (500 µl) and the cells were allowed to attach to the surface of the filter membrane overnight thus incubated at 37°C under

5% CO_2. After 24 hours, the monolayer was exposed to 9.6 µg/ml of CSS, empty and CSS-loaded NPs, daily for 24, 48, 72 and 96 hours.

3.2.7.2.4 Measuring the transendothelial resistance across the bEnd5 cell monolayer

The culture plates were removed from the incubator and placed into the laminar flow to for 20-30 min to allow for acclimatization. The electrodes were placed in 70% ethanol and PBS (for 15 mins consecutively to encourage electrode surface stabilization).

TEER electrodes were submerged into the plates containing the inserts; the shorter electrode was placed in the luminal compartment; the longer electrode was placed in the basolateral compartment. For accuracy and precision, the electrodes were kept steady for 5 mins whilst the readings were underway. Each reading was performed cautiously ensuring that the shorter electrode did not come into contact with the monolayer on filter surface-this could pierce the cellulose membrane and significantly alter the integrity of the monolayer. All readings were performed in triplicates twice per day also for 24-96 hours.

TEER values obtained from the control readings (devoid of cells) were subtracted from the values from experimental readings (with cells) - this signifies the *true resistance* which was calculated as follows:

True resistance = (Experimental reading - Blank reading) X 0.6cm^2 (effective filtration area) (Srinivasan *et al*., 2005).

3.2.7.3 High-Resolution Scanning Electron Microscopy

3.2.7.3.1 Operating principle of the SEM

High-Resolution Scanning Electron Microscopy (HR-SEM) was used to analyze the topographical localization and interaction of the CS-DS NPs with the bEnd5 cell monolayer. SEM results in the production of three-dimensional images with great magnification and field of depth. The SEM instrument has six main components; an electron column, a scanning system, detector(s), a display, a vacuum system and electronic controls. Contained within is an electron gun which is the source of the electrons that will be passed through the electron column and thus bombarded on the specimen surface. A series of lenses (condenser and objects) that controls the diameter of the electron beam emanating from the electron column (JEOL, 2006). Additionally, there is a series of apertures (micron-scale holes in the metal film) which direct and manipulate the properties of the electron beam. This is also facilitated by the adaptation of functional controls for the position of the specimen position relative to height and orientation (allowing for the tilting and rotation of specimen). Also included in SEM is a beam-specimen interaction area that allows for the scanning and processing of specimens in response to electron stimuli resulting in an image. Finally is the vacuum system which facilitates the regulation of working pressure atmosphere of the upper column and specimen chamber (Figure 3.5) (Goldstein *et al*., 2017).

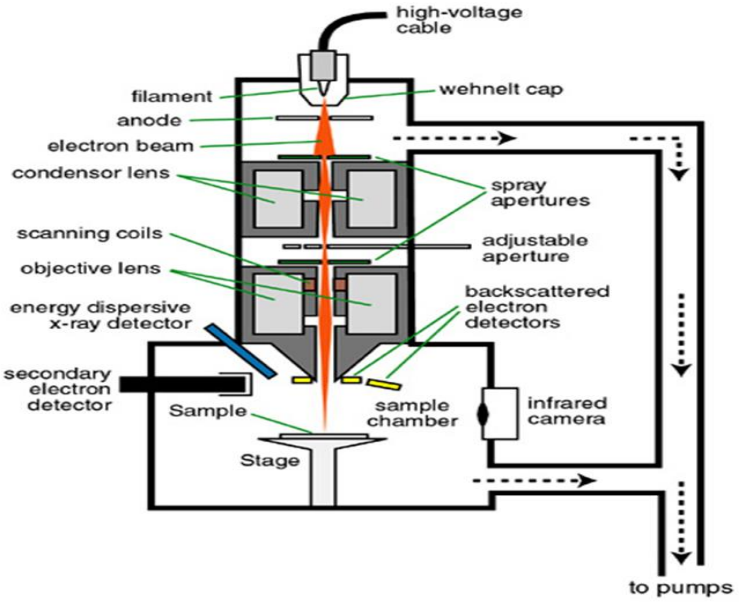

Figure 3.5 Schematic diagram showing the functional components of SEM (http://saturno.fmc.uam.es/web/superficies/instrumentacion/Instrumentation.htm)

Contained within the SEM electron column is a thermionic electron gun (TE gun) with multiple electromagnetic lenses under a vacuum. The TE gun is the generates and accelerates free electrons (Reichelt, 2007). These electrons are generated by heating a thin cathode filament made of 0.1 nm tungsten wire. When high temperatures of approximately 2800K are reached the electrons are emitted from the cathode filament. Subsequently, the electrons are collected as an electron beam that is passed through to the anode (metal plate) by applying a positive voltage to the anode (1-30kV) (Goldstein *et al*., 2017). Ultimately, electron lenses create a small, streamline ultra-focused electron beam containing accelerated electrons (possessing energies between 1-40 keV) for the specimen. Once the focused beam hits the specimen, the interaction is detailed a series of signals in the form of electromagnetic radiation. These signals include secondary electrons (SE) which are refractory electrons from the primary focus beam and/or backscattered electrons (BSE). The SE become attracted to a Scintillator coated on the tip of the secondary electron detector due to a high voltage being applied to the detector. Interaction of the SE and the detector results in the generation of light which is directed by a photomultiplier tube. This light is converted into an electrical signal which is then amplified and transmitted to the display unit for imaging (Figure 3.6) (Oatley *et al*., 1966).

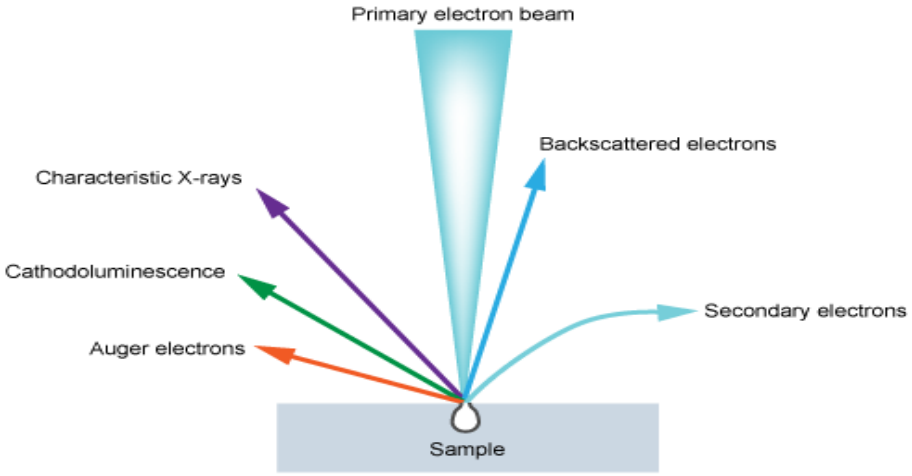

Figure 3.6 Schematic diagram showing backscattered and secondary electrons from SEM primary electron beam (http://www.ammrf.org.au/myscope/sem/background/concepts/interactions.php).

3.2.7.3.2 Bend5 preparation: fixation and dehydration

The culture medium was removed from the well of the inserts then flipped right-side down onto a tissue paper sprayed with ethanol. A sterilized scalpel was used to gently indent the edges forming the circumference of the cellulose membrane. This was performed until the membrane was dissociated from the plastic rim of the insert. Forceps were used to place the membranes into 6 well plates ensuring that the surface containing bEnd5 monolayer was orientated right-side up.

The bEnd5 cells were fixed in 2 ml of 2.5% glutaraldehyde in PBS solution. After an hour, the cells were washed twice with 2 ml 100% PBS solution for 5 minutes then twice with distilled water for 5 mins.

The bEnd5 cells were Dehydrated using increasing concentrations of ethanol (50, 70, 90, 95, and 100% ethanol for 10 minutes sequentially). This was followed by a secondary exposure to 100% ethanol (10mins) performed just before critical point drying (CPD). The membrane was handled with caution during the dehydration phase.

3.2.7.3.3 Critical point drying

Critical point drying was carried out using Hitachi hcp-2. The dryer was cooled to 10°C before submerging the specimen holder. The vessel was filled with 50-80% with liquefied carbon dioxide (three cycles). After the critical point, 37°C (73kg/cm), fixed samples were removed

from the chamber by allowing the chamber to cool down to 20-22°C. The gas was discharged from the chamber. The membranes were removed from the specimen holder and mounted on carbon adhesive tape applied on an aluminium studs (12.5 mm and 8 mm). Each stud was sputter coated (Q150T, GS Quorum sputter coater) with gold-palladium for 2 mins and viewed with the Auriga HR-SEM F50 with a voltage of 5 KV (Zeiss Auriga high-resolution field SEM, South Africa).

3.3 Statistical analysis

The data is presented as the mean ± standard error (SE) for all data denoting to cell culturing and as the mean ± standard deviation (SD) for particle size (nm), ζ-potential (mV) and PDI n=3.The data was captured and analyzed using GraphPad Prism (version 6.01). The data was analyzed using one-way or two-way ANOVA. Differences were considered significant at $p < 0.05$. Significance levels of the data were determined using a Tukey range test in conjunction with an ANOVA. The degree of significance was presented for p-value if; $p < 0.05$(*), $p < 0.01$(**) or $p < 0.001$(***).

CHAPTER FOUR: RESULTS

4.1 Chemical characterization in of CS-DS NPs in deionized water

Inherent NP physicochemical properties correspond to their biological performance. Hydrodynamic diameter, PDI and ζ-potential properties are important factors that ultimately determine drug loading capacity, the rate of drug release, bioavailability, biodistribution, stability and toxicity (Kharia *et al.*, 2012). Hence, physicochemical characterization is rudimentary in understanding and predicting NP behaviour (Nguyena and Paika, 2012). In this study, DLS was used to elucidate the relationship between charge index (N:P) and CS-DS NPs physiochemical properties. The charge index of CS-DS NPs was expressed as the ratio of negatively charged DS sulphate functional groups (N) to positively charged CS amino functional groups (P).

4.1.1. The effect of charge index (N:P) on the hydrodynamic diameter of CS-DS NPs

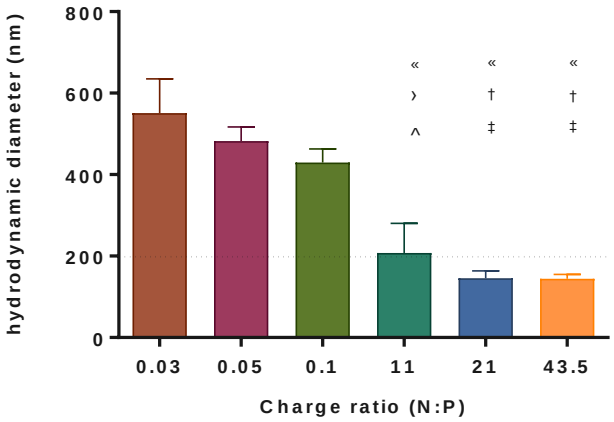

Figure 4.1 The effect of charge index (N:P) on CS-DS hydrodynamic diameter (nm). NPs were synthesized using negatively charged DS (0.1% w/v) and positively charged CS (0.1% w/v), pH3.2. Statistically significant differences are annotated as: (") significant difference from charge ratio 0.03, $P < 0.0001$. (†) significant difference from charge ratio 0.05, $P < 0.001$. (>) significant difference from charge ratio 0.05, $P < 0.0001$. (‡) significant difference from charge ratio 0.1, $P < 0.01$. (^) significant difference from charge ratio 0.1, $P < 0.001$. The dotted line signifies hydrodynamic diameter less than 200 nm. Data representation; n=3; mean ± SD (see methods, Section 3.3).

In Figure 4.1; holistically, an inverse relationship existed between the hydrodynamic diameter and the charge index, i.e. an increase in the charge index correlated to a statistically significant decrease in hydrodynamic diameter. This was observed between the range of the lowest charge index value 0.03 (551 ± 84.05 nm) to the highest charge index value 43.5 (144.4 ± 10.89 nm) ($P < 0.0001$). However, within certain intervals the proportion of change in the charge index did not influence the hydrodynamic diameter, hence, no significant differences were observed in increasing the charge index from 0.03 (551 ± 84.05 nm), 0.05 (482.6 ± 34.25 nm) and 0.1 (429.8 ± 33.33 nm). Similarly, there was no statistically significant difference when the charge index was increased from 11 (207.8 ± 72.54 nm) to 21 (145.7 ± 17.97 nm) and 43.5 (144.4 ± 10.89 nm). Hence, the crucial points of determination seemed to be charge index 0.1 and 11. A dramatic decrease in hydrodynamic diameter was noted when the charge ratio increased from 0.1 (429.8 ± 33.33 nm) to 11 (207.8 ± 72.54 nm) ($P < 0.0001$). As a result, all charge indices greater than 11 pertained to hydrodynamic diameters that were significantly smaller than those obtained before charge index 0.1. The results showed that charge index 21 and 43 yielded the smallest sizes of 145.7 ± 17.97 nm and 144.4 ± 10.89 nm, respectively.

4.1.2. The effect of charge index (N:P) on the ζ-potential CS-DS NPs

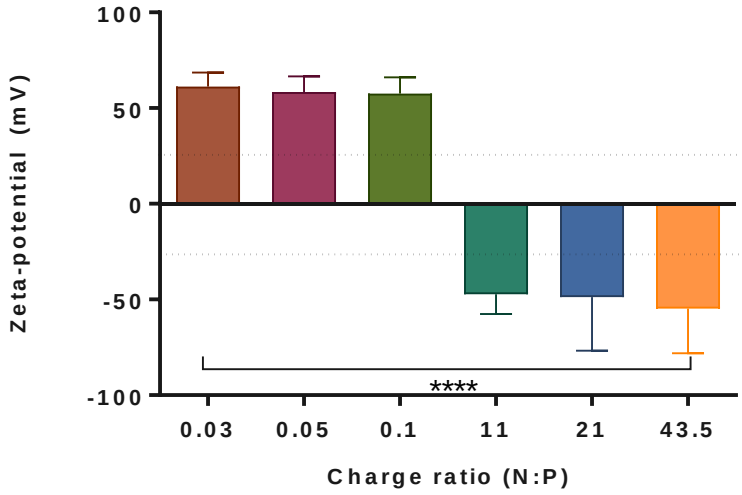

Figure 4.2 The effect of charge index (N:P) on CS-DS ζ-potential (mV). NPs were synthesized using negatively charged DS (0.1% w/v) and positively charged CS (0.1% w/v), pH3.2. Statistically significant differences are annotated by asterisks (**** $P < 0.0001$). The dotted line signifies NPs with ζ-potential $-30 \geq mV \geq 30$. Data representation; n=3; mean ± SD (see methods, Section 3.3).

As the charge index increased from 0.03 to 43.5, the net charge of the NPs significantly decreased from a highly positive ζ-potential (61.27 ± 7.27 mV) to negative ζ-potential (-54.77 ± 23.29 mV), respectively (P<0.0001) (Figure 4.2). The charge index determined the ζ-potential profile of the CS-DS NPs thus divided the NPs into discriminatory groups of positive and negative charge. Hence, charge index 0.03 (61.27 ± 7.27 mV), 0.05 (58.37 ±8.20 mV) and 0.1 (57.63 ± 8.37 mV) pertained to positively charged NPs. On the other hand, charge index 11 (-47.27 ± 10.35 mV), 21 (-48.73 ± 28.02 mV) and 43.5(-54.77 ± 23.29 mV) pertained to negatively charged NPs. The discriminatory points of charge profiling were observed to be between charge index 0.1 and 11. Herein a statistically significant decline and subsequent change in the ζ-potential profile was observed (57.63 ± 8.37 mV to -47.27 ± 10.35 mV), respectively (P<0.0001).

4.1.3. The effect of charge index (N:P) on the PDI of CS-DS NPs

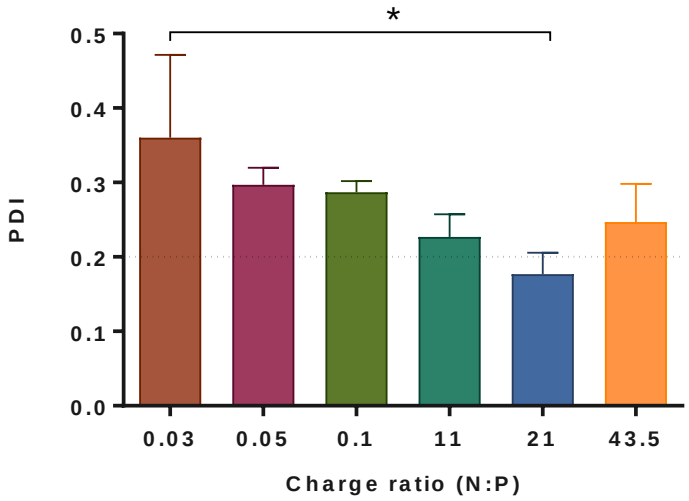

Figure 4.3 The effect of charge ratio (N:P) on CS-DS NPs PDI. NPs were synthesized using negatively charged DS (0.1% w/v) and positively charged CS (0.1% w/v), pH3.2. Statistically significant differences annotated by asterisks (*P < 0.05). The dotted line signifies NPs with PDI 0.0 > dispersity index ≤ 0.2. Data representation; n=3; mean ± SD (see methods, Section 3.3).

An observable decrease in NP dispersity was noted with an increase in charge index; however, this decrease was statistically insignificant (Figure 4.3). Statistically, only charge index 21 (0.17 ± 0.02) significantly differed to 0.03 (0.36 ± 0.11) (P<0.05). All the charge indices displayed a degree of colloidal uniformity with a PDI range between 0.1 and 0.4 with 21 (0.17 ± 0.02) yielding NP with the highest observable degree of uniformity.

4.2 Chemical characterization of NPs in biological milieu

Utilization of NPs in biological milieu has gained significant traction. This, in part, is due to the exponential and prospective applications of NPs as drug delivery systems. (Aggarwal *et al*, 2009). *In vivo*, NP interaction is primarily initiated in plasma. Plasma, however, contains an array of proteins that compete and subsequently bind to the chemically active and large surface area-to-volume ratio of NPs. This alters the native physicochemical profile of the NPs thus affecting subsequent biological performance. Hence, characterization of the differences between the synthetic and biological identity of NPs is significant in predicting their biological behaviour (Lynch and Dawson, 2008; Casals *et al.*, 2010). However, due to the exponential NPs types as well as cell culture environments, data pertaining to the functionality of NPs in bEnd5 specific media is yet still limited. This section of work involves the characterization of CS-DS NPs physicochemical properties in biological media; DMEM (serum-free and serum-containing) as well as PBS.

4.2.1 The effect of biological media on the hydrodynamic diameter of CS-DS NPs

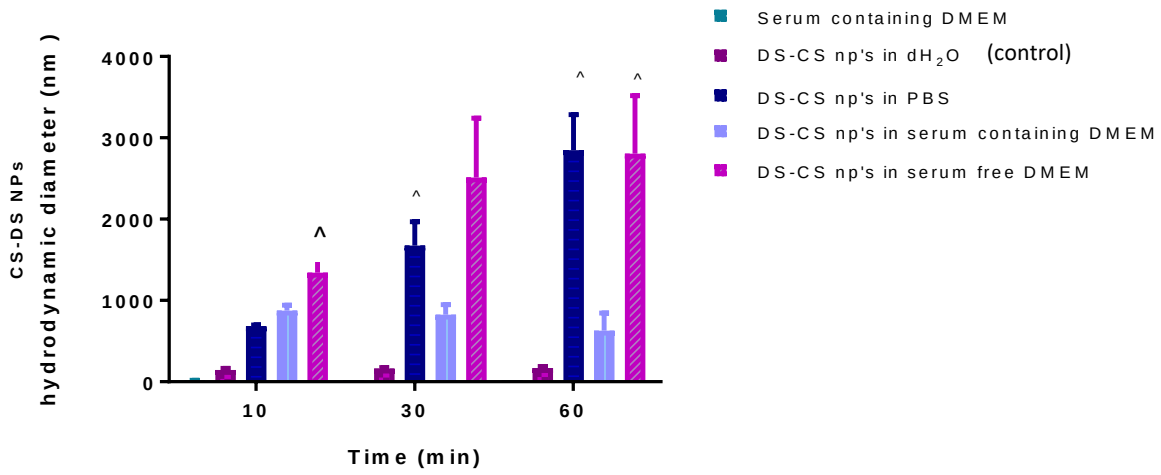

Figure 4.4 The effect of biological media on the hydrodynamic diameter of CS-DS NPs synthesized using charge index (N:P) 21. CS-DS NPs incubated for 10, 30 and 60 min at 37 ^{0}C in DMEM (serum-free and containing), PBS and control (NPs in DI)-pH 7.4 and 3.2, respectively. (^) denotes statistically significant differences from control ($P<0.001$). Data representation; n=3; mean ± SD (see methods, Section 3.3).

At 10 min, although observable increases were noted, no statistically significant differences were found in the hydrodynamic diameters of CS-DS NPs exposed to serum-containing DMEM and PBS relative to the control (NPs in water) (Figure 4.4). CS-DS NPs exposed to serum-free DMEM were, statistically, significantly larger than the control. These differences were noted as an increase to from 146.43 ± 17.38 nm to 1342.67 ± 203.56 nm ($P<0.01$).

At 30 min, although observable increases were displayed, no statistically significant differences were noted in the hydrodynamic diameter of CS-DS NPs exposed to serum-containing DMEM relative to the control. However, yet again, CS-DS NPs exposed to serum-free DMEM were significantly larger than the control. Herein, a statistically significant increase to 2511 ± 421.46 from 160.26 ± 7.56 nm was observed (respectively, $P<0.01$). This was also true for CS-DS NPs exposed to PBS relative to the control, NP hydrodynamic diameter increased to 1673.6 ± 169.33 nm from 160.26 ± 7.56 nm (respectively, $P<0.0001$). Moreover, CS-DS NPs exposed to serum-free DMEM (2511 ± 421.46 nm) were significantly larger than those in serum-containing DMEM (824.56 ± 72.21) as well as PBS (1673.6 ± 169.33 nm) ($P<0.01$, $P<0.0001$, respectively).

At 60 min, although observable increases were displayed, no statistically significant differences were noted in the hydrodynamic diameter of CS-DS NPs exposed to serum-containing DMEM relative to the control. However, CS-DS NPs exposed to serum-free DMEM were significantly larger relative to the control. The hydrodynamic diameter increased to 2805.33 ± 412 nm from 167.47 ± 19.52 nm. This was also true for CS-DS NPs exposed to PBS relative to the control with a significant increase to 2847.33 ±251.9 nm from 167.47 ± 19.52 nm (respectively, $P<0.0001$). No significant differences were observed between CS-DS NPs exposed to serum-free DMEM in comparison to PBS.

No significant differences were observed in CS-DS NPs in serum-containing DMEM from 10, 30 to 60 min. On the other hand, CS-DS NPs exposed to serum-free DMEM incurred significant increases from 10 to 60 min (1342.67 ± 203.56 nm to 2805.33) ($P<0.001$). This was also true for CS-DS NPs exposed to PBS as significant increases from 10 to 30 min (682.8 ± 8.71 nm to 1673.6 ± 169.33 nm, respectively) ($P<0.01$), Hence, the interaction of CS-DS NPs with serum-free DMEM was characterized by an initial and sustained increase over time. Conversely, CS-DS NPs exposed to PBS gradually increased over time.

4.2.2 The effect of biological media on the ζ-potential of CS-DS NPs

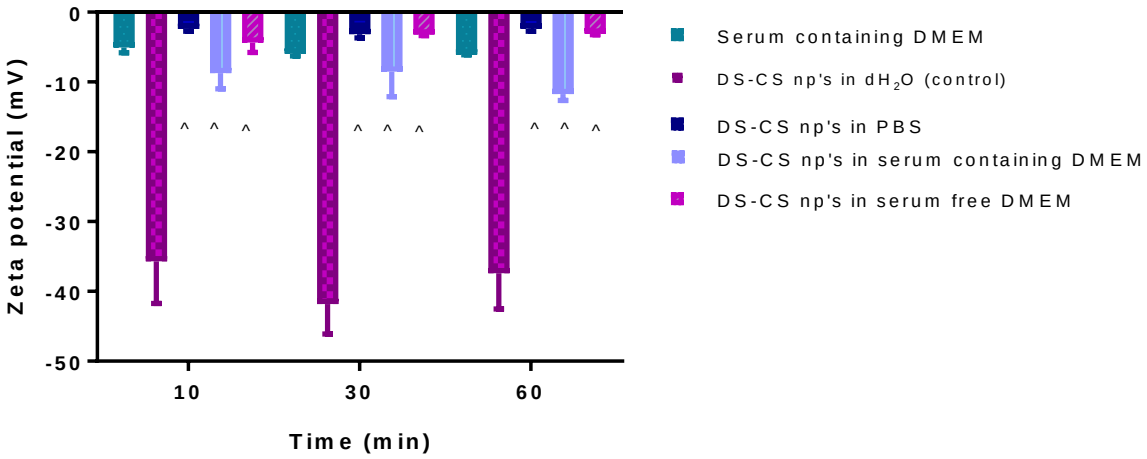

Figure 4.5 The effect of biological media on the ζ-potential of CS-DS NPs synthesized using charge index (N:P) 21. CS-DS NPs incubated for 10, 30 and 60 min at 37 ^{0}C in DMEM (serum-free and containing), PBS and control (NPs in DI)-pH 7.4 and 3.2, respectively. Data is represented in triplicates (mean ± SD). (^) denotes statistically significant differences from control (P<0.001). Data representation; n=3; mean ± SD (see methods, Section 3.3).

The interaction of CS-DS NPs with biological media was marked by a significant increase in the ζ-potential (Figure 4.5). After 10 min of incubation, an observable increase in ζ-potential (migration of ζ-potential values towards positive values) occurred in PBS, serum-containing and serum-free DMEM. The innate charge of DMEM was found to be significantly higher than that of the control (-5.08 ± 0.41 mV and -35.7 ± 3.47 mV, respectively (P<0.0001)).

At 10 min, a statistically significant increase in the ζ-potential was observed when the CS-DS NPs were exposed to serum-containing DMEM relative to the control, from -35.7 ± 3.47 mV to -8.74 ± 1.27 mV (P<0.0001). When exposed to serum-free DMEM, a statistically significant increase in ζ-potential was observed relative to the control, from -35.7 ± 3.47 mV and - 4.35 ± 0.80 mV (P<0.0001). These results were synonymous to those of CS-DS NPs exposed to PBS relative to the control, where a statistically significant increase in ζ-potential was observed from -35.7 ± 3.47 mV to -2.39 ± 0.19 mV, respectively (P<0.0001).

At 30 min, the innate ζ-potential of DMEM was found to be significantly higher than that of the control (-5.94 ± 0.41 mV and -41.8 ± 2.48 mV, respectively (P<0.0001). Hence, when the CS-DS NPs were exposed to serum-containing DMEM, a significant increase was observed in the ζ-potential relative to the control, from -41.8 ± 2.48 mV to -8.51 ± 2.06 mV (P<0.0001).

Similarly, a significant increase in the ζ-potential of CS-DS NPs exposed to serum-free DMEM was observed relative to the control from -41.8 ± 2.48 mV to -3.17 ± 0.1 mV respectively (P<0.0001). CS-DS NPs exposed to PBS also displayed a significantly higher ζ-potential than the control (-3.15 ± 0.29 mV and 41.8 ± 2.48 mV, respectively (P<0.0001))

At 60 min, the innate ζ-potential of DMEM was found to be significantly higher than that of the control (-6.07 ± 0.02 mV and -37.4 ± 2.48 mV, respectively (P<0.05)). Hence, when the CS-DS NPs were exposed to serum-containing DMEM, a significant increase was observed in the ζ-potential relative to the control; from -37.4 ± 2.48 mV to -11.74 ± 0.52 mV, (P<0.0001). CS-DS NPs exposed to serum-free DMEM also incurred a significant increase in ζ-potential relative to the control, from -37.4 ± 2.48 mV to -3.05 ± 0.1 mV (P<0.0001). CS-DS NPs exposed to PBS also displayed a significant increase in ζ-potential relative to the control; from -37.4 ± 2.48 mV to -2.35 ± 0.21 mV (P<0.0001).

4.2.3 The effect of biological media on the PDI of CS-DS NPs

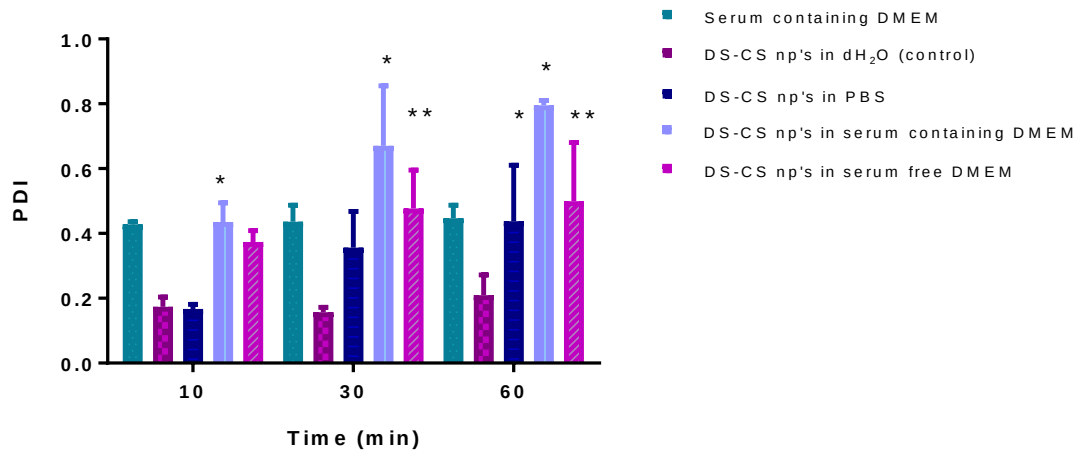

Figure 4.6 The effect of biological media on the PDI of CS-DS NPs synthesized using charge index (N:P) 21. The control was set as CS-DS NPs in DI. CS-DS NPs incubated for 10, 30 and 60 min at 37 ^{0}C in DMEM (serum-free and containing), PBS and control (NPs in DI)-pH 7.4 and 3.2, respectively. Asterisks (*) denotes statistically significant differences from control (*P<0.05, ** P<0.01) Data representation; n=3; mean ± SD (see methods, Section 3.3).

At 10 min, the PDI of serum-containing DMEM was observed to be inherently high with a value of 0.428 ± 0.005 (Figure 4.6). This was significantly higher than that of the control (CS-DS NPs in DI) (0.173 ±0.018) (P<0.05). Hence, when the CS-DS NPs were exposed to serum-containing DMEM, the degree of dispersity was significantly high (0.435 ± 0.034) relative to the control (respectively, P<0.05). CS-DS NPs exposed to serum-containing DMEM also

displayed a higher degree of dispersity than PBS (0.167 ± 0.008) ($P<0.05$). However, no significant differences were observed between CS-DS NPs exposed to serum-containing and serum-free DMEM.

At 30 min, the PDI of serum-containing DMEM remained significantly higher than the control (0.437 ± 0.029 and 0.157 ± 0.009, respectively ($P<0.05$)). This was also significantly higher than CS-DS NPs exposed to PBS (0.356 ± 0.06, ($P<0.05$)). When the CS-DS NPs were exposed to serum-containing DMEM, a significantly higher degree of dispersity was obtained, relative to the control (0.67 ± 0.107 and 0.157 ± 0.009, respectively ($P<0.05$)). This was also true for CS-DS NPs exposed to serum-free DMEM. Herein, a significantly higher degree of dispersity was observed, relative to the control (0.477 ± 0.68 and 0.157 ± 0.009, respectively ($P<0.05$)).

At 60 min, the dispersity index of serum-containing DMEM remained significantly higher than the control (0.447 ± 0.023 and 0.210 ± 0.036, respectively ($P<0.05$)). Exposure of the CS-DS NPs to serum-containing DMEM pertained to significantly higher degree of dispersity relative to the control (0.447 ± 0.023 and 0.210 ± 0.036, respectively ($P<0.0001$)). Moreover, CS-DS NPs exposed to serum-containing DMEM displayed a higher degree of dispersity relative to PBS and serum-free DMEM (0.438 ± 0.1 and 0.447 ± 0.023 ($P<0.001$, $P<0.001$), respectively)

CS-DS NPs exposed to serum-containing DMEM exhibited a greater degree of non-uniformity relative to the control over time. The relatively high PDI values were synonymous with those found in serum DMEM overtime. This is also true for CS-DS NPs exposed to serum-free DMEM and PBS in comparison to the control.

4.3. Quantification of CSS encapsulated in CS-DS NPs

NPs have gained a considerable amount of attention pertaining to their drug loading characteristics. This has allowed for the design of drug loaded NPs capable of delivering a specific concentration of active compounds to the targeted tissue (Martinho, 2011; Kulkarni and Feng, 2013). The advantage of encapsulating active drugs into NPs serves to improve therapeutic efficiency, enhance bioavailability and protect the chemically active therapeutic compounds (Wallace *et al*., 2010). Hence, this section of work pertained to quantifying the EE (%) of CS-DS NPs. A standard curve was established as a factor of the (ultraviolet) light absorbance of CSS relative to its' concentration. The standard curve was utilized in characterizing the quantity of CSS incorporated into CS-DS NPs. Reproducibility and accuracy assays were performed for the standard curve as a form of method validation.

4.3.1 Establishing the standard curve for CSS

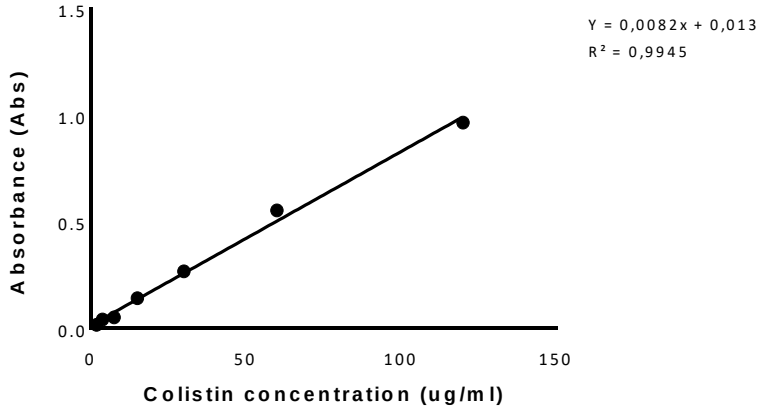

Figure 4.7 Standard calibration curve for CSS, absorbance versus concentration (range 0.175µg/ml to 120µg/ml), in DI water, measured at 210 nm wavelength. Data representation; n=3; mean ± SD (see methods, Section 3.3).

The standard curve generated for CSS showed high regression coefficient of 0.99 with a linear regression equation of y=0.0082x+0.013. The mean slope was 0.007738 to 0.008581 and the y-intercept when x = 0 was -0.009084 to 0.03506 whereas the x-intercept when y=o was -4.452 to 1.077 (Figure 4.7).

4.3.2 Method validation: reproducibility and accuracy assay for CSS standard calibration curve

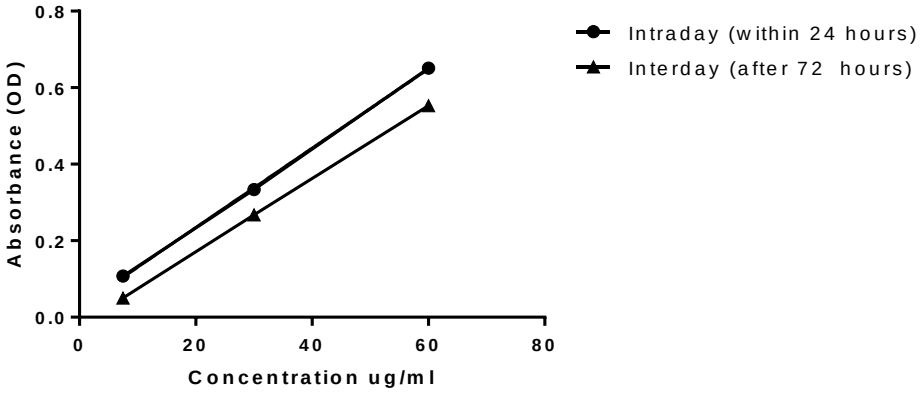

Figure 4.8 Absorbance readings obtained for intraday and interday analysis for CSS concentration 60, 30 and 7.5 µg/ml, in DI water, measured at 210 nm wavelength. Data representation; n=3; mean ± SD (see methods, Section 3.3).

High regression coefficients for the intra-and- inter-day assays were observed (0.92 and 0.97, respectively) (Figure 4.8). The linear regression equations for the assays were y = 0.008417x + 0, 04168 and y = 0.009565x – 0.02059 with mean slope of 0.005879 to 0.01486 and 0.008091 to 0.01104, respectively. Furthermore, no significant differences were noted for the absorbance's obtained at 60, 30 and 7.5 µg/ml at 24 hours relative to after 72 hours. This confirmed that the absorbance of the intra and interday at fixed concentrations, were constant. Hence, intra-and- inter-day assay demonstrated that the UV method utilized was reproducible, accurate and thus appropriate for the quantification of CSS encapsulated in CS-DS NPs.

4.3.3 Determining EE (%)

The encapsulation of CSS in CS-DS NPs was achieved using the incorporation method which entailed the addition of CSS during NP synthesis. This resulted in the spontaneous formation of CSS loaded CS-DS NPs. The indirect method was utilized in the quantification of CSS encapsulated within the NPs. This involved measuring the concentration of CSS found in the aqueous supernatant of CSS incorporated NPs. Using the linear regression equation y=0.0082x+0.0013, based on the calibration curve, the EE (%) was calculated from the absorbance value of the sample supernatant. The EE (%) of the NPs was found to be 9.6 µg/ml (24%).

4.4. Biological characterization in of CS-DS NPs

4.4.1 Cytotoxicity

The appropriation of polymeric NPs as drug delivery systems has gained significant momentum (Rizzello *et al*., 2012). This is especially considering the malleability of physicochemical properties such as hydrodynamic diameter, surface charge, as well as the utilization of biocompatible materials during polymeric NP synthesis such as CS and DS (Tiyaboonchai and Limpeanchob, 2007). Moreover is the ability to rationally design custom polymers for the encapsulation of hydrophobic or hydrophilic drugs that generally show poor permeability across biological barriers like the BBB (Jin *et al*, 2009). Hence, the development of efficient and effective NP entails identifying the correlation of the physiochemical properties of NPs to their biological activity (Khanna *et al*., 2015). In this study, the biological performance of CS-DS NPs was determined by ascertaining the innate *in vitro* toxicity of empty and CSS loaded CS-DS NP relative to free drug. Bend5 cell monolayer was used as a response model to represent the BBB. The experimental set-up included an acute ‘once off’ exposure in order to assess the primary response of the bend5 cells over time. Then, a chronic ‘daily exposure’ to ascertain the response of the bend5 cells to a continuous dose of CS-DS NPs over time.

4.4.1.1 The effects of acute CSS, empty and CSS loaded CS-DS NPs on the bEnd5 cell monolayer

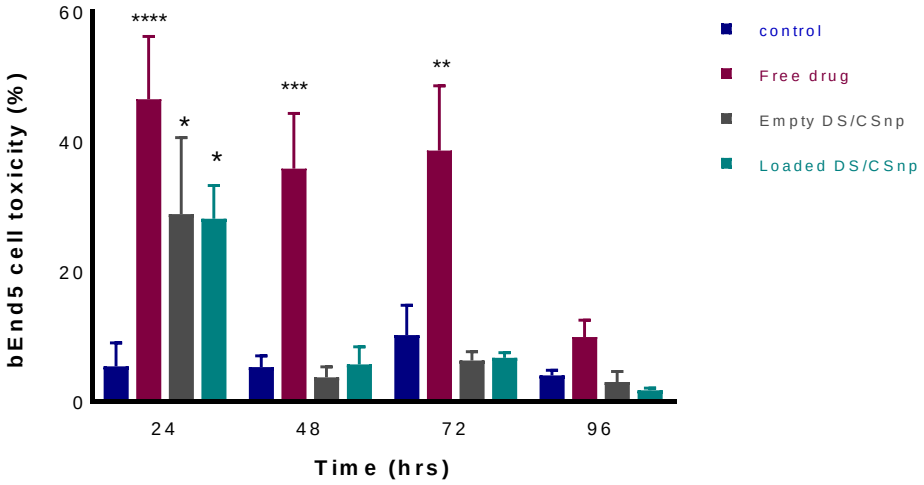

Figure 4.9 The Toxicity (%) to bend5 cells after acute treatment using CSS, empty and CSS loaded CS-DS NPs (0.96 mg/ml for all) for 24-96 hrs. The NPs were synthesized using charge index 21 (0.1% w/v CS/DS) The mean diameter for empty and CSS loaded NPs was 145.7 ± 17.97 nm and 125.8 ± 1.8 nm, respectively. Statistically significant differences are denoted with an asterisk(s) (*statistically different from the control; * P<0.05, ** P<0.01, *** P<0.001, **** P<0.0001). Data is expressed as mean ± SEM, represented in quintuplets (n = 5).

At 24 h, relative to the control (5.4 ± 3.6%), there was a significant increase in cellular toxicity in cell populations exposed to the free drug (46.5 ± 9.63 %), (P<0.0001) (Figure 4,.9). This was also true for empty CS-DS NPs (28.8 ± 11.79 %) and CSS loaded CS-DS NPs (28 ± 5.12 %), (P<0.05, respectively) relative to the control.

Interestingly, at 48 h, no statistically significant differences were observed between empty and CSS loaded CS-DS NPs relative to the control. In fact, a significant decrease in cellular toxicity was observed in cell populations exposed to empty (3.7 ± 1.63 %) and CSS loaded CS-DS NPs (5.7 ± 2.6 %) in comparison to the free drug (35.8 ± 8.52 %) (P<0.01 and P<0.0001, respectively). Alarmingly, relative to the control (5.3 ± 1.7 %), there was a significant increase in cellular toxicity in cell populations exposed to the free drug (35.8 ± 8.52 %) (P< 0.001).

At 72 h, the cellular toxicity was significantly higher in free drug populations in comparison to the control (10 ± 4.57 %), empty (6.3 ± 1.35 %) and CSS loaded CS-DS NPs (6.7 ± 0.81 %)

(P<0.01 and P<0.001 respectively). Conversely, at 96 h, no significant differences were noted between the control, free drug, empty and CSS loaded CS-DS NPs.

4.4.1.2 The effects of chronic CSS, empty and CSS loaded CS-DS NPs on bEnd5 cell monolayer

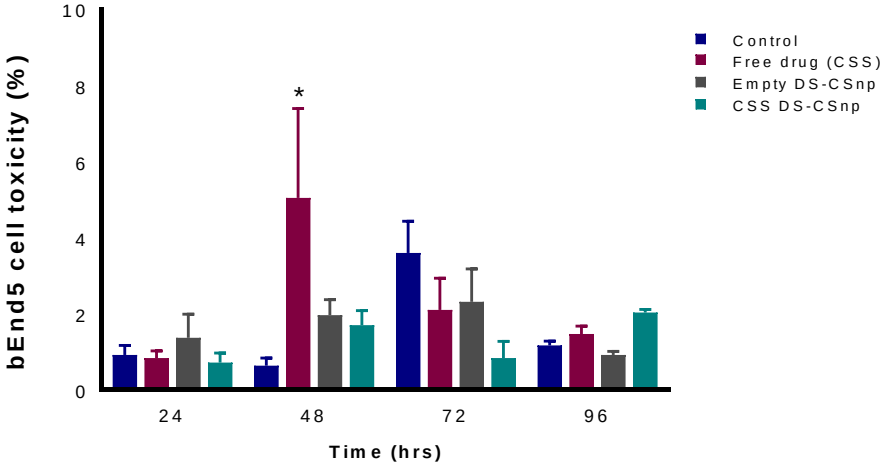

Figure 4.10 The Toxicity (%) to bend5 cells after chronic treatment using CSS, empty and CSS loaded CS-DS NPs (9.6 µg/ml for all) for 24-96 hrs. The NPs were synthesized using charge index 21(0.1% w/v CS/DS). The mean diameter for empty and CSS loaded NPs was 145.7 ± 17.97 nm and 125.8 ± 1.8 nm, respectively. Statistically significant differences are denoted with an asterisk(s) (*statistically different from the control), (* P<0.05). Data is expressed as mean ± SEM, represented in quintuplets (n = 5).

At 24 h, no significant differences were observed in cell populations exposed to the free drug, empty and CSS loaded CS-DS NPs (Figure 4.10). At 48 h however, a significant peak in cellular toxicity in cell populations exposed to the free drug (5.05 ± 2.34 %) in relation to the control (0.63 ± 0.20 %), (P< 0.001) was observed. This increase was also significantly higher than the toxicity denoted by empty and CSS loaded CS-DS NPs. These effects were diminished by 72h as no statistically significant differences were noted between the control and the free drug as well empty and CSS loaded CS-DS NPs. Moreover, at 96 h no significant differences were observed amongst all populations. Notably, the empty and CSS loaded CS-DS NPs exhibited little toxicity (under 2%) sustained over 96 hours. Hence, no statistically significant differences were noted relative to the control.

4.4.2 Evaluating the paracellular permeability of bEnd5 cell monolayer

The endothelial cells lining the neuronal microvasculature constitute a paracellular-limiting barrier between the blood and the neuronal microenvironment formed by TJs. This barrier impedes the movement of substances between adjacent endothelial cells, as well as establishing the tautness of the BBB (Rempe *et al*, 2011). An *in vitro* BBB model entailing a cultured monolayer of bEnd5 cells was utilized in order to predict the *in vivo* performance of CS-DS NPs. Inferences regarding the tautness of the BBB model were based on TEER- a measure of the electrical resistance denoted by junctional complexes, mainly TJs. TEER was measured on Transwell® inserts using an ohmmeter (Ohms, Ω-cm^2). A relation of inverse proportion exists between the electrical resistance across the bEdn5 monolayer and the paracellular permeability. That is, an increase in resistance equates to a decrease in the permeability across the monolayer.

4.4.2.1 The effects of chronic CSS, empty and CSS loaded CS-DS NP on the transendothelial electrical resistance

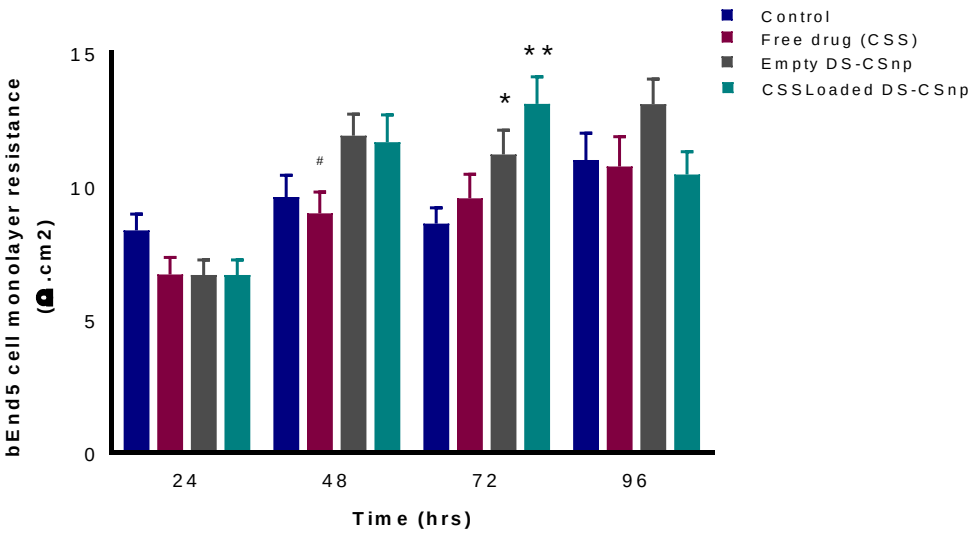

Figure 4.11 TEER readings of bend5 cells after chronic treatment using CSS, empty and CSS loaded CS-DS NPs (9.6 µg/ml for all) for 24-96 hrs. The NPs were synthesized using charge index 21(0.1% w/v CS/DS). The mean diameter for empty and CSS loaded NPs was 145.7 ± 17.97 nm and 125.8 ± 1.8 nm, respectively. Statistically significant differences from the control denoted with an asterisk (* P<0.05, ** P<0.01). Statistically significant differences from empty CS-DS NPs denoted with a hash (#) (# P<0.05). Data is expressed as mean ± SEM, represented in quintuplets (n = 5).

At 24 h, no significant differences were observed between the free drug, empty and CSS loaded CS-DS NPs relative to the control (Figure 4.11). At 48 h, the only statistically significant

observations were noted in cell populations exposed to empty CS-DS NPs to free drug. Herein, there was a significant increase in resistance in empty CS-DS NPs (11.2 ± 0.907 Ω-cm^2), thus decrease in paracellular permeability, relative to free drug (9.5 ± 0.9 Ω-cm^2) ($P<0.05$). At 72 h, a significant increase in resistance was observed in CSS loaded CS-DS NPs (13.1 ± 1 Ω-cm^2) relative to the control (8.6 ± 0.59 Ω-cm^2) ($P<0.01$). This was also noted in free drug (9.5 ± 0.9 Ω-cm^2) relative to the control (8.6 ± 0.59 Ω-cm^2) ($P<0.05$). However, at 96 h no significant differences were noted the exposed populations and the control.

4.4.3 Evaluation of the topographical localization of CS-DS NPs on bEnd5 cell monolayer using High-Resolution Scanning Electron Microscopy

In the control (Figure 4.12, A, E and I) the bEnd5 cells were represented as spherical cells, contrasted on the Transwell® cellulose membrane. The endothelial cell diameter reached approximately 8-9 µm. The EC surface was observed to be densely populated by ultrastructural membranous components. These membranous components were atypical to each other; varying in morphology, hydrodynamic diameter and surface density. The confluent EC monolayer was also characterized by extracellular protrusions extending from adjacent ECs. Collectively these inter-endothelial protrusions formed an elongated sheath that effectively covered the paracellular junction. The intermingling of the adjacent ECs adjoined the paracellular space thus forming a continuous EC monolayer. However, in bEnd5 cultures exposed to free drug CSS (Figure 4.12, B, F and J), the confluent EC monolayer was now represented by scanty flattened regions. There was an absence of the distinctive elongated ECs paracellular protrusions. Hence the monolayer was characterized by few areas of intermingling between adjacent ECs. The EC surface, however, was still observed to be abundant in amorphous cell membranous components.

In bEnd5 cell cultures exposed to Empty CS-DS NPs (Figure 4.12, C, G and K), healthy bend5 cells with distinctive membranous components much like that of the control were observed. Moreover, a confluent, intact EC monolayer was present. Colloidal Empty CS-DS NPs were also found to be scattered around and engaging with the inter-endothelial cleft. The presence of CSS-loaded CS-DS NP was signified by an observation of an apically located np between adjacent ECs (Figure 4.12, D, H and L). This NP, however, was approximately 200 nm, incandescent with a smooth surface. The topographical localization of the NPs was observed to be on a confluent, intact and healthy EC monolayer that expressed paracellular protrusions. The paracellular space was characterized by a meshwork of smooth continuous extracellular protrusions adjoining the adjacent EC.

Control | Colistin 'free drug' | Empty CS-DS NPs | Colistin-Loaded CS-DS NPs

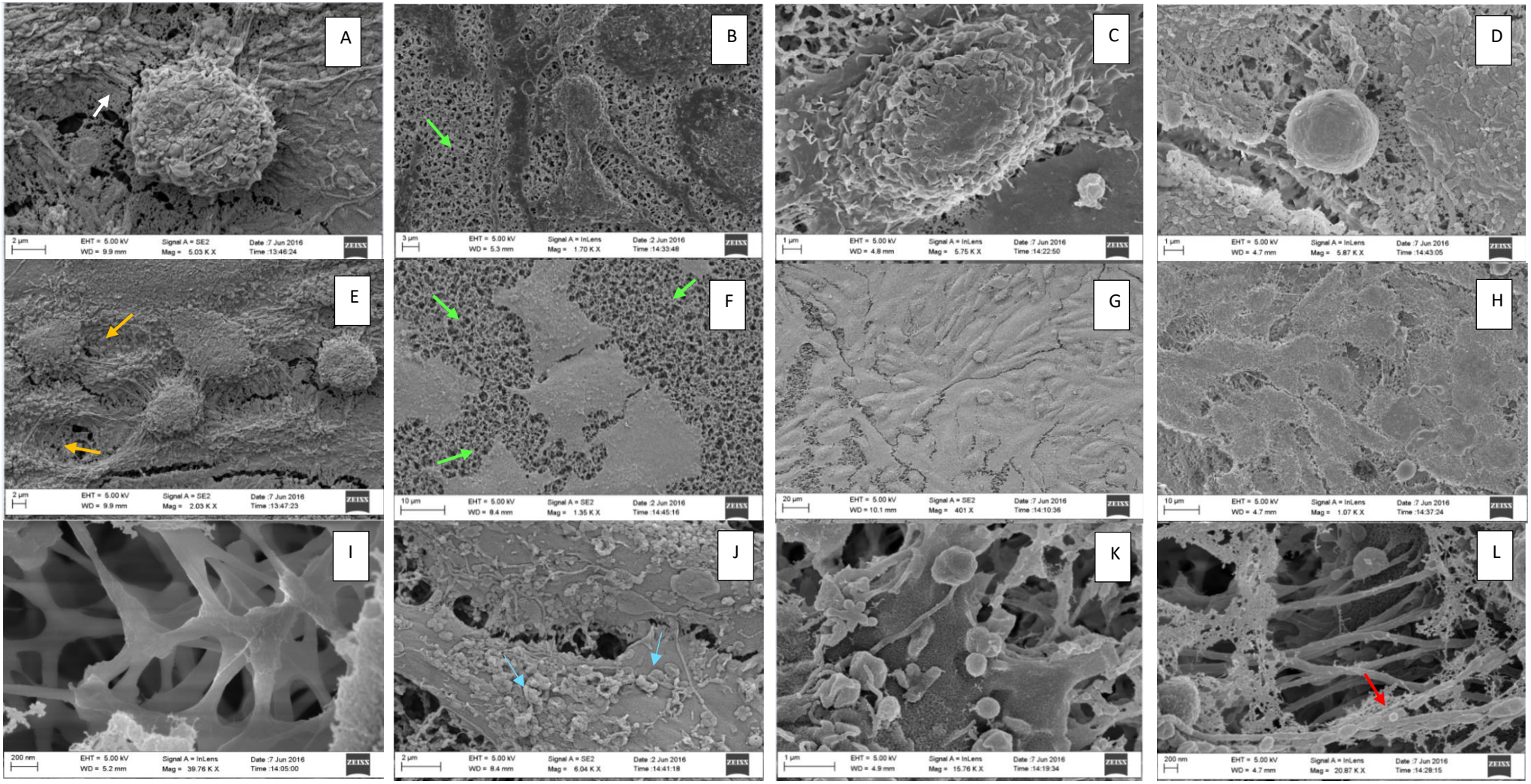

Figure 4.12 SEM images showing the interaction of NPs with confluent bEnd5 cells monolayer seeded at a density of 50000 cells per well per insert on a mixed cellulose Transwell insert membrane (12mm diameter with 0.45µm pore size) (Millicell^{TM}) for 24 hours. A, E and I are the control cells in DMEM only. B, F and J are cells exposed to 9.6 µg/ml colistin. C, G and K are cells exposed to empty NPs. D, H and L are cells exposed to colistin loaded NPs. Arrows WHITE; covering of the inter-endothelial space. ORANGE; cell protrusions between adjacent endothelia. LIME; scanty space. BLUE; amorphous cell membrane components RED; CS-DS NP.

CHAPTER FIVE: DISCUSSION

5.1 Chemical characterization of CS-DS NPs in Deionized water

5.1.1 Introduction

5.1.1.1 Biological significance of NP hydrodynamic diameter to the BBB

It has become evident that modifications to NP hydrodynamic diameter, ζ-potential and PDI have significant biological implications with regards to biodistribution, (Alexis *et al*., 2008) as well as the mechanism of cellular uptake (Yin *et al*., 2009). Several size parameters have also been associated with NP drug delivery systems crossing biological barriers; more specifically the BBB and the gastrointestinal barrier. The general size parameters have been shown as less than 50 nm for paracellular passage, less than 500 nm for endocytosis and less than 5,000 nm for enterocytes (Kulkarni and Feng, 2013). It has been suggested that NP less 100 nm such as thiamine ligand functionalized polymeric NPs (Lockman *et al*., 2003) as well as polysorbate 80-coated PBCA NPs (loaded with dalargin (opioid)) crossed the BBB in therapeutically significant doses (Kreuter *et al*., 1995). Additionally, breviscapine (a flavonoid) loaded Poly (lactic acid) (PLA) NPs, traversed the BBB in a size-dependent manner. Herein, NPs with a hydrodynamic diameter of 300 nm had a higher brain uptake versus NPs of 200 nm (Liu *et al*., 2008). Surely then, NP physicochemical properties have to be considered during synthesis. The choice of the physicochemical parameters, however, is determined by the therapeutic goal of the NP system (Voigt *et al*., 2014).

5.1.1.2 Biological significance of NP ζ-potential on the BBB

Positively charged NPs have the advantage of electrostatically interacting with anionic sialic acid glycoproteins residues on negatively charged cell membranes. However, negatively charged NP can also interact with the BBB due to a few cationic sites on the endothelial membrane (Honary and Zahir, 2013a). This electrostatic interaction results in the formation of NP clusters on the cell membrane due to electrostatic repulsion by neighboring anionic membrane residues. (Honary and Zahir, 2013b). NPs binding to these residues may lead to localized neutralization and membrane in-folding thus endorsing endocytosis (Saptarshi *et al*., 2013). Some positively charged NPs have not been approved by the FDA due to their enhanced cytotoxicity in comparison to negatively charged NPs (Faraji and Wipft, 2009). The positive charge has a membrane destabilizing component and thus destructive to the cells. With respect to the BBB, it has been established that positively charged NP induce vascular permeability

leading to alteration and subsequent breakdown in barrier properties. Hence, the use of less cytotoxic negatively charged NPs has been favored (Ranaldi *et al*., 2002).

5.1.2 Correlation between charge index and CS-DS NPs hydrodynamic diameter

The charge index denoted a binary effect on the physicochemical properties of the CS-DS NPs. The trend observed was that an increase in charge index correlated to, firstly, a decrease in NP size; a statistically significant difference from 0.03 (551 ± 84.05 nm) to 43.5 (144.4 ± 10.89 nm) ($P < 0.0001$) (Figure 4.1). These results were consistent with those reported by Chen *et al* (2003) where an increase in CS:DS from 5:5 to 5:10 correlated to significant decrease in NP size from 554 ± 12 nm to 220 ± 2nm. The same effect was also shown in studies replacing DS with an anionic alternative, TTP. It was observed that increasing the CS to TTP ratio increased NP size from 396 ± 106 to 15 ± 9 nm to 615 ± 9 nm (Koukaras *et al.*, 2012).

When the N:P ratio is high there is a greater concentration of DS than CS in the formulation. The higher the DS concentration the greater the degree of cationic CS group neutralization. This is achieved by DS molecule infiltrating and subsequently penetrating the inter-and-intramolecular space within the CS molecule. Consequently, as CS draws towards neutral there is a higher degree of in-folding and condensation thus forming small compact CS-DS NPs (Chen *et al.*, 2007). Contrarily, at low N:P ratio, there is a greater concentration of CS than DS within the synthesis system. The electrostatic forces within the CS molecule cause hydration and stretching, thus forming large complexes (Fan *et al.*, 2012; Chen *et al.*, 2003) Additionally, the presence of CS N–acetyl groups encourages 'loop' formations thus hindering CS crosslinking to the D–glucosamine residues of DS (Goycoolea *et al.*, 2007).

5.1.3 Correlation between charge index and CS-DS NPs hydrodynamic diameter with respect to CS, DS Mwt

Chen *et al* (2007) attributed the influence of charge index on hydrodynamic diameter to be a result of the difference in the Mwt of the two polymers. When the charge index is high, larger NPs are formed supposedly due to the Mwt of CS being greater than that of DS. However, in our study the Mwt of CS and DS was relatively close, 5 kDa and 6.5 kDa, respectively, therefore, Mwt may not have played a significant role on the hydrodynamic diameter of the NPs formed. Other studies also showed that increasing the charge index resulted in the formation of small NPs despite variances in Mwt, (Tiyaboonchai and Limpeanchob, 2007). This begs the question, is it possible to identify the optimal physicochemical parameters for

synthesizing CS-DS NPs based on variances in Mwt. Alternatively, are the discrepancies in hydrodynamic diameter an attribution of differences in experimental conditions?

Other studies demonstrated that independently manipulating the DD of CS as well as Mwt had no significant effect on the hydrodynamic diameter obtained. (Alameh *et al*., 2012). Our data also suggest that, at a constant Mwt, increasing the N:P ratio had no significant effect on hydrodynamic diameter (for certain values). For example, the first three indices 0.03, 0.05 and 0.1 had large NPs that were not significantly different from each other. Similarly, the last three indices 11, 21 and 43.5 had small NPs that were also not significantly different from each other (Figure 4.1). Theoretically, DS has 2.3 negative sulphate groups per monomer and CS has 0.85 protonable amino groups per monomer Therefore, there is a critical ionic quantity required for DS to neutralize and condense CS after which the system reaches equilibrium and is relatively impartial to excess DS (Chen et al., 2007). Our data suggest that the critical ionic quantity required for the formation of small CS-DS NPs lies between 0.1 and 11(Figure 4.1). The same was demonstrated in Grenha *et al* (2010) where complexation was achieved using sulphate groups found in carrageen (natural polymer obtained from seaweed) instead of DS. It was found that a higher degree of carrageenan, in comparison to CS amino groups available for neutralization, lead to precipitation. However, a lower degree of carrageenan resulted in insufficient counter-anion interaction for NP formation.

5.1.4 Correlation between charge index and CS-DS NP ζ-potential

The secondary effect denoted by charge index pertained to the CS-DS NPs ζ-potential. An increase in charge index was a result of an increase in DS (N) of N: P. The data showed that increasing the charge index determined the ζ-potential profile of the NPs, shifting from positive to negative. These results were consistent with work reported in literature (Chen *et al.,* 2007; Sarmento *et al*., 2007). This is thought to be a due to anionic DS charge neutralizing the CS amino groups (Fan *et al.*, 2012). Therefore, the greater the concentration of DS, the greater the degree of CS neutralization, the lower the ζ-potential. However, charge indices 11, 21 and 43.5 had negatively charged NPs with no significant difference from each other either. Similarly, charge indices 0.03, 0.05, 0.1 had positively charged NPs with no statistical significance from each other (Figure 4.2). This illustrates that there is also a critical ionic quantity required for the determination of ζ-potential. After this point has been reached the system seems to be impartial to excess DS hence plays no effect on the magnitude of the ζ-potential. It is thought that, simply, the excess DS localized itself on NP surface facilitating as steric hindrance thus preventing NP agglomeration (Chen *et al.*, 2007). The stability of the colloidal system is

inferred by the ζ-potential which in essence takes into account the balance between the net van der Waal's forces and the electrical repulsion, according to the DLVO theory (Toman, 2012). Generally, ζ-potential above +30 mV or below -30 mV infers good stability whereas ζ-potential between -30 mV and +30 mV potentiates aggregation (due to the reduction of repulsive forces between NPs) (Sarvaiya and Agrawal, 2015). Our data suggest that the charge indices used yielded a strong NP surface charge sufficient for colloidal stability in the synthesis media.

5.2 Chemical characterization of CS-DS NPs in biological milieu

5.2.1 Introduction

5.2.1.1 The relevance of serum on the physicochemical properties of NPs with respect to the BBB

Physicochemical stability of NP properties in biological milieu can be a formidable issue for clinical application (Honary and Zahir, 2013a). There have been a number of successful drug delivery systems targeting the CNS, however, the majority of them involve local administration. However, local CNS administration limits clinical acceptability as it is deemed invasive. Another alternative delivery route involves intranasal administration which bypasses the systemic circulation and gains direct access to the brain through the intra- and extra-neuronal pathways through the along both the olfactory and trigeminal nerves pathways (Masserini *et al*., 2013; Elnaggar *et al*., 2015) however clinical translation of these methods may be difficult. Ideally, a drug delivery NP should be able to cross the BBB subsequent to systemic administration as it is the most viable route in delivering therapeutic agents to the CNS (Mc Carthy *et al*, 2015). However, due to the highly reactive large surface area-to-volume ratio of NPs, they often adsorb serum proteins (albumin, fibrinogens, immunoglobulins) forming a protein corona when exposed to a biological (Hellstrand *et al*., 2009; Saptarshi *et al*., 2013; Wilhelm and Krizbai, 2014).

The NP-protein corona complex primarily offsets the physiochemical properties denoted during synthesis, secondarily, influences biological activity (Casals *et al*., 2010; Cedervall *et al*., 2007). Studies have shown than large NP-protein complexes can undergo cellular uptake, however, the mechanism of uptake (caveolae-mediated endocytosis) was conditional to albumin being complexed onto the NP surface. Additionally, it was also shown that the caveolae cell membrane invaginations contained varying sizes of NP (20 and 240 nm); suggesting that the invaginations were flexible to even larger NP-protein complexes (Agyare *et al*, 2008). Since NP-protein complexes are formed instantaneously after intravenous administration, it can be presumed that NP cell interactions occur as a factor of the adsorbed protein complex rather than bare NP (Saptarshi *et al*., 2013). Moreover, adsorption of proteins on NP surface may be advantageous to cellular uptake. The efficacy of NPs functionalized with cationic albumin as drug delivery system to the brain has been reported extensively (Liu *et al*., 2013; Parikh *et al*., 2010). Even so, NP-protein complexation is a multifactorial process that is

unique to each NP, protein and culture medium. Hence, in order to elucidate the fate of NPs in a biological context, it is imperative to understand their behaviour in biological media first.

5.2.2 The effect of DMEM on CS-DS NP hydrodynamic diameter

As a control, it was found that serum containing media (10% FBS in DMEM) possessed small sized particles (19.52± 3.090 nm (SD)) with a relatively low negative ζ-potential of -5.69 ± 0.53 mV (Figure 4.4 and 4.5).

In the presence of serum, observable increases in CS-DS NP hydrodynamic diameters were observed (though not statistically significant). Interestingly, after 10 min, there was stabilization in NP hydrodynamic diameter (Figure 4.4). It is possible that serum proteins ionically bound to NP surface forming a corona that effectively covered NP reactive sites. In this way, the serum proteins would act as a colloidal stabilizer thus preventing further interactions via steric hindrance (Alonso-Sande *et al*., 2006). Hyaluronic acid-CS NPs were found to be stable in EMEM due to serum protein stabilization (Parajó *et al*., 2010). Protein corona composition for CS functionalized NPs has been detailed to be albumin, fetuin-A and IgG as part of the 'hard corona'. Moreover, it was suggested that albumin and fetuin comprised the dominant fractions of the corona due to their abundance in FBS (Abouelmagd *et al*., 2015).

Our data also showed that exposure to serum containing DMEM had a neutralizing effect on the CS-DS NPs, drawing the ζ-potential close to zero (Figure 4.5). Since ζ-potential gauges NP stability according to the classical definition (ζ-potential above +30 mV or below - 30 mV infers good stability) (Honary and Zahir, 2013a). The ζ-potential after incubation in serum suggested that there was a reduction in the repulsive forces between the NPs, hence they were "unstable". These results were similar to those in literature where an immediate and significant decrease in CS-DS NP ζ-potential after 10min incubation in FBS was shown (Katas *et al*., 2013). The difference between our study and the reported data is the innate charge of the CS-DS NPs; ours being negative and theirs positive. It is acceptable that positively charged CS-DS NPs can bind negatively charged BSA via electrostatic interactions. However, it is also thought that negatively charged NPs can also bind BSA. Although this may not have been the initial desired effect, coating with BSA (or the presence of serum in culture medium) has shown to lessen the cytotoxicity of NPs (Fröhlich, 2012). In fact, when cultured with serum, polystyrene, PLGA and most polysaccharide NPs were less toxic to nonphagocytic cells (Agashe *et al*., 2009). Studies detailing BBB endothelial cell uptake of Methoxy PEG–PLA coated with thiolated cationized bovine serum BSA (CBSA) versus bare PEG–PLA NPs

showed that A) conjugation of cationic BSA onto NP surface resulted in a shift in ζ-potential from -39 mV to -19 mV and B) cellular uptake was preferential for -19 mV BSA NP than -39 mV uncoated NP (Parikh *et al*., 2010). This signifies that NP interaction with serum proteins may be advantageous to their biological performance.

Statistically significant increases in CS-DS NP hydrodynamic were observed in serum-free DMEM and PBS. Studies have shown that differences in ionic strength of the biological media, of the same pH, effected the stability of NPs. For example, in comparison to PBS, CS NPs exposed to HBSS (Hanks Balanced Salt Solution, pH 7.4) were more unstable due to 8-fold increase in PO_4^{2-} and CO_3^{2-} concentration (Oyarzun-ampuero *et al*., 2009). Ionic concentration is thought to directly affect the hydration layer as well as the water surrounding the NP surface, thus causing swelling (López-león *et al*, 2005; Parajó et al., 2010). CS-DS NPs synthesized using high N:P are thought to be compact due to stronger electrostatic interactions and steric hindrance denoted by the DS sulphate groups. This compact structure should impede the incubation media from penetrating the NP matrix as there are less NP surface sites available for crosslinking (Katas *et al*., 2013). However, this effect was not seen in our data, it is possible that the steric hindrance was not enough to overcome the influence of the ionic composition and concentration of the media. Despite difference in ionic strength and pH, it is also likely that the absence of electrostatic repulsive forces between the NP due to a shift in ζ-potential, from highly negative to near neutral, potentiated increases throughout all samples. The low ζ-potential experienced by NP in PBS is most likely due to charge cancellation by PBS phosphate groups (Katas *et al*., 2013).

5.2.3 The effect of DMEM on CS-DS NP PDI

On the other hand, when observing the size distribution (PDI) of serum containing samples, it was noted that they displayed a high degree of dispersity (Figure 4.6). This suggests that hydrodynamic diameter obtained was not a true representation of the sample, as it contained a variety of sizes. This then partially negates the arguments of protein-functionalized stabilization by serum. Additionally, serum-free and PBS samples also had increased hydrodynamic diameters and a high degree of dispersity. The commonality between the samples is their neutral pH (7.4). The CS network in the CS-DS NPs contains pH-ionizable functional groups. Modification of pH from acidic to basic potentiates the deprotonation of the CS NH_2 groups - thus destabilizing the intramolecular electric repulsion within the NP (López-león *et al*., 2005). This signifies that the changes in hydrodynamic diameter were a factor of pH modification (from 3.2 to 7.4) rather than the presence of proteins. Literature shows that the hydrodynamic diameter of CS NP increases in the presence of PBS (pH7.4) ((Parajó et al., 2010). Other studies show that CS NPs formed insoluble microparticles (2 µm) in the presence of serum-free and serum containing DMEM (pH7.4, size determined by DLS). Nevertheless, cells lose their ability to internalize CS NPs in serum-free media at pH 7.4 due to the inability of the slightly electronegative particle to bind to the membrane (Hoemann *et al*., 2013). The tendency of CS to crosslink with anionic counter-parts (Mohammadpour *et al*., 2012) renders it susceptible to disruptions due to the presence of phosphates and borates in the media (López-león *et al*., 2005). Hence differences in ionic composition may have different influences in the physiochemical properties. However, considering the relatively high PDI values obtained for CS-DS NPs in all samples. It is difficult to denote the effects of the intrinsic composition on the hydrodynamic diameters due to the multitude of ions in each media (Hoemann *et al*., 2013). Most significant is the large degree of variances in the CS-DS NP size distribution obtained in each sample. Although the media has a significant influence on the physicochemical properties of the NPs, it is unclear if this influence was based solely on protein binding or the ionic strength and composition of the media. Therefore, further analysis is required.

5.3 Biological characterization: in vitro effects of CS-DS NPs on Bend5 cell monolayer

5.3.1 Bend5 cytotoxicity

5.3.1.1 Introduction

The BBB is a multifunctional partition between the blood and brain. It resembles an anatomical, metabolic and transportation barrier that selectively facilitates the movement of molecules into and out of the CNS. The integrity of this dynamic interface is crucial in maintaining the homeostatic milieu required for optimal neuronal synapses (Cardoso *et al*., 2010; Hawkins *et al*., 2014). Perturbation of barrier properties renders the neuronal microenvironment vulnerable to changes in ionic composition resulting in abnormal neuronal activities (manifestation of seizures) and many other disease states (Vliet *et al*., 2015). Albeit essential, the BBB itself is a therapeutic challenge due to its highly specialized nature. Approximately 98% of small molecules, including therapeutics, do not cross the BBB (Deli, 2009). Hence, treatment of CNS infections is still a formidable. This issue is exacerbated by the rise in MDR CNS infections. Although it has shown high nephro-and-neurotoxicity colistin has been revived as a last line of defense. However, it is a large polycationic peptide that displays poor distribution into the brain (Dai *et al*., 2013; Levin *et al*., 1999; Spapen *et al*., 2011). Hence, there is a great need to develop systemic drug delivery systems that efficiently and effectively transport drugs across the BBB resulting in sufficient parenchyma distribution in therapeutically significant doses (Pardridge, 2012; Wilhelm and Krizbai, 2014). The FDA has not approved the use some NPs due to toxicity (Honary and Zahir, 2013b; Alameh, 2012). Given the significance of the BBB in neuronal functioning, it is essential to characterize the cytotoxic effects of NP before they can be used as a drug delivery system.

5.3.1.2 The effect of acute and chronic CS-DS NP treatment on endothelial toxicity

The toxicity of NPs was tested on mouse brain endothelial cells (bend5) using trypan blue cell viability assay. Both empty and CSS loaded NPs were compared to free drug CSS. Our data showed that after single exposure CSS had a long-term suppression of cell viability. Thus, within this concentration, CSS compromised to the integrity of the BBB (Figure 4.9).

At 24 h, empty and CSS loaded NPs had some level of toxicity although to a lesser degree than CSS (Figure 4.9). This was contrary to literature where incubation of CS NP with rat neuronal b50 cells showed no impact on toxicity for 10 min to 24 h (Malatesta *et al*., 2012). However, it has been shown that the active toxicity of NPs differs between cell lines due to variances in cell-line characteristics, media-specifications and the physicochemical properties of the NPs

(Nafee *et al*., 2009). The attraction to CS and DS in their utilization as drug delivery systems is due to their biodegradability, under physiological conditions molecular chains can be degraded by lysozymes to non-toxic by-products (Rodrigues *et al*., 2012). Perhaps interaction of CSS loaded CS NPs with the endothelia resulted in their degradation and subsequent intracellular release of CSS hence the toxicity. However, toxicity was also displayed by the empty NPs, hence, at this point; no inferences can be made pertaining to the mechanism of the toxicity displayed at 24 h.

Interestingly, by 48 h no toxicity was due to empty and loaded NP whilst CSS sustained toxicity. Encapsulation of CSS in CS-DS NPs had a protective effect on the BBB (Figure 4.9). Several reports have detailed the occurrence of CS NPs in the cytoplasm devoid of vesicle; the pharmaceutical relevance of which substantiates CS NPs notoriety in effectively protecting their therapeutic cargo from intracellular enzymatic degradation by escaping from endosomes (Malatesta *et al*., 2012; Sato *et al*., 2001; Köping-Höggård *et al*., 2001) and entering the cytosol (Serda *et al*., 2011). Studies have shown that CS NPs, complexed with novel dextran derivative, were not toxic to mouse (bend3) and human (hCMEC/D3) brain endothelial cells. Moreover, it was found the NPs from the DS derivatives were rapidly taken up by the cells bend3 cells and localized around the nuclei (Toman, 2012). Other studies suggest that NPs synthesized using LMW-CS were less toxic than HMW-CS (Alameh, 2012).

5.3.1.3 The relationship between the colloidal stability of the CS-DS NPs and endothelial toxicity

The toxicity of NPs is, in part, determined by the ζ-potential **(**positive charges effectively bind anionic cell membranes which facilitates membrane destabilization). In turn, the ζ-potential is determined by the pH of the media. *In vitro,* the ideal conditions required for cell culture is pH 7.4, it was in these very same conditions that our data showed that the hydrodynamic diameter of CS-DS NPs significantly enlarged. This was postulated as a combined effect of serum protein adsorption and NP swelling (due to shift in PH from 3.2 to 7.4) (López-león *et al*., 2005; Oyarzun-ampuero *et al*., 2009; Parajó et al., 2010). NP utilization heavily relies on small sizes. Hence, in order to avoid colloidal instability/agglomeration, studies use buffers in the culture media that vary significantly from *in vivo* conditions. Nevertheless, NP agglomeration in media has shown to effectively reduce toxicity (Nafee *et al*., 2009). This notion has been displayed by our data as the NPs were still biocompatible with the bend5 cells and significantly combated the cytotoxic effect denoted by CSS. It is thought that reduced toxicity is due to serum protein binding and masking the NP active sites (Goycoolea *et al*., 2007; Katas *et al*.,

2013). This interaction enhances cellular uptake due to the unfolding of the adsorbed protein to access cell membrane receptors (Saptarshi *et al*., 2013). Moreover, the pH 7.4 of the culture media is conducive to CS being non-ionized and thus not toxic (Rodrigues *et al*., 2012). Some studies suggest that there is a dose-dependent effect of serum on the uptake of CS NPs, in that the serum regulates the cell metabolism essential for micropinocytosis (Swanson and Watts, 1995). Contrarily, others show that in certain sera the soluble CS chains are taken up through high energy dependent mechanisms (Hoemann *et al*., 2013).

5.3.2 The effect of CS-DS NPs on TEER of confluent endothelial monolayer

5.3.2.1 Introduction: The relationship between tight junction permeability and BBB integrity with respect to CS

Several reports have demonstrated the ability of CS to induce transient opening of TJs in various epithelial cell lines (Maher *et al*., 2016; Thanou *et al*., 2000). As such CS has been the focus for enhanced drug absorption and penetration hence its potential use as an excipient has been extrapolated to other barriers including the BBB (Deli, 2009). It is thought that the CS cationic moieties bind anionic cell membranes and thus through a series of events decrease TEER in cell monolayers whilst increasing TJ permeability (Ranaldi *et al*., 2002). TJs have a complex of integral transmembrane proteins that span the paracellular junction, thus maintaining BBB tautness (Valenzano *et al*., 2015). Although lipophilic molecules have free transcellular diffusion, TJ impede the free flow of hydrophilic molecules through the paracellular clefts hence enhancing a rate-limiting paracellular function (Fu, 201). Until recently, literature on the molecular configuration and regulation of TJs was relatively sparse. Occludin was the first integral membrane protein to be detailed in 1993 (Tsukita and Furuse, 1999; Wolburg *et al*., 1994) although now the ZO-1 and ZO-2 are the best characterized transmembranous proteins (Salama *et al*., 2006; Sears *et al*., 2000). Paracellular permeability enhancers (PPE) were discovered before the TJs were fully outlined (Deli, 2009). Studies have shown that PPE modulate ZO-1 and the actin-cytoskeleton (Dodane *et al*., 1999; Schipper *et al*., 1997). Other studies showed that PPE's increased the apical membrane permeability followed by a significant reduction in cell viability (Duizer *et al*., 1998). The transient opening of TJs facilitates the indiscriminate movement of blood-borne and exogenous molecules from the circulatory system into the brain parenchyma (Ranaldi *et al*., 2002). This has detrimental effects on ionic microenvironment essential for normal neuronal synapses. Hence, the opening of TJs and subsequent increase in paracellular permeability can be regarded as a sub-lethal toxic effect (De Angelis *et al*., 1998; Ferruzza *et al*., 1999). However, due to its biocompatibility, biodegradability, solubility, mucoadhesive properties, CS has been denoted as a potential candidate as a drug delivery system in a clinical setting. However, controlling transient TJ opening (to facilitate efficient and safe drug delivery across biological barriers) is still yet in its infancy (Deli, 2009).

5.3.2.2 The effect of chronic CS-DS NPs treatment on BBB permeability

The integrity of the endothelial monolayer was maintained in the presence of CS-DS NPs after 24 h exposure, as no significant differences were observed (Figure 4.11). This suggests that CS containing formulation had no observable effects on the permeability of the BBB, therefore no inferences to sub-lethal toxicity could be made. Significant changes were only noted during 72hr of the chronic exposure relative to the control. Surprisingly, Loaded CS-DS NPs denoted an increase in TEER; decrease in the TJ permeability. This suggests that the NPs may have contributed to barrier properties by enhancing the tautness of the monolayer. These findings are contrary to other cell lines demonstrated in literature where CS enhanced permeability (Fluorescein isothiocyanate labelled dextran) (Vllasaliu *et al*., 2010). However, other studies indicated that the effect on TJ permeability was based on the type and the concentration of the polycation, as well as the extracellular concentration of divalent cations. It is possible that the concentration used in our study was too low to elicit transient TJ opening (Ranaldi *et al*., 2002). Alternatively, it is possible that TJ permeability only pertains to free CS and its derivatives, perhaps the PPE effects of CS are mitigated when CS is in a formulation. However, in other studies when CS NPs were compared to CS solution, a sharp and reversible decrease in TEER was observed, suggesting that CS effects can still be attributed even when in a formulation (Nafee *et al*., 2009). Moreover, CS NPs displayed TJ modulation via ZO-1 distribution in the same manner as the solution.

5.3.3 Evaluation of the topographical localization of CS-DS NPs on bEnd5 cell monolayer using High-Resolution Scanning Electron Microscopy

SEM analysis was based on observations made on bEnd5 cells seeded at a density of 50000 cells per well per insert on a mixed cellulose Transwell insert membrane (12mm diameter with 0.45µm pore size) (Millicell^{TM}) for 24 hours. The morphology of the NP was found to be synonymous with those reported in literature describing spherical NPs structures with a smooth surface (Chaiyasan *et al*., 2013; Chen *et al*, 2007). SEM images showed spherical incandescent NPs close to the nominal size (Figure 4.12, L). The NPs were engaging with cellular processes of junctional complexes on intact healthy monolayers. NP sizes were similar to those obtained from DLS (Malvern Zetasizer Nano S90°) for NPs in DI for charge index 21; 145.7 ± 17.97 nm (section 4.1.1.). However, considering the effects of cell culture media on NPs, size parameters are not comparable to NPs in DI due to wide distribution. When exposed to culture media, although observable increases were noted, no statistically significant differences were noted in the hydrodynamic diameter of CS-DS NPs relative to NPs in DI (section 4.2.1). However, the size distribution was relatively high 0.435 ± 0.034 as the PDI suggested that the NPs had a high degree of dispersity (section 4.2.3). Hence, it is plausible to find NPs less than 200 nm. Theoretical description of TJ is intricate interconnected transmembranous protein structures (claudins, occludins, and JAMS) that span the width of the inter-endothelial space. These structures form complexes that constitute the paracellular space and maintain the tautness of the BBB (Valenzano et al., 2015). In our SEM images, inter-endothelial protrusions spanning the paracellular space were present. However, interestingly these protrusions formed an elongated sheath that covered the paracellular space (Figure 4.12, E). Due to the limitations of SEM, we could not, however, differentiate between the individual substructures of the junctional complexes. Therefore, no inferences could be made regarding the specification of the junctional proteins present. In observation, the junctional complexes were still found to be intact in bEnd5 cells treated with colistin (considering magnification 6.04 K X) (Figure 4.12, J), although, macroscopically the endothelial cells were found to be scanty and unhealthy (1.35 K X) (Figure 4.12, F). With reference to TEER (Figure 4.11**)** the notion of intact junctional complexes is plausible as at 24 h, no significant differences were observed in permeability between colistin and the control. Most significant is that the NPs mitigated the effects of colistin on monolayer morphology. The encapsulation of colistin into NPs denoted healthy intact cell morphologies (Figure 4.12, D and H). To our knowledge, this has not yet been demonstrated in literature.

CHAPTER SIX: CONCLUSION

This study focused on the characterization of CS-DS NPs as drug delivery systems according to their physicochemical properties; hydrodynamic diameter, dispersity index, ζ-potential and drug encapsulation efficacy. As well as biocompatibility with the BBB measured as physiological parameters of cytotoxicity, permeability and topographical localization. The hypothesis was that varying the charge index would influence the physicochemical properties of CS-DS NPs. Moreover, the encapsulation of colistin into CS-DS NPs would have a biocompatible effect on the BBB.

The charge index had a dual effect on the CS-DS NPs. Increasing the charge index divided the CS-DS NPs into positively charged populations (with larger hydrodynamic diameters) and negatively charged populations (with smaller hydrodynamic diameters). There was no statistical correlation between the increased value of the charge index and the magnitude of hydrodynamic diameter and ζ-potential.

Studies suggest that, in a high N:P formulation, the excess DS denotes a strong negative charge on the NP surface. Not only do high N:P formulations form smaller NPs, also observed in our study, the excess DS also acts as colloidal protectant via steric hindrance thus preventing agglomeration (Chen *et al*., 2003). This, however, only pertains to NP's solely in their innate synthesis media (mainly DI) outside of a biological environment. To our surprise, our data suggested that NPs grew larger only in serum-free media than serum-containing media. However, considering the high degree of dispersity found for all samples, DLS may not have been an adequate tool for characterization of NPs in biological milieu. Therefore, the notion of NP protein interaction could still hold true, it is possible that a fraction of serum proteins complexed with chitosan chains on the NP surface. A more conclusive answer could be found by using confirmatory analyses i.e. Mass spectroscopy to identify the serum proteins bound on NP surface (Saptarshi *et al*., 2013). The data suggests that the behaviour of NP's in biological is milieu is a multifactorial process that is governed not only by intrinsic characteristics (i.e. hydrophobicity, functional groups) of the NP but also as to the composition of the medium (i.e. pH, ionic strength) (Hoemann *et al*., 2013). This highlights the unpredictable nature of NP in a biological environment. *In vivo,* the presence of serum proteins is the epitome of a highly dynamic biological system. Hence such environments may denote modifications to an otherwise 'well-characterized' NP, the extent of which as of yet is not well understood.

Remarkably, although the media influenced NP agglomeration, this did not have a negative influence on their biological activity. The data shows the protective effects of CS-DS NPs on the BBB after treatment with antibiotic colistin. The data also showed that the NPs were biologically compatible with the endothelial cells (as shown in SEM). Moreover, although they were expected to transiently induce paracellular permeability, surprisingly the CS-DS NPs had the opposite effect on the confluent monolayer. That is, a decrease in permeability was observed suggesting that possibly the NPs enhanced barrier properties. However, inferences to TJ modulation cannot be extrapolated from this assay.

Our study highlights the *in vitro* neuroprotective and biocompatible nature of CS-DS NPs on the BBB.

CHAPTER SEVEN: FUTURE WORKS

There are some ideas that I would have liked to implement during the synthesis and the characterization of the NPs in Chapter 3. This thesis mainly focused on the use of polyelectrolyte complexation, with respect to the charge of the functional polymer groups, to synthesis CS-DS NPs. Dynamic light scattering (DLS) was used to measure the physicochemical properties of the NPs, however, the conformation of electrostatic interaction (to form NPs) was based on following previously described articles from literature (i.e. Chaiyasan *et al.,* 2013 and Chen *et al*., 2003). Additionally, it became apparent that DLS was not a sufficient tool in fully characterizing NPs in biological media. This meant that characterizing the NP protein surface profile was outside the scope of the thesis. Considering that the interaction of proteins and the NPs may have a role in cellular uptake (Lynch and Dawson, 2008; Casals *et al.,* 2010), characterization of surface proteins would have yielded a deeper understanding of the interaction between the CS-DS NPs and the Bend5 cells.

The following ideas could be tested:

1. It would be interesting to characterize type and affinity of protein binding on the NP surface. Considering which proteins would constitute the hard and soft corona, whether protein binding would induce protein unfolding and any conformational changes to the NP surface
2. As a secondary confirmatory analysis, Fourier-transform infrared spectroscopy could have been used to assess electrostatic interactions that are responsible for NP formation.
3. A more definitive strategy for the TEER study would have been to fluorescently label the NPs and perform a tracking study. In this, the initial concentration (in the luminal compartment) and the final concentration (in the basolateral compartment) could have been compared. This would have shown whether the NPs crossed the BBB. Since the thesis was aimed at assessing the biocompatible nature of the CS-DS NPs, permeation abilities would have been the next logical step in potentiating NP use as a BBB drug delivery system.
4. Since brain cells have limited regenerative capacity (Hawkins *et al*., 2005), inferences to NP biocompatibility could have been made through the use of immunoassays to assess for inflammatory agents caused by the NPs.

As this was a mini-thesis, the above mentioned was above the required scope. However, it would be interesting and beneficial to include such parameters in a project that allows for a grander scope.

CHAPTER EIGHT: REFERENCES

Abbott, N. J. (2005). Dynamics of CNS barriers: evolution, differentiation, and modulation. *Cellular and Molecular Neurobiology*, *25*(1), 5-23.

Abbott, N. J., Rönnbäck, L., & Hansson, E. (2006). Astrocyte–endothelial interactions at the blood–brain barrier. *Nature Reviews Neuroscience*, *7*(1), 41-53.

Abdelwahed, W., Degobert, G., Stainmesse, S., & Fessi, H. (2006). Freeze-drying of nanoparticles: Formulation, process and storage considerations. *Advanced Drug Delivery Reviews*, *58*(15), 1688–1713.

Abouelmagd, S. A., Ku, Y. J., & Yeo, Y. (2015). Low molecular weight chitosan-coated polymeric nanoparticles for sustained and pH-sensitive delivery of paclitaxel. *Journal of Drug Targeting*, *23*(7-8), 725-735.

Agashe, H. B., Dutta, T., Garg, M., & Jain, N. K. (2006). Investigations on the toxicological profile of functionalized fifth-generation poly (propylene imine) dendrimer. *Journal of Pharmacy and Pharmacology*, *58*(11), 1491-1498.

Aggarwal, P., Hall, J. B., Mcleland, C. B., Dobrovolskaia, M. A., & Mcneil, S. E. (2009). Nanoparticle interaction with plasma proteins as it relates to particle biodistribution , biocompatibility and therapeutic eficacy. *Advanced Drug Delivery Reviews*, *61*(6), 428–437.

Agnihotri, S.A., Mallikarjuna, N.N. & Aminabhavi, T.M. (2004). Recent advances on chitosan-based micro-and nanoparticles in drug delivery. *Journal of Controlled Release*, 100(1), pp.5-28.

Agulhon, C., Petravicz, J., McMullen, A. B., Sweger, E. J., Minton, S. K., Taves, S. R., & McCarthy, K. D. (2008). What is the role of astrocyte calcium in neurophysiology?. *Neuron*, *59*(6), 932-946.

Agyare, E. K., Curran, G. L., Ramakrishnan, M., Caroline, C. Y., Poduslo, J. F., & Kandimalla, K. K. (2008). Development of a smart nano-vehicle to target cerebrovascular amyloid deposits and brain parenchymal plaques observed in Alzheimer's disease and cerebral amyloid angiopathy. *Pharmaceutical Research*, *25*(11), 2674-2684.

Ahing, F. A., & Wid, N. (2016). Optimization of shrimp shell waste deacetylation for chitosan production. *International Journal of Advanced and Applied Sciences*, *3*(10), 31-36.

Ahmed, T. A., & Aljaeid, B. M. (2016). Preparation, characterization, and potential application of chitosan, chitosan derivatives, and chitosan metal nanoparticles in pharmaceutical drug delivery. *Drug Design, Development and Therapy*, *10*, 483–507.

Ainsworth, G.C., Brown, A.M. & Brownlee, G. (1947). Aerosporin, an antibiotic produced by Bacillus aerosporus Greer. *Nature*, 160(263), p.878.

Alameh, M., DeJesus, D., Jean, M., Darras, V., Thibault, M., Lavertu, M., & Merzouki, A. (2012). Low molecular weight chitosan nanoparticulate system at low N: P ratio for nontoxic polynucleotide delivery. *International Journal of Nanomedicine*, *7*, 1399.

Alexis, F., Pridgen, E., Molnar, L. K., & Farokhzad, O. C. (2008). Factors affecting the clearance and biodistribution of polymeric nanoparticles. *Molecular Pharmaceutics*, *5*(4), 505-515.

Alonso-Sande, M., Cuña, M., Remuñán-López, C., Teijeiro-Osorio, D., Alonso-Lebrero, J. L., & Alonso, M. J. (2006). Formation of new glucomannan− chitosan nanoparticles and study of their ability to associate and deliver proteins. *Macromolecules*, *39*(12), 4152-4158.

Andrianov, A. K. (2006). Water-soluble polyphosphazenes for biomedical applications. *Journal of Inorganic and Organometallic Polymers and Materials*, *16*(4), 397-406.

Auburtin, M., Wolff, M., Charpentier, J., Varon, E., Le Tulzo, Y., Girault, C., Mohammedi, I., Renard, B., Mourvillier, B., Bruneel, F. & Ricard, J.D. (2006). Detrimental role of delayed antibiotic administration and penicillin-nonsusceptible strains in adult intensive care unit patients with pneumococcal meningitis: the PNEUMOREA prospective multicenter study. *Critical Care Medicine*, 34(11), pp.2758-2765.

Baeten, K.M. & Akassoglou, K. (2011). Extracellular matrix and matrix receptors in blood–brain barrier formation and stroke. *Developmental Neurobiology*, 71(11), pp.1018-1039.

Bagnard, D., Vaillant, C., Khuth, S. T., Dufay, N., Lohrum, M., Püschel, A. W., & Thomasset, N. (2001). Semaphorin 3A–vascular endothelial growth factor-165 balance mediates migration and apoptosis of neural progenitor cells by the recruitment of shared receptor. *Journal of Neuroscience*, *21*(10), 3332-3341.

Bai, L., Ma, Z., Yang, G., Yang, J., & Cheng, J. (2011). A Simple HPLC Method for the Separation of Colistimethate Sodium and Colistin Sulphate. *Journal of Chromatography*

& Separation Techniques, *2*(1), 2–5.

Ballabh, P., Braun, A., & Nedergaard, M. (2004). The blood-brain barrier: An overview: Structure, regulation, and clinical implications. *Neurobiology of Disease*, *16*(1), 1–13.

Banks, W. A. (1999). Physiology and pathology of the blood-brain barrier: implications for microbial pathogenesis, drug delivery and neurodegenerative disorders. *Journal of Neurovirology*, *5*(6), 538-555.

Begley, D.J. (2004). Delivery of therapeutic agents to the central nervous system: the problems and the possibilities. *Pharmacology & Therapeutics*, 104(1), pp.29-45.

Bellavance, M. A., Blanchette, M., & Fortin, D. (2008). Recent advances in blood–brain barrier disruption as a CNS delivery strategy. *The AAPS Journal*, *10*(1), 166-177.

Benedict, R.G. & Langlykke, A.F. (1947). Antibiotic activity of Bacillus polymyxa. *Journal of Bacteriology*, 54(1), p.24.

Benson, K., Cramer, S., & Galla, H. J. (2013). Impedance-based cell monitoring: barrier properties and beyond. *Fluids and Barriers of The Cns*, *10*(1), 5.

Berger, J., Reist, M., Mayer, J. M., Felt, O., & Gurny, R. (2004). Structure and interactions in chitosan hydrogels formed by complexation or aggregation for biomedical applications. *European Journal of Pharmaceutics and Biopharmaceutics*, *57*(1), 35-52.

Bernkop-Schnürch, A., Humenberger, C. & Valenta, C. (1998). Basic studies on bioadhesive delivery systems for peptide and protein drugs. *International Journal of Pharmaceutics*, 165(2), pp.217-225.

Blanchette, M., Pellerin, M., Tremblay, L., Lepage, M., & Fortin, D. (2009). Real-time monitoring of gadolinium diethylenetriamine penta-acetic acid during osmotic blood-brain barrier disruption using magnetic resonance imaging in normal wistar rats. *Neurosurgery*, *65*(2), 344-351.

Bodilsen, J., Dalager-Pedersen, M., Schønheyder, H.C. & Nielsen, H. (2011). Dexamethasone treatment and prognostic factors in community-acquired bacterial meningitis: a Danish retrospective population-based cohort study. *Scandinavian Journal of Infectious Diseases*, 46(6), pp.418-425.

Brightman, M. W. (1977). Morphology of blood-brain interfaces. *Experimental Eye Research*, *25*, 1-25.

Brown, W. (1996). Light scattering: principles and development (Vol. 53). Oxford University Press. Retrieved from http://books.google.com

Burgess, D.J., Duffy, E., Etzler, F. & Hickey, A.J. (2004). Particle size analysis: AAPS workshop report, cosponsored by the Food and Drug Administration and the United States *Pharmacopeia*. The AAPS Journal, 6(3), pp.23-34.

Busquets, M., Espargaró, A., Sabaté, R., & Estelrich, J. (2015). Magnetic Nanoparticles Cross the Blood-Brain Barrier: When Physics Rises to a Challenge. *Nanomaterials*, *5*(4), 2231–2248.

Butt, A. M., Jones, H. C., & Abbott, N. J. (1990). Electrical resistance across the blood-brain barrier in anaesthetized rats: a developmental study. *The Journal of Physiology*, *429*(1), 47-62.

Cardoso, F. L., Brites, D., & Brito, M. A. (2010). Looking at the blood-brain barrier: Molecular anatomy and possible investigation approaches. *Brain Research Reviews*, *64*(2), 328–363.

Casals, E., Pfaller, T., Duschl, A., Oostingh, G. J., & Puntes, V. (2010). Time evolution of the nanoparticle protein corona. *Acs Nano*, *4*(7), 3623-3632.

Cedervall, T., Lynch, I., Foy, M., Berggård, T., Donnelly, S. C., Cagney, G., & Dawson, K. A. (2007). Detailed identification of plasma proteins adsorbed on copolymer nanoparticles. *Angewandte Chemie International Edition*, *46*(30), 5754-5756.

Chaiyasan, W., Srinivas, S. P., & Tiyaboonchai, W. (2013). Mucoadhesive Chitosan–Dextran Sulfate Nanoparticles for Sustained Drug Delivery to the Ocular Surface. *Journal of Ocular Pharmacology and Therapeutics*, *29*(2), 200–207.

Charig, E.M., Anderson, I.M., Robinson Sen, J.M., Nutt, D.J. & Cowen, P.J. (1986). L-Tryptophan and prolactin release: Evidence for interaction between 5-HT1 and 5-HT2 receptors. *Human Psychopharmacology: Clinical and Experimental*, 1(2), pp.93-97.

Chemmangattu Radhakrishnan, R., Jacob, S., Pathak, H. R., & Tamilarasi, V. (2015). Colistin Induced Neurotoxicity in a Patient with End Stage Kidney Disease and Recovery with Conventional Hemodialysis. *The Open Urology & Nephrology Journal*, *8*, 53–55.

Chen, Y., & Liu, L. (2012). Modern methods for delivery of drugs across the blood-brain barrier. *Advanced Drug Delivery Reviews*, *64*(7), 640–665.

Chen, Y., Mohanraj, V. J., & Parkin, J. E. (2003). Chitosan-dextran sulfate nanoparticles for

delivery of an anti-angiogenesis peptide. *Letters In Peptide Science*, *10*(5-6), 621-629.

Chen, Y., Mohanraj, V. J., Wang, F., & Benson, H. a E. (2007). Designing chitosan-dextran sulfate nanoparticles using charge ratios. *AAPS PharmSciTech*, *8*(4), 131–139.

Choonara, Y.E., Pillay, V., Ndesendo, V.M., du Toit, L.C., Kumar, P., Khan, R.A., Murphy, C.S. & Jarvis, D.L. (2011). Polymeric emulsion and crosslink-mediated synthesis of super-stable nanoparticles as sustained-release anti-tuberculosis drug carriers. *Colloids and Surfaces B: Biointerfaces*, 87(2), pp.243-254.

Choosakoonkriang, S., Supaluknari, S., & Puangkaew, P. (2013). High Performance Liquid Chromatographic Method for Determination of Colistin Sulfate and its Application in Medicated Premixand Animal Feed. *World Academy of Science, Engineering and Technology, International Journal of Chemical, Molecular, Nuclear, Materials and Metallurgical Engineering*, *7*(4), 224-228.

Cordell, C. B., Borson, S., Boustani, M., Chodosh, J., Reuben, D., Verghese, J., & Fried, L. B. (2013). Alzheimer's Association recommendations for operationalizing the detection of cognitive impairment during the Medicare Annual Wellness Visit in a primary care setting. *Alzheimer's & Dementia: The Journal of The Alzheimer's Association*, *9*(2), 141-150.

Cummings, J.L., Morstorf, T. & Zhong, K. (2011). Alzheimer's disease drug-development pipeline: few candidates, frequent failures. *Alzheimer's Research & Therapy*, 6(4), p.37.

Curry, F.E. (1986). Determinants of capillary permeability: a review of mechanisms based on single capillary studies in the frog. *Circulation Research*, 59(4), pp.367-380.

Dai, C., Li, J., & Li, J. (2013). Experimental and Toxicologic Pathology New insight in colistin induced neurotoxicity with the mitochondrial dysfunction in mice central nervous tissues. *Experimental and Toxicologic Pathology*, *65*(6), 941–948.

Dakhara, S., & Anajwala, C. (2010). Polyelectrolyte complex: A pharmaceutical review. *Systematic Reviews In Pharmacy*, *1*(2), 121.

Dawson, K.A., Salvati, A. & Lynch, I. (2009). Nanotoxicology: nanoparticles reconstruct lipids. *Nature Nanotechnology*, 4(2), pp.84-85.

De Angelis, I., Vincentini, O., Brambilla, G., Stammati, A., & Zucco, F. (1998). Characterization of furazolidone apical-related effects to human polarized intestinal cells. *Toxicology and Applied Pharmacology*, *152*(1), 119-127.

De Rosa, G., Salzano, G., Caraglia, M. & Abbruzzese, A. (2012). Nanotechnologies: a strategy to overcome blood-brain barrier. *Current Drug Metabolism*, 13(1), pp.61-69.

De, S. & Robinson, D. (2003). Polymer relationships during preparation of chitosan–alginate and poly-l-lysine–alginate nanospheres. *Journal of Controlled Release*, 89(1), pp.101-112.

Delgado, A.V., González-Caballero, F., Hunter, R.J., Koopal, L.K. & Lyklema, J. (2005). Measurement and interpretation of electrokinetic phenomena. *Pure Appl. Chem*, 77(10), pp.1753-1805.

Deli, M. A. (2009). Biochimica et Biophysica Acta Potential use of tight junction modulators to reversibly open membranous barriers and improve drug delivery. *BBA - Biomembranes*, *1788*(4), 892–910.

Deng, Z. J., Liang, M., Monteiro, M., Toth, I., & Minchin, R. F. (2011). Nanoparticle-induced unfolding of fibrinogen promotes Mac-1 receptor activation and inflammation. *Nature Nanotechnology*, *6*(1), 39.

Dodane, V., Khan, M. A., & Merwin, J. R. (1999). Effect of chitosan on epithelial permeability and structure. *International Journal of Pharmaceutics*, *182*(1), 21-32.

Duizer, E., Van Der Wulp, C., Versantvoort, C. H., & Groten, J. P. (1998). Absorption enhancement, structural changes in tight junctions and cytotoxicity caused by palmitoyl carnitine in Caco-2 and IEC-18 cells. *Journal of Pharmacology and Experimental Therapeutics*, *287*(1), 395-402.

Ehrenberg, M. S., Friedman, A. E., Finkelstein, J. N., Oberdörster, G., & McGrath, J. L. (2009). The influence of protein adsorption on nanoparticle association with cultured endothelial cells. *Biomaterials*, *30*(4), 603-610.

Elnaggar, Y. S., Etman, S. M., Abdelmonsif, D. A., & Abdallah, O. Y. (2015). Intranasal piperine-loaded chitosan nanoparticles as brain-targeted therapy in Alzheimer's disease: optimization, biological efficacy, and potential toxicity. *Journal of Pharmaceutical Sciences*, *104*(10), 3544-3556.

Elsabahy, M., & Wooley, K. L. (2012). Design of polymeric nanoparticles for biomedical delivery applications. *Chemical Society Reviews*, *41*(7), 2545-2561.

Engelhardt, B. & Sorokin, L. (2009). The blood–brain and the blood–cerebrospinal fluid barriers: function and dysfunction. *Seminars In Immunopathology* (Vol. 31, No. 4, pp.

497-511). Springer-Verlag.

Everett, D.H. (2007). Basic principles of colloid science. *Royal Society of Chemistry*.ISBN 0851864430

Faraji, A. H., & Wipf, P. (2009). Bioorganic & Medicinal Chemistry Nanoparticles in cellular drug delivery. *Bioorganic & Medicinal Chemistry*, *17*(8), 2950–2962.

Fellner, S., Bauer, B., Miller, D. S., Schaffrik, M., Fankhänel, M., Spruß, T., & Buschauer, A. (2002). Transport of paclitaxel (Taxol) across the blood-brain barrier in vitro and in vivo. *The Journal of clinical investigation*, *110*(9), 1309-1318.

Feng, S. S. (2011). Chemotherapeutic engineering: concept, feasibility, safety and prospect—a tribute to Shu Chien's 80th birthday. *Cellular and Molecular Bioengineering*, *4*(4), 708-716.

Ferruzza, S., Scarino, M. L., Rotilio, G., Ciriolo, M. R., Santaroni, P., Muda, A. O., & Sambuy, Y. (1999). Copper treatment alters the permeability of tight junctions in cultured human intestinal Caco-2 cells. *American Journal of Physiology-Gastrointestinal and Liver Physiology*, *277*(6), G1138-G1148.

Feustel, S.M., Meissner, M. & Liesenfeld, O. (2012). Toxoplasma gondii and the blood-brain barrier. *Virulence*, 3(2), pp.182-192.

Filosa, J. A., Morrison, H. W., Iddings, J. A., Du, W., & Kim, K. J. (2016). Beyond neurovascular coupling, role of astrocytes in the regulation of vascular tone. *Neuroscience*, *323*, 96-109.

Fischer, H. C., & Chan, W. C. (2007). Nanotoxicity: the growing need for in vivo study. *Current Opinion In Biotechnology*, *18*(6), 565-571.

Fischer, H., Gottschlich, R., & Seelig, A. (1998). Blood-brain barrier permeation: molecular parameters governing passive diffusion. *Journal of Membrane Biology*, *165*(3), 201-211.

Fitch, M.T. & van de Beek, D. (2007). Emergency diagnosis and treatment of adult meningitis. *The Lancet Infectious Diseases*, 7(3), pp.191-200.

Fröhlich, E. (2012). The role of surface charge in cellular uptake and cytotoxicity of medical nanoparticles. *International Journal of Nanomedicine*, *7*, 5577.

Fu, B. M. M. (2012). Experimental Methods and Transport Models for Drug Delivery Across the Blood-Brain Barrier. *Current Pharmaceutical Biotechnology*, *13*(7), 1346–1359.

Gaillard, P.J., Appeldoorn, C.C., Rip, J., Dorland, R., van der Pol, S.M., Kooij, G., de Vries, H.E. & Reijerkerk, A. (2012). Enhanced brain delivery of liposomal methylprednisolone improved therapeutic efficacy in a model of neuroinflammation. *Journal of Controlled Release*, 164(3), pp.364-369.

Gallardo-Godoy, A., Muldoon, C., Becker, B., Elliott, A. G., Lash, L. H., Huang, J. X., & Phetsang, W. (2016). Activity and predicted nephrotoxicity of synthetic antibiotics based on polymyxin B. *Journal of Medicinal Chemistry*, *59*(3), 1068-1077.

Gan, Q., Wang, T., Cochrane, C. & McCarron, P. (2005). Modulation of surface charge, particle size and morphological properties of chitosan–TPP nanoparticles intended for gene delivery. *Colloids and Surfaces B: Biointerfaces*, 44(2), pp.65-73.

Gao, K., & Jiang, X. (2006). Influence of particle size on transport of methotrexate across blood brain barrier by polysorbate 80-coated polybutylcyanoacrylate nanoparticles. *International Journal of Pharmaceutics*, *310*(1–2), 213–219.

George, M. & Abraham, T.E. (2006). Polyionic hydrocolloids for the intestinal delivery of protein drugs: alginate and chitosan—a review. *Journal of Controlled Release*, 114(1), pp.1-14.

Gojova, A., Guo, B., Kota, R.S., Rutledge, J.C., Kennedy, I.M. & Barakat, A.I. (2007). Induction of inflammation in vascular endothelial cells by metal oxide nanoparticles: effect of particle composition. *Environmental Health Perspectives*, 115(3), p.403.

Goldstein, J. I., Newbury, D. E., Michael, J. R., Ritchie, N. W., Scott, J. H. J., & Joy, D. C. (2017). *Scanning Electron Microscopy and X-Ray Microanalysis*. Springer.

Goycoolea, F. M., El Gueddari, N. E., Remuñán-López, C., Coggiola, A., Lollo, G., Domard, A., & Alonso, M. J. (2007). Effect of Molecular Weight and Degree of Acetylation on the Physicochemical Characteristics of Chitosan Nanoparticles. *Advances In Chitin Science*, *10*, 542–547.

Gref, R. & Couvreur, P. (2006) . Nanocapsules: preparation, characterization and therapeutic applications. *Nanoparticulates As Drug Carriers* (pp. 255-276).

Grenha, A., Gomes, M. E., Rodrigues, M., Santo, V. E., Mano, J. F., Neves, N. M., & Reis, R. L. (2010). Development of new chitosan/carrageenan nanoparticles for drug delivery applications. *Journal of Biomedical Materials Research Part A*, *92*(4), 1265-1272.

Griffon, D.J., Sedighi, M.R., Schaeffer, D.V., Eurell, J.A. & Johnson, A.L. (2006) . Chitosan

scaffolds: interconnective pore size and cartilage engineering. *Acta Biomaterialia*, 2(3), pp.313-320.

Groothuis, D. R., Warkne, P. C., Molnar, P., Lapin, G. D., & Mikhael, M. A. (1990). Effect of hyperosmotic blood-brain barrier disruption on transcapillary transport in canine brain tumors. *Journal of Neurosurgery*, *72*(3), 441-449.

Haas, H.L. & Jefferys, J.G. (1984) . Low-calcium field burst discharges of CA1 pyramidal neurones in rat hippocampal slices. *The Journal of Physiology*, 354(1), pp.185-201.

Halmos, T., Santarromana, M., Antonakis, K., & Scherman, D. (1996). Synthesis of glucose-chlorambucil derivatives and their recognition by the human GLUT1 glucose transporter. *European Journal of Pharmacology*, *318*(2-3), 477-484.

Halnes, G., Mäki-Marttunen, T., Keller, D., Pettersen, K. H., Andreassen, O. A., & Einevoll, G. T. (2016). Effect of Ionic Diffusion on Extracellular Potentials in Neural Tissue. *PLoS Computational Biology*, *12*(11), 1–38.

Hasbun, R., Abrahams, J., Jekel, J. & Quagliarello, V.J. (2001). Computed tomography of the head before lumbar puncture in adults with suspected meningitis. *New England Journal of Medicine*, 345(24), pp.1727-1733.

Hawkins, B. T., & Davis, T. P. (2005). The Blood-Brain Barrier / Neurovascular Unit in Health and Disease. *Pharmacological Reviews*, *57*(2), 173–185.

Hawkins, R. A., O'kane, R. L., Simpson, I. A., & Vina, J. R. (2006). Structure of the blood–brain barrier and its role in the transport of amino acids. *The Journal of Nutrition*, *136*(1), 218S-226S.

He, P., Davis, S.S. & Illum, L. (1998) . In vitro evaluation of the mucoadhesive properties of chitosan microspheres. *International Journal of Pharmaceutics*, 166(1), pp.75-88.

Heinemann, U., Konnerth, A., Pumain, R. & Wadman, W.J. (1986). Extracellular calcium and potassium concentration changes in chronic epileptic brain tissue. *Advances In Neurology*, 44, pp.641-661.

Hellstrand, E., Lynch, I., Andersson, A., Drakenberg, T., Dahlbäck, B., Dawson, K. A., & Cedervall, T. (2009). Complete high-density lipoproteins in nanoparticle corona. *The FEBS Journal*, *276*(12), 3372-3381.

Hirani, J. J., Rathod, D. A., & Vadalia, K. R. (2009). Orally disintegrating tablets: a

review. *Tropical Journal of Pharmaceutical Research*, *8*(2).

Hoemann, C. D., Guzmán-Morales, J., Tran-Khanh, N., Lavallée, G., Jolicoeur, M., & Lavertu, M. (2013). Chitosan rate of uptake in HEK293 cells is influenced by soluble versus microparticle state and enhanced by serum-induced cell metabolism and lactate-based media acidification. *Molecules*, *18*(1), 1015-1035.

Honary, S., & Zahir, F. (2013a). Effect of zeta potential on the properties of nano-drug delivery systems-a review (Part 1). *Tropical Journal of Pharmaceutical Research*, *12*(2), 255-264.

Honary, S., & Zahir, F. (2013b). Effect of zeta potential on the properties of nano-drug delivery systems-a review (Part 2). *Tropical Journal of Pharmaceutical Research*, *12*(2), 265-273.

Hornig, S., & Heinze, T. (2007). Nanoscale structures of dextran esters. *Carbohydrate Polymers*, *68*(2), 280-286.

Iravani, S. (2011). Green synthesis of metal nanoparticles using plants. *Green Chemistry*, *13*(10), 2638-2650.

Jafar Mazumder, M. A. (2014). Polyelectrolyte complexation between cationic and anionic polyelectrolytes with complementary polymer-bound reactive groups of amine and acetoacetate: effect of mono- and divalent salts. *Iranian Polymer*, *23*, 445–455.

Jain, K. K. (2012). Nanobiotechnology-based strategies for crossing the blood–brain barrier. *Nanomedicine*, *7*(8), 1225-1233.

Jensen, M. S., & Yaari, Y. (1997). Role of intrinsic burst firing, potassium accumulation, and electrical coupling in the elevated potassium model of hippocampal epilepsy. *Journal of Neurophysiology*, *77*(3), 1224–1233.

JEOL. (2006). Scanning Electron Microscope A To Z. *Serving Advanced Technology*, 32.

Jin, L., Li, J., Nation, R. L., & Nicolazzo, J. A. (2009). Brain penetration of colistin in mice assessed by a novel high-performance liquid chromatographic technique. *Antimicrobial Agents and Chemotherapy*, *53*(10), 4247–4251.

Jouyban, A., & Soltani, S. (2012). Blood brain barrier permeation. *Toxicity and Drug Testing*. InTech. Retrieved from https://www.intechopen.com/books/toxicity-and-drug-testing/blood-brain-barrier-penetration

Kaibara, K., Okazaki, T., Bohidar, H.B. & Dubin, P.L. (2000). pH-induced coacervation in complexes of bovine serum albumin and cationic polyelectrolytes. *Biomacromolecules*, 1(1), pp.100-107.

Karlowsky, J.A., Jones, M.E., Draghi, D.C., Thornsberry, C., Sahm, D.F. & Volturo, G.A. (2004). Prevalence and antimicrobial susceptibilities of bacteria isolated from blood cultures of hospitalized patients in the United States in 2002. *Annals of Clinical Microbiology and Antimicrobials*, 3(1), p.7.

Kasper, J. C., & Friess, W. (2011). The freezing step in lyophilization: Physico-chemical fundamentals, freezing methods and consequences on process performance and quality attributes of biopharmaceuticals. *European Journal of Pharmaceutics and Biopharmaceutics*, *78*(2), 248–263.

Katas, H., Hussain, Z., & Awang, S. A. (2013). Bovine serum albumin-loaded chitosan/dextran nanoparticles: preparation and evaluation of ex vivo colloidal stability in serum. *Journal of Nanomaterials*, 2013, 34.

Kawasaki, K., Traynelis, S.F. & Dingledine, R. (1990). Different responses of CA1 and CA3 regions to hypoxia in rat hippocampal slice. *Journal of Neurophysiology*, 63(3), pp.385-394.

Kay, G.G. (2000). The effects of antihistamines on cognition and performance. *Journal of Allergy and Clinical Immunology*, 105(6), pp.S622-S627.

Kemper, E. M., Boogerd, W., Thuis, I., Beijnen, J. H., & van Tellingen, O. (2004). Modulation of the blood–brain barrier in oncology: therapeutic opportunities for the treatment of brain tumours?. *Cancer Treatment Reviews*, *30*(5), 415-423.

Kesharwani, P., Gajbhiye, V. & Jain, N.K. (2012). A review of nanocarriers for the delivery of small interfering RNA. *Biomaterials*, 33(29), pp.7138-7150.

Khanna, P., Ong, C., Bay, B., & Baeg, G. (2015). Nanotoxicity: An Interplay of Oxidative Stress, Inflammation and Cell Death. *Nanomaterials*, *5*(3), 1163–1180.

Kharia, A. A., Singhai, A. K., & Verma, R. (2012). Formulation and evaluation of polymeric nanoparticles of an antiviral drug for gastroretention. *International journal of pharmaceutical sciences and nanotechnology*, *4*(4), 1557-1562.

Ko, J.A., Park, H.J., Hwang, S.J., Park, J.B. & Lee, J.S. (2002). Preparation and characterization of chitosan microparticles intended for controlled drug delivery. *International Journal of Pharmaceutics*, 249(1), pp.165-174.

Koczulla, A.R. & Bals, R. (2003) . Antimicrobial peptides. *Drugs*, 63(4), pp.389-406.

Köping-Höggård, M., Tubulekas, I., Guan, H., Edwards, K., Nilsson, M., Vårum, K. M., & Artursson, P. (2001). Chitosan as a nonviral gene delivery system. Structure–property relationships and characteristics compared with polyethylenimine in vitro and after lung administration in vivo. *Gene Therapy*, *8*(14), 1108.

Korting, H.C. & Schäfer-Korting, M. (2010) . Carriers in the topical treatment of skin disease. *Drug Delivery* (pp. 435-468).

Kowal, S. L., Dall, T. M., Chakrabarti, R., Storm, M. V., & Jain, A. (2013). The current and projected economic burden of Parkinson's disease in the United States. *Movement Disorders*, *28*(3), 311-318.

Krafft, C., Steiner, G., Beleites, C. & Salzer, R. (2009) . Disease recognition by infrared and Raman spectroscopy. *Journal of Biophotonics*, 2(1-2), pp.13-28.

Kreuter, J. (2004). Influence of the surface properties on nanoparticle-mediated transport of drugs to the brain. *Journal of Nanoscience and Nanotechnology*, 4(5), pp.484-488.

Kulkarni, S. A., & Feng, S. S. (2013). Effects of particle size and surface modification on cellular uptake and biodistribution of polymeric nanoparticles for drug delivery. *Pharmaceutical Research*, *30*(10), 2512-2522.

Kumar, M., Pandey, R.S., Patra, K.C., Jain, S.K., Soni, M.L., Dangi, J.S. & Madan, J. (2013). Evaluation of neuropeptide loaded trimethyl chitosan nanoparticles for nose to brain delivery. *International Journal of Biological Macromolecules*, 61, pp.189-195.

Kurita, K., Kaji, Y., Mori, T. & Nishiyama, Y. (2000). Enzymatic degradation of β-chitin: susceptibility and the influence of deacetylation. *Carbohydrate Polymers*, 42(1), pp.19-21.

Lee, J.W., Kim, S.Y., Kim, S.S., Lee, Y.M., Lee, K.H. & Kim, S.J. (1999). Synthesis and characteristics of interpenetrating polymer network hydrogel composed of chitosan and poly (acrylic acid). *Journal of Applied Polymer Science*, 73(1), pp.113-120.

Levin, A. S., Barone, A. A., Penço, J., Santos, M. V., Marinho, I. S., Arruda, E. A. G., & Costa,

S. F. (1999). Intravenous Colistin as Therapy for Nosocomial Infections Caused by Multidrug-Resistant Pseudomonas aeruginosa and Acinetobacter baumannii. *Clinical Infectious Diseases*, *28*(5), 1008–1011.

Levin, V. (1980). Relationship of octanol/water partition coefficient and molecular weight to rat brain capillary permeability. *Journal of Medicinal Chemistry*, *23*(6), 682–684.

Lindahl, P., Johansson, B. R., Levéen, P., & Betsholtz, C. (1997). Pericyte loss and microaneurysm formation in PDGF-B-deficient mice. *Science*, *277*(5323), 242-245.

Lipinski, C. A., Lombardo, F., Dominy, B. W., & Feeney, P. J. (1997). Experimental and Computational Approaches to Estimate Solubility and Permeability in Drug Discovery and Develop ment Settings. *Advanced Drug Delivery Reviews*, *23*, 3–25.

Lipinski, C.A. (2000). Drug-like properties and the causes of poor solubility and poor permeability. *Journal of Pharmacological and Toxicological Methods*, 44(1), pp.235-249.

Liu, M., Li, H., Luo, G., Liu, Q., & Wang, Y. (2008). Pharmacokinetics and biodistribution of surface modification polymeric nanoparticles. *Archives of Pharmacal Research*, *31*(4), 547-554.

Liu, W. Y., Wang, Z. B., Zhang, L. C., Wei, X., & Li, L. (2012). Tight junction in blood-brain barrier: an overview of structure, regulation, and regulator substances. *CNS Neuroscience and Therapeutics*, *18*(8), 609-615.

Liu, X., An, C., Jin, P., Liu, X., & Wang, L. (2013). Biomaterials Protective effects of cationic bovine serum albumin-conjugated PEGylated tanshinone IIA nanoparticles on cerebral ischemia. *Biomaterials*, *34*(3), 817–830.

Lockman, P. R., Oyewumi, M. O., Koziara, J. M., Roder, K. E., Mumper, R. J., & Allen, D. D. (2003). Brain uptake of thiamine-coated nanoparticles. *Journal of Controlled Release*, *93*(3), 271-282.

López-León, T., Carvalho, E. L. S., Seijo, B., Ortega-Vinuesa, J. L., & Bastos-González, D. (2005). Physicochemical characterization of chitosan nanoparticles: electrokinetic and stability behavior. *Journal of Colloid and Interface Science*, *283*(2), 344-351.

Lorenzo, P., Adriana, A., Jessica, S., Carles, B., Marinella, F., Marta, L., & Pierre, S. (2018).

Antibiotic resistance in urban and hospital wastewaters and their impact on a receiving freshwater ecosystem. *Chemosphere*.

Luissint, A.C., Artus, C., Glacial, F., Ganeshamoorthy, K. & Couraud, P.O. (2012). Tight junctions at the blood brain barrier: physiological architecture and disease-associated dysregulation. *Fluids and Barriers of The CNS*, 9(1), p.23.

Lyklema, J. (2005). Fundamentals of interface and colloid science*: Soft Colloids* (Vol. 5). Elsevier.

Lynch, I., & Dawson, K. A. (2008). Protein-nanoparticle interactions. *Nano Today*, *3*(1–2), 40–47.

Ma, X. L., Chen, C., & Yang, J. (2005). Predictive model of blood-brain barrier penetration of organic compounds. *Acta Pharmacologica Sinica*, *26*(4), 500–512.

Madan, J., Pandey, R.S., Jain, V., Katare, O.P., Chandra, R. & Katyal, A. (2013). Poly (ethylene)-glycol conjugated solid lipid nanoparticles of noscapine improve biological half-life, brain delivery and efficacy in glioblastoma cells. *Nanomedicine: Nanotechnology, Biology and Medicine*, 9(4), pp.492-503.

Maher, S., Mrsny, R. J., & Brayden, D. J. (2016). Intestinal permeation enhancers for oral peptide delivery. *Advanced Drug Delivery Reviews*, *106*, 277–319.

Mahmoud Abbas, A. O. (2010). Chitosan for biomedical applications. University of Iowa, 1–329.

Malatesta, M., Giagnacovo, M., Costanzo, M., Conti, B., Genta, I., Dorati, R., & Zancanaro, C. (2012). Diaminobenzidine photoconversion is a suitable tool for tracking the intracellular location of fluorescently labelled nanoparticles at transmission electron microscopy. *European Journal of Histochemistry: EJH*, *56*(2).

Malhotra, M., & Prakash, S. (2011). Targeted Drug Delivery Across Blood-Brain-Barrier Using Cell Penetrating Peptides Tagged Nanoparticles. *Current Nanoscience*, *7*(1), 81–93.

Martinho, N. (2011). Recent Advances in Drug Delivery Systems. *Journal of Biomaterials and Nanobiotechnology*, *02*(05), 510–526.

Martìn-Padura, I., Lostaglio, S., Schneemann, M., Williams, L., Romano, M., Fruscella, P., & Simmons, D. (1998). Junctional adhesion molecule, a novel member of the immunoglobulin superfamily that distributes at intercellular junctions and modulates monocyte transmigration. *The Journal of Cell Biology*, *142*(1), 117-127.

Mason, T.G. (2000). Estimating the viscoelastic moduli of complex fluids using the generalized Stokes–Einstein equation. *Rheologica Acta*, 39(4), pp.371-378.

Masserini, M. (2013). Nanoparticles for Brain Drug Delivery. *ISRN Biochemistry*, *2013*, 1–18.

Mc Carthy, D. J., Malhotra, M., O'Mahony, A. M., Cryan, J. F., & O'Driscoll, C. M. (2015). Nanoparticles and the blood-brain barrier: Advancing from in-vitro models towards therapeutic significance. *Pharmaceutical Research*, *32*(4), 1161–1185.

McConnell, H. L., Kersch, C. N., Woltjer, R. L., & Neuwelt, E. A. (2017). The translational significance of the neurovascular unit. *Journal of Biological Chemistry*, *292*(3), 762-770.

McNaught, A.D. (1997). Compendium of chemical terminology. *Blackwell Science.*Retreived from http://goldbook.iupac.org/pdf/goldbook.pdf. [ISBN 0865426848]

Md, S., Khan, R. A., Mustafa, G., Chuttani, K., Baboota, S., Sahni, J. K., & Ali, J. (2013). Bromocriptine loaded chitosan nanoparticles intended for direct nose to brain delivery: pharmacodynamic, pharmacokinetic and scintigraphy study in mice model. *European Journal of Pharmaceutical Sciences*, *48*(3), 393-405.

Mikitsh, J. L., & Chacko, A. M. (2014). Pathways for small molecule delivery to the central nervous system across the blood-brain barrier. *Perspectives In Medicinal Chemistry*, *6*, PMC-S13384.

Misra, A., Ganesh, S., Shahiwala, A. & Shah, S.P. (2003). Drug delivery to the central nervous system: a review. *Journal of Pharmacy and Pharmaceutical Sciences*, 6(2), pp.252-273.

Mitra, S., Gaur, U., Ghosh, P. C., & Maitra, A. N. (2001). Tumour targeted delivery of encapsulated dextran-doxorubicin conjugate using chitosan nanoparticles as carrier. *Journal of Controlled Release*, *74*(1–3), 317–323.

Mohammadpour Dounighi, N., Eskandari, R., Avadi, M. R., Zolfagharian, H., Mir Mohammad Sadeghi, A., & Rezayat, M. (2012). Preparation and in vitro characterization of chitosan nanoparticles containing Mesobuthus eupeus scorpion venom as an antigen delivery system. *Journal of Venomous Animals and Toxins including Tropical Diseases*, *18*(1), 44-52.

Morita, K., Furuse, M., Fujimoto, K., & Tsukita, S. (1999). Claudin multigene family encoding four-transmembrane domain protein components of tight junction strands. *Proceedings of the National Academy of Sciences*, *96*(2), 511-516.

Morris, G. A., Castile, J., Smith, A., Adams, G. G., & Harding, S. E. (2009). Macromolecular conformation of chitosan in dilute solution: A new global hydrodynamic approach. *Carbohydrate Polymers*, *76*(4), 616–621.

Morrison, D.C. & Jacobs, D.M. (1976). Binding of polymyxin B to the lipid A portion of bacterial lipopolysaccharides. *Immunochemistry*, 13(10), pp.813-818.

Muoio, V., Persson, P. B., & Sendeski, M. M. (2014). The neurovascular unit - concept review. *Acta Physiologica*, *210*(4), 790–798.

Nafee, N., Schneider, M., Schaefer, U. F., & Lehr, C. M. (2009). Relevance of the colloidal stability of chitosan/PLGA nanoparticles on their cytotoxicity profile. *International Journal of Pharmaceutics*, *381*(2), 130-139.

Nag, S. ed. (2003). The blood-brain barrier: biology and research protocols (Vol. 89). Springer Science & Business Media.

Nagpal, K., Singh, S. K., & Mishra, D. N. (2010). Chitosan nanoparticles: a promising system in novel drug delivery. *Chemical and Pharmaceutical Bulletin*, *58*(11), 1423-1430.

Nagpal, K., Singh, S. K., & Mishra, D. N. (2013). Drug targeting to brain: a systematic approach to study the factors, parameters and approaches for prediction of permeability of drugs across BBB. *Expert Opinion on Drug Delivery*, *10*(7), 927–955.

Nagy, J. I., & Rash, J. E. (2003). Astrocyte and oligodendrocyte connexins of the glial syncytium in relation to astrocyte anatomical domains and spatial buffering. *Cell Communication & Adhesion*, *10*(4-6), 401-406.

Nakagawa, H., Groothuis, D., & Blasberg, R. G. (1984). The effect of graded hypertonic intracarotid infusions on drug delivery to experimental RG-2 gliomas. *Neurology*, *34*(12), 1571-1571.

National Institute of Neurological Disorders and Stroke (2012). National Institute of Neurological Disorders and Stroke Updated Feb, 18.

Nau, R., Sörgel, F., & Eiffert, H. (2010). Penetration of drugs through the blood-cerebrospinal fluid/blood-brain barrier for treatment of central nervous system infections. *Clinical*

Microbiology Reviews, *23*(4), 858-883.

Neuwelt, E. A., Goldman, D. L., Dahlborg, S. A., Crossen, J., Ramsey, F., Roman-Goldstein, S., & Dana, B. (1991). Primary CNS lymphoma treated with osmotic blood-brain barrier disruption: prolonged survival and preservation of cognitive function. *Journal of Clinical Oncology*, *9*(9), 1580-1590.

Nguyena, H., & Paika, S. S.-Y.-R. (2012). Preparation of size-tailored, similar surface characteristic chitosan nanoparticles by ionotropic gelation. *International Culture & Educational Foundation Organisation*, 2–5.

Nidhi, K., Indrajeet, S., Khushboo, M., Gauri, K., & Sen, D. J. (2011). Hydrotropy: A promising tool for solubility enhancement: A review. *International Journal of Drug Development and Research*, *3*(2), 26–33.

Nireesha, G. R., Divya, L., Sowmya, C., Venkateshan, N., Babu, M. N., & Lavakumar, V. (2013). Lyophilization/freeze drying-an review. *International Journal of Novel Trends In Pharmaceutical Sciences*, *3*(4), 87-98.

Nuriya, M., Shinotsuka, T., & Yasui, M. (2012). Diffusion properties of molecules at the blood–brain interface: potential contributions of astrocyte endfeet to diffusion barrier functions. *Cerebral Cortex*, *23*(9), 2118-2126.

O ’neill, J. (2016). Tackling drug-resistant infections globally: final report and recommendations the review on antimicrobial resistance.

Oatley, C.W., Nixon, W.C. & Pease, R.F.W. (1966). Scanning electron microscopy. *Advances in Electronics and Electron Physics*, 21, pp.181-247.

Oberdörster, G., Sharp, Z., Atudorei, V., Elder, A., Gelein, R., Kreyling, W. and Cox, C. (2004). Translocation of inhaled ultrafine particles to the brain. *Inhalation Toxicology*, 16(6-7), pp.437-445.

Ohtsuki, S. & Terasaki, T. (2007). Contribution of carrier-mediated transport systems to the blood–brain barrier as a supporting and protecting interface for the brain; importance for CNS drug discovery and development. *Pharmaceutical Research*, 24(9), pp.1745-1758.

Oldendorf, W. H., Hyman, S., Braun, L., & Oldendorf, S. Z. (1972). Blood-brain barrier: penetration of morphine, codeine, heroin, and methadone after carotid injection. *Science*, *178*(4064), 984-986.

Olesen, J., Gustavsson, A., Svensson, M., Wittchen, H. U., & Jönsson, B. (2012). The economic cost of brain disorders in Europe. *European Journal of Neurology*, *19*(1), 155-162.

O'Mahony, A.M., Godinho, B.M., Cryan, J.F. & O'Driscoll, C.M. (2013). Non-Viral Nanosystems for Gene and Small Interfering RNA Delivery to the Central Nervous System: Formulating the Solution. *Journal of Pharmaceutical Sciences*, 102(10), pp.3469-3484.

Orthmann, A., Zeisig, R., Süss, R., Lorenz, D., Lemm, M. & Fichtner, I.(2012). Treatment of experimental brain metastasis with MTO-liposomes: impact of fluidity and LRP-targeting on the therapeutic result. *Pharmaceutical Research*, 29(7), pp.1949-1959.

Oyarzun-Ampuero, F. A., Brea, J., Loza, M. I., Torres, D., & Alonso, M. J. (2009). Chitosan–hyaluronic acid nanoparticles loaded with heparin for the treatment of asthma. *International Journal of Pharmaceutics*, *381*(2), 122-129.

Pajouhesh, H., & Lenz, G. R. (2005). Medicinal chemical properties of successful central nervous system drugs. *NeuroRx*, *2*(4), 541-553.

Parajó, Y., d'Angelo, I., Welle, A., Garcia-Fuentes, M., & Alonso, M. J. (2010). Hyaluronic acid/Chitosan nanoparticles as delivery vehicles for VEGF and PDGF-BB. *Drug delivery*, *17*(8), 596-604.

Pardridge, W. M. (1998). Blood-brain barrier carrier-mediated transport and brain metabolism of amino acids. *Neurochemical research*, *23*(5), 635-644.

Pardridge, W. M. (2002). Why is the global CNS pharmaceutical market so under-penetrated?. *Drug Discovery Today*, 7(1), 5-7.

Pardridge, W. M. (2005). The blood-brain barrier: Bottleneck in brain drug development. *NeuroRX*, *2*(1), 3–14.

Pardridge, W. M. (2012). Drug Transport across the Blood–Brain Barrier. *Journal of Cerebral Blood Flow & Metabolism*, *32*(11), 1959–1972.

Parikh, T., Bommana, M. M., & Iii, E. S. (2010). European Journal of Pharmaceutics and Biopharmaceutics Efficacy of surface charge in targeting pegylated nanoparticles of sulpiride to the brain. *European Journal of Pharmaceutics and Biopharmaceutics*, *74*(3), 442–450.

Pecora, R. (Ed.). (2013). Dynamic light scattering: applications of photon correlation spectroscopy. Springer Science & Business Media.

Perkampus, H.H. & Grinter, H.C. (1992). UV-VIS Spectroscopy and its Applications (pp. 220-22). Berlin: Springer-Verlag.

Petushkov, A., Intra, J., Graham, J. B., Larsen, S. C., & Salem, A. K. (2009). Effect of crystal size and surface functionalization on the cytotoxicity of silicalite-1 nanoparticles. *Chemical Research In Toxicology*, *22*(7), 1359-1368.

Prokop, A., Hunkeler, D., DiMari, S., Haralson, M.A. & Wang, T.G. (1998). Water soluble polymers for immunoisolation I: Complex coacervation and cytotoxicity. *Advances in Polymer Science*, 136, pp.1-52.

Qi, J., Yao, P., He, F., Yu, C., & Huang, C. (2010). Nanoparticles with dextran / chitosan shell and BSA / chitosan core — Doxorubicin loading and delivery. *International Journal of Pharmaceutics*, *393*(1–2), 176–184.

Ranaldi, G., Marigliano, I., Vespignani, I., Perozzi, G., & Sambuy, Y. (2002). The effect of chitosan and other polycations on tight junction permeability in the human intestinal Caco-2 cell line1. *The Journal of Nutritional Biochemistry*, *13*(3), 157-167.

Rapoport, S. I., & Robinson, P. J. (1986). Tight-junctional modification as the basis of osmotic opening of the blood-brain barrier. *Annals of the New York Academy of Sciences*, *481*(1), 250-267.

Rapoport, S. I., Fredericks, W. R., Ohno, K., & Pettigrew, K. D. (1980). Quantitative aspects of reversible osmotic opening of the blood-brain barrier. *American Journal of Physiology-Regulatory, Integrative and Comparative Physiology*, *238*(5), R421-R431.

Reichelt, R. (2007). Scanning electron microscopy. *Science of Microscopy* (pp. 133-272).

Rempe, R., Cramer, S., Hüwel, S., & Galla, H. J. (2011). Transport of Poly(n-butylcyano-acrylate) nanoparticles across the blood-brain barrier in vitro and their influence on barrier integrity. *Biochemical and Biophysical Research Communications*, *406*(1), 64–69.

Review on Antimicrobial Resistance. (2016). Tackling drug-resistant infections globally: final report and recommendations. Review on Antimicrobial Resistance.

Rizzello, L., Vecchio, G., Brunetti, V., Maiorano, G., Malvindi, M. A., Galeone, A., & Pompa, P. P. (2012). Impact of nanomaterials on in vitro and in vivo systems: role of nanoscale

features in nanotoxicology. *Colloidal Nanocrystals for Biomedical Applications VII* (Vol. 8232, p. 82320E). International Society for Optics and Photonics.

Rodrigues, S., Dionísio, M., López, C. R., & Grenha, A. (2012). Biocompatibility of chitosan carriers with application in drug delivery. *Journal of Functional Biomaterials*, *3*(3), 615-64.

Rodríguez-Baeza, A., Reina-de la Torre, F., Poca, A., Martí, M., & Garnacho, A. (2003). Morphological features in human cortical brain microvessels after head injury: a three-dimensional and immunocytochemical study. *The Anatomical Record*, *273*(1), 583-593.

Rosa, A., Yan, M., Fernandez, R., Wang, X., & Zegarra, E. (n.d.). Top-down and Bottom-up approaches to nanotechnology. Portland State University.

Roy, A. G., Panicker, J., & Kumar, A. (2014). Acute CNS infections. *Amrita Journal of Medicine*, *10*, 8–14.

Rubin, L. L., & Staddon, J. M. (1999). The cell biology of the blood-brain barrier. *Annual Review of Neuroscience*, *22*(1), 11-28.

Rüdiger, F., Greger, R., Nitschke, R., Henger, A., Mundel, P., & Pavenstädt, H. (1999). Polycations induce calcium signaling in glomerular podocytes. *Kidney International*, *56*(5), 1700-1709.

Saboktakin, M. R., Tabatabaie, R. M., Maharramov, A., & Ramazanov, M. A. (2011). Synthesis and characterization of pH-dependent glycol chitosan and dextran sulfate nanoparticles for effective brain cancer treatment. *International Journal of Biological Macromolecules*, *49*(4), 747–751.

Sadeghi, A. M. M., Dorkoosh, F. A., Avadi, M. R., Weinhold, M., Bayat, A., Delie, F., & Junginger, H. E. (2008). Permeation enhancer effect of chitosan and chitosan derivatives: comparison of formulations as soluble polymers and nanoparticulate systems on insulin absorption in Caco-2 cells. *European Journal of Pharmaceutics and Biopharmaceutics*, *70*(1), 270-278.

Salama, N. N., Eddington, N. D., & Fasano, A. (2006). Tight junction modulation and its relationship to drug delivery. *Advanced Drug Delivery Reviews*, *58*(1), 15-28.

Sangster, J. (1989). Octanol-water partition coefficients of simple organic compounds. *Journal of Physical and Chemical Reference Data*, *18*(3), 1111-1229.

Saptarshi, S. R., Duschl, A., & Lopata, A. L. (2013). Interaction of nanoparticles with proteins: relation to bio-reactivity of the nanoparticle. *Journal of Nanobiotechnology*, *11*(1), 26.

Sarvaiya, J., & Agrawal, Y. K. (2015). Chitosan as a suitable nanocarrier material for anti-Alzheimer drug delivery. *International Journal of Biological Macromolecules*, *72*, 454–465.

Satalkar, P., Elger, B.S. & Shaw, D.M. (2016). Defining nano, nanotechnology and nanomedicine: why should it matter?. *Science and Engineering Ethics*, 22(5), pp.1255-1276.

Sato, T., Ishii, T., & Okahata, Y. (2001). In vitro gene delivery mediated by chitosan. Effect of pH, serum, and molecular mass of chitosan on the transfection efficiency. *Biomaterials*, *22*(15), 2075-2080.

Saunders, N. R., Dreifuss, J. J., Dziegielewska, K. M., Johansson, P. A., Habgood, M. D., Møllgård, K., & Bauer, H. C. (2014). The rights and wrongs of blood-brain barrier permeability studies: a walk through 100 years of history. *Frontiers in Neuroscience*, *8*, 404.

Sawchuk, R.J. & Elmquist, W.F. (2000). Microdialysis in the study of drug transporters in the CNS. *Advanced Drug Delivery Reviews*, 45(2), pp.295-307.

Schönhoff, M. (2003). Layered polyelectrolyte complexes: physics of formation & molecular properties. *Journal of Physics: Condensed Matter*, 15(49), p.R1781.

Sears, C. L. (2000). Molecular physiology and pathophysiology of tight junctions V. assault of the tight junction by enteric pathogens. *American Journal of Physiology-Gastrointestinal and Liver Physiology*, *279*(6), G1129-G1134.

Serda, R. E., Mack, A., Van De Ven, A. L., Ferrati, S., Dunner, K., Godin, B., & Bean, A. J. (2010). Logic-Embedded Vectors for Intracellular Partitioning, Endosomal Escape, and Exocytosis of Nanoparticles. *Small*, *6*(23), 2691-2700.

Seyrek, E., & Dubin, P. (2010). Glycosaminoglycans as polyelectrolytes. *Advances In Colloid and Interface Science*, *158*(1-2), 119-129.

Shaw, D.J. & Costello, B. (1993). Introduction to colloid and surface chemistry. *Journal of Dispersion Science and Technology*,*15*(1), 306.

Shetab, M. A., & Lamprecht, A. (2015). Nanoparticles as drug carriers : current issues with in

vitro testing. *Nanomedicine*, *10*, 3213–3230.

Shima, D. T., & Mailhos, C. (2000). Vascular developmental biology: getting nervous. *Current Opinion In Genetics & Development*, *10*(5), 536-542.

Siddharth, S., Nayak, A., Nayak, D., Bindhani, B. K., & Kundu, C. N. (2017). Chitosan-Dextran sulfate coated doxorubicin loaded PLGA-PVA-nanoparticles caused apoptosis in doxorubicin resistance breast cancer cells through induction of DNA damage. *Scientific Reports*, *7*(1), 2143.

Siliciano, J. D., & Goodenough, D. A. (1988). Localization of the tight junction protein, ZO-1, is modulated by extracellular calcium and cell-cell contact in Madin-Darby canine kidney epithelial cells. *The Journal of Cell Biology*, *107*(6), 2389-2399.

Smith, E. & Dent, G., (2005). The Raman Experiment–Raman Instrumentation, Sample Presentation, Data Handling and Practical Aspects of Interpretation. *Modern Raman Spectroscopy-A Practical Approach*, pp.23-70.

Sohaebuddin, S.K., Thevenot, P.T., Baker, D., Eaton, J.W. & Tang, L. (2010). Nanomaterial cytotoxicity is composition, size, and cell type dependent. *Particle and Fibre Toxicology*, 7(1), p.22.

Somand, D. & Meurer, W. (2009). Central nervous system infections. *Emergency Medicine Clinics of North America*, 27(1), pp.89-100.

Song, J., Shi, F., Zhang, Z., Zhu, F., Xue, J., Tan, X., & Jia, X. (2011). Formulation and evaluation of celastrol-loaded liposomes. *Molecules*, *16*(9), 7880–7892.

Soni, V., Kohli, D.V. & Jain, S.K. (2008). Transferrin-conjugated liposomal system for improved delivery of 5-fluorouracil to brain. *Journal of Drug Targeting*, 16(1), pp.73-78.

Sosunov, A. A., Wu, X., Tsankova, N. M., Guilfoyle, E., McKhann, G. M., & Goldman, J. E. (2014). Phenotypic heterogeneity and plasticity of isocortical and hippocampal astrocytes in the human brain. *Journal of Neuroscience*, *34*(6), 2285-2298.

Spapen, H., Jacobs, R., Gorp, V. Van, Troubleyn, J., & Honoré, P. M. (2011). Renal and neurological side effects of colistin in critically ill patients. *Annals of Intensive Care*, *1*(1),

Spectronic, T. (2012). Basic UV-Vis Theory, Concepts and Applications. *Thermo Spectronic*, pp.1-28.

Squire, J. M., Chew, M., Nneji, G., Neal, C., Barry, J., & Michel, C. (2001). Quasi-periodic

substructure in the microvessel endothelial glycocalyx: a possible explanation for molecular filtering?. *Journal of Structural Biology*, *136*(3), 239-255.

Srinivasan, B., Kolli, A.R., Esch, M.B., Abaci, H.E., Shuler, M.L. & Hickman, J.J. (2015). TEER measurement techniques for in vitro barrier model systems. *Journal of Laboratory Automation*, 20(2), pp.107-126.

Stamford, T. C. M., Stamford-Arnaud, T. M., de Medeiros Cavalcante, H. M., Macedo, R. O., & de Campos-Takaki, G. M. (2013). Microbiological chitosan: Potential application as anticariogenic agent. *Practical Applications in Biomedical Engineering*.

Stansly, P.G., Shepherd, R.G. & White, H.J. (1947). Polymyxin: a new chemotherapeutic agent. *Bulletin of the Johns Hopkins Hospital*, 81(1), p.43.

Statistics South Africa. (2016). Mid-year population estimates. Retrieved from https://www.statssa.gov.za/publications/P0302/P03022016.pdf

Steed, E., Balda, M. S., & Matter, K. (2010). Dynamics and functions of tight junctions. *Trends In Cell Biology*, *20*(3), 142-149.

Swanson, J. A., & Watts, C. (1995). Macropinocytosis. *Trends In Cell Biology*, *5*(11), 424-428.

Szymańska, E., & Winnicka, K. (2015). Stability of chitosan - A challenge for pharmaceutical and biomedical applications. *Marine Drugs*, *13*(4), 1819–1846.

Thanabalasundaram, G., Pieper, C., Lischper, M., & Galla, H. J. (2010). Regulation of the blood–brain barrier integrity by pericytes via matrix metalloproteinases mediated activation of vascular endothelial growth factor in vitro. *Brain Research*, *1347*, 1-10.

Thanou, M. M., Kotze, A. F., Scharringhausen, T., Luessen, H. L., De Boer, A. G., Verhoef, J. C., & Junginger, H. E. (2000). Effect of degree of quaternization of N-trimethyl chitosan chloride for enhanced transport of hydrophilic compounds across intestinal Caco-2 cell monolayers. *Journal of Controlled Release*, *64*(1-3), 15-25.

Tian, X. hua, Wei, F., Wang, T. xiao, Wang, P., Lin, X. ning, Wang, J., & Ren, L. (2012). In vitro and in vivo studies on gelatin-siloxane nanoparticles conjugated with SynB peptide to increase drug delivery to the brain. *International Journal of Nanomedicine*, *7*, 1031–1041.

Tiyaboonchai, W., & Limpeanchob, N. (2007). Formulation and characterization of amphotericin B–chitosan–dextran sulfate nanoparticles. *International Journal of Pharmaceutics*, *329*(1-2), 142-149.

Tiyaboonchai, W., Woiszwillo, J. & Middaugh, C.R. (2003a). Formulation and characterization of DNA–polyethylenimine–dextran sulfate nanoparticles. *European Journal of Pharmaceutical Sciences*, 19(4), pp.191-202.

Tiyaboonchai, W., Woiszwillo, J., Sims, R.C. & Middaugh, C.R. (2003b). Insulin containing polyethylenimine–dextran sulfate nanoparticles. *International Journal of Pharmaceutics*, 255(1), pp.139-151.

Toman, P. (2012). From alkylglyceryl-modified polysaccharides for drug delivery to the brain. https://scholar.google.co.za/scholar?hl=en&as_sdt=0%2C5&q=From+alkylglyceryl-modified+polysaccharides+for+drug+delivery+to+the+brain&btnG=

Träuble, H. (1971). The movement of molecules across lipid membranes: a molecular theory. *Journal of Membrane Biology*, 4(1), pp.193-208.

Traynelis, S.F. & Dingledine, R. (1988). Potassium-induced spontaneous electrographic seizures in the rat hippocampal slice. *Journal of Neurophysiology*, 59(1), pp.259-276.

Tsuji, A., & Tamai, I. (1999). Carrier-mediated or specialized transport of drugs across the blood–brain barrier. *Advanced Drug Delivery Reviews*, *36*(2-3), 277-290.

Tsukita, S., & Furuse, M. (1999). Occludin and claudins in tight-junction strands: leading or supporting players?. *Trends In Cell Biology*, *9*(7), 268-273.

Turci, F., Ghibaudi, E., Colonna, M., Boscolo, B., Fenoglio, I., & Fubini, B. (2010). An integrated approach to the study of the interaction between proteins and nanoparticles. *Langmuir*, *26*(11), 8336-8346.

Tute, M.S. (1990). History and objectives of quantitative drug design. *Comprehensive Medicinal Chemistry*, 4, pp.1-32.

Ueno, M., Sakamoto, H., Liao, Y.J., Onodera, M., Huang, C.L., Miyanaka, H. & Nakagawa, T. (2004). Blood-brain barrier disruption in the hypothalamus of young adult spontaneously hypertensive rats. *Histochemistry and Cell Biology*, 122(2), pp.131-137.

Umut, E. (2013). Surface Modification of Nanoparticles Used in Biomedical Applications. *Modern Surface Engineering Treatments*, 185–208.

Upadhyay, R. K. (2014). Drug delivery systems, CNS protection, and the blood brain barrier. *Biomed Research International*, *2014*.

Vaara, M.A. & Viljanen, P.E. (1985). Binding of polymyxin B nonapeptide to gram-negative bacteria. *Antimicrobial Agents and Chemotherapy*, 27(4), pp.548-554.

Valenzano, M. C., DiGuilio, K., Mercado, J., Teter, M., To, J., Ferraro, B., & Wertheimer, J. (2015). Remodeling of tight junctions and enhancement of barrier integrity of the CACO-2 intestinal epithelial cell layer by micronutrients. *Plos One*, *10*(7), e0133926.

Valiño, V., San Román, M.F., Ibáñez, R., Benito, J.M., Escudero, I. & Ortiz, I. (2011). Accurate determination of key surface properties that determine the efficient separation of bovine milk BSA and LF proteins. *Separation and Purification Technology*, 135, pp.145-157.

Van Thienen, T. (2007). Biodegradable dextran and PEG micro-and nanogels: physicochemical properties and sustained drug delivery features. Ghent University

Vliet, E. A. Van, Aronica, E., & Gorter, J. A. (2015). Seminars in Cell & Developmental Biology Blood – brain barrier dysfunction , seizures and epilepsy. *Seminars in Cell and Developmental Biology*, *38*, 26–34.

Vllasaliu, D., Exposito-harris, R., Heras, A., Casettari, L., Garnett, M., Illum, L., & Stolnik, S. (2010). Tight junction modulation by chitosan nanoparticles : Comparison with chitosan solution. *International Journal of Pharmaceutics*, *400*(1–2), 183–193.

Voigt, N., Henrich-Noack, P., Kockentiedt, S., Hintz, W., Tomas, J., & Sabel, B. A. (2014). Surfactants, not size or zeta-potential influence blood-brain barrier passage of polymeric nanoparticles. *European Journal of Pharmaceutics and Biopharmaceutics*, *87*(1), 19–29.

Wagner, S., Kufleitner, J., Zensi, A., Dadparvar, M., Wien, S., Bungert, J., & von Briesen, H. (2010). Nanoparticulate transport of oximes over an in vitro blood-brain barrier model. *PLoS ONE*, *5*(12).

Wallace, S.. (2017). Formulation approaches to pulmonary delivery of colistin combination antibiotic therapy. Retrieved from https://figshare.com/articles/Formulation_approaches_to_pulmonary_delivery_of_colistin_combination_antibiotic_therapy/4597600

Wallace, S.J., Li, J., Nation, R.L., Prankerd, R.J., Velkov, T. & Boyd, B.J. (2010). Self-assembly behavior of colistin and its prodrug colistin methanesulfonate: implications for solution stability and solubilization. *The Journal of Physical Chemistry B*, 114(14), pp.4836-4840.

Wangoo, N., Suri, C.R. & Shekhawat, G. (2008). Interaction of gold nanoparticles with protein: a spectroscopic study to monitor protein conformational changes. *Applied Physics Letters*, 92(13), p.133104.

Wilhelm, I., & Krizbai, I. A. (2014). In Vitro Models of the Blood-Brain Barrier for the Study of Drug Delivery to the Brain. *Molecular Pharmaceutics*, *11*(7), 1949–1963.

Williams, P. C., Henner, W. D., Simon, R. G., Dahlborg, S. A., Brummett, R. E., Tableman, M., & Neuwelt, E. A. (1995). Toxicity and efficacy of carboplatin and etoposide in conjunction with disruption of the blood-brain tumor barrier in the treatment of intracranial neoplasms. *Neurosurgery*, *37*(1), 17-28.

Win, K. Y., & Feng, S. S. (2005). Effects of particle size and surface coating on cellular uptake of polymeric nanoparticles for oral delivery of anticancer drugs. *Biomaterials*, *26*(15), 2713-2722.

Wolburg, H., Neuhaus, J., Kniesel, U., Krauss, B., Schmid, E. M., Ocalan, M., & Risau, W. (1994). Modulation of tight junction structure in blood-brain barrier endothelial cells. Effects of tissue culture, second messengers and cocultured astrocytes. *Journal of Cell Science*, *107*(5), 1347–1357.

World Health Organization. (2012). Dementia: a public health priority. World Health Organization.

Yang, S., Mei, S., Jin, H., Zhu, B., Tian, Y., Huo, J., & Zhao, Z. (2017). Identification of two immortalized cell lines, ECV304 and bEnd3, for in vitro permeability studies of blood-brain barrier. *Plos One*, *12*(10), e0187017.

Yang, Y., Wang, S., Wang, Y., Wang, X., Wang, Q., & Chen, M. (2014). Advances in self-assembled chitosan nanomaterials for drug delivery. *Biotechnology Advances*, *32*(7), 1301–1316.

Yousefpour, P., Atyabi, F., Farahani, E. V., Sakhtianchi, R., & Dinarvand, R. (2011). Polyanionic carbohydrate doxorubicin-dextran nanocomplex as a delivery system for anticancer drugs: in vitro analysis and evaluations. *International Journal of*

Nanomedicine, *6*, 1487–1496.

Zaccaria, M. L., Di Tommaso, F., Brancaccio, A., Paggi, P., & Petrucci, T. C. (2001). Dystroglycan distribution in adult mouse brain: a light and electron microscopy study. *Neuroscience*, *104*(2), 311-324.

Zeng, Y., Ebong, E.E., Fu, B.M. & Tarbell, J.M. (2012). The structural stability of the endothelial glycocalyx after enzymatic removal of glycosaminoglycans. *PLoS One*, 7(8), p.e43168.

Zhang, H. & Neau, S.H. (2001). In vitro degradation of chitosan by a commercial enzyme preparation: effect of molecular weight and degree of deacetylation. *Biomaterials*, 22(12), pp.1653-1658.

Zhang, L., Gu, F.X., Chan, J.M., Wang, A.Z., Langer, R.S. & Farokhzad, O.C. (2008). Nanoparticles in medicine: therapeutic applications and developments. *Clinical Pharmacology and Therapeutics*, 83(5), pp.761-769.

Zhang, X., Chen, G., Wen, L., Yang, F., Shao, A.L., Li, X., Long, W. & Mu, L. (2013). Novel multiple agents loaded PLGA nanoparticles for brain delivery via inner ear administration: in vitro and in vivo evaluation. *European Journal of Pharmaceutical Sciences*, 48(4), pp.595-603.

Zlokovic, B. V. (2008). The blood-brain barrier in health and chronic neurodegenerative disorders. *Neuron*, *57*(2), 178-201.

Zünkeler, B., Carson, R. E., Olson, J., Blasberg, R. G., Devroom, H., Lutz, R. J., ... & Dedrick, R. L. (1996). Quantification and pharmacokinetics of blood-brain barrier disruption in humans. *Journal of Neurosurgery*, *85*(6), 1056-1065.